Purdue University
Purdue e-Pubs

Department of Electrical and Computer Engineering Technical Reports

Department of Electrical and Computer Engineering

7-1-1988

Final Report on NASA Grant NAG 3-433. Solar Energy Conversion Through the Interaction of Plasmons with Tunnel Junctions. Part A Solar Cell Analysis. Part B Photoconductor Analysis

R. E. Welsh
Purdue University

R. J. Schwartz
Purdue University

Follow this and additional works at: https://docs.lib.purdue.edu/ecetr

Welsh, R. E. and Schwartz, R. J., "Final Report on NASA Grant NAG 3-433. Solar Energy Conversion Through the Interaction of Plasmons with Tunnel Junctions. Part A Solar Cell Analysis. Part B Photoconductor Analysis" (1988). *Department of Electrical and Computer Engineering Technical Reports.* Paper 618.
https://docs.lib.purdue.edu/ecetr/618

This document has been made available through Purdue e-Pubs, a service of the Purdue University Libraries. Please contact epubs@purdue.edu for additional information.

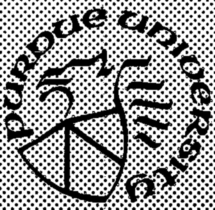

Final Report on
NASA Grant NAG 3-433

Solar Energy Conversion Through the Interaction of Plasmons with Tunnel Junctions

Part A Solar Cell Analysis
Part B Photoconductor Analysis

P. E. Welsh
R. J. Schwartz

TR-EE 88-37
July 1988

School of Electrical Engineering
Purdue University
West Lafayette, Indiana 47907

Final Report on

NASA Grant NAG 3-433

Solar Energy Conversion Through the Interaction of Plasmons with Tunnel Junctions

Part A Solar Cell Analysis

Part B Photoconductor Analysis

By
P. E. Welsh
R. J. Schwartz

School of Electrical Engineering
Purdue University
West Lafayette, IN 47907

TR-EE 88-37

July 1988

This work was supported under grant NAG 3-433.

TABLE OF CONTENTS

Page

LIST OF TABLES vi
LIST OF FIGURES vii
LIST OF SYMBOLS ix
SUMMARY xii

INTRODUCTION 1

Part A - SOLAR CELL ANALYSIS

A-1. INTRODUCTION 4

A-1.1 The purpose of part A 4
A-1.1.1 Conventional solar cell weaknesses and the multiple cell concepts 4
A-1.1.2 The purpose of part A 4
A-1.2 The conventional tandem cell concept and the conventional spectrum splitting concept 4
A-1.2.1 Description of the tandem cell and spectrum splitting concepts 5
A-1.2.2 The importance of the losses in the conventional multiple cell concepts 5
A-1.3 Operation of the multiple effective gap solar cell(MEG-SC) and associated problems 10
A-1.3.1 Description and operation 10
A-1.3.2 Problems 11

A-2. REVIEW OF THE PREVIOUS TECHNICAL REPORT 12

A-2.1 Introduction 12
A-2.2 A problem with metal layers in the solar cell 12
A-2.3 Problem with tunneling through an oxide 17
A-2.4 Important conclusions of the previous report 17

A-3. POSSIBLE ABSORPTION JUNCTIONS 19

A-3.1 Introduction 19

Page

A-3.2 Semiconductor-Insulator-Semiconductor(SIS) diodes - stacked SIS diodes 20
A-3.3 pn junction - nipi(or doping) superlattices 22
A-3.4 Heterojunction - type I superlattice 26
A-3.5 Heterojunction - type II superlattice 26
A-3.6 Comparison of the various absorption junctions 30
A-3.7 Conclusion 30

A-4. CONCLUSIONS 32

Part B - PHOTOCONDUCTOR ANALYSIS

B-1. OPERATION OF THE PHOTOCONDUCTOR 34

B-1.1 Introduction 34
B-1.2 Problems encountered by conventional photodetectors at long wavelengths 34
B-1.3 Description of the superlattice intraband-absorption photoconductor(SLIP) 35
B-1.4 Important physical relationships for the SLIP 39
B-1.4.1 Free carrier absorption 39
B-1.4.2 $E_{cb}-E_F$ 40
B-1.4.2.1 Open well case 40
B-1.4.2.2 Partly closed well case 43
B-1.4.2.3 Temperature and quantum efficiency 43
B-1.4.2.4 What others have done 43
B-1.4.3 E_F-E_{cw} 44
B-1.4.4 Impact ionization 44
B-1.5 Advantages and disadvantages of the SLIP 45

B-2. SURVEY OF THE COMPETING PHOTODETECTORS 47

B-2.1 Three alternatives for photodetection 47
B-2.2 Conventional and novel photoconductors 47
B-2.2.1 Graded well SLIP 50
B-2.2.2 Intersubband photoconductor(IS-PC) 50
B-2.2.2.1 Intersubband absorption 50
B-2.2.2.2 Intersubband photoconductor(IS-PC) 53
B-2.2.3 Tunneling IS-PC 53
B-2.2.4 Resonant IS-PC 53
B-2.2.5 Effective mass filter IS-PC 56
B-2.2.6 Quantum well IS-PC 56
B-2.2.7 Grating IS-PC 58

Page

B-2.2.8 Sampling IR detector 58
B-2.3 Conventional and novel avalanche photodiodes(APDs) 58
B-2.3.1 Separate absorption and multiplication region APD(SAM-APD) 59
B-2.3.2 Superlattice APD 62
B-2.3.3 Staircase APD 64
B-2.3.4 Quantum well APD 64
B-2.3.5 Graded gap APD 64
B-2.3.6 Resonant tunneling superlattice APD(RTS-APD) 68
B-2.3.7 Channeling APD 68
B-2.4 Conclusion 68

B-3. FREE CARRIER ABSORPTION 69

B-3.1 Experimental free carrier absorption results 69
B-3.2 Free carrier absorption limits 69
B-3.3 Classical calculation of free carrier absorption 71
B-3.4 Quantum calculation of free carrier absorption 72

B-4. PROPAGATION OF RADIATION 73

B-4.1 Three cases of incidence 73
B-4.2 Perpendicular incidence 73
B-4.3 Oblique incidence 73
B-4.4 Parallel incidence 74

B-5. CALCULATION OF THE CURRENT IN THE SLIP 75

B-5.1 Description of the current terms 75
B-5.2 Calculation of the signal current 75
B-5.2.1 Signal current for a conventional photodetector 75
B-5.2.2 Signal current for the SLIP 76
B-5.3 Calculation of the background current 77
B-5.4 Calculation of the thermionic emission current 78
B-5.5 Calculation of the tunnel current 79
B-5.5.1 Triangular barrier 80
B-5.5.2 Trapezoidal barrier 82
B-5.5.3 Comparison between the triangular barrier and the trapezoidal barrier 85

B-6. QUANTUM EFFICIENCY 87

B-6.1 Definition of quantum efficiency in the SLIP 87
B-6.2 Comparison of quantum efficiencies in open and partly closed wells 87

Page

B-6.2.1 Description of scattering mechanisms 87
B-6.2.2 Definition of open well and partly closed well 88
B-6.2.3 Physical significance of open and partly closed well 89
B-6.3 Analysis of quantum efficiency in an open well 89
B-6.4 Analysis of quantum efficiency in a partly closed well 91

B-7. NOISE AND D^* 96

B-7.1 Introduction 96
B-7.2 Noise terms 96
B-7.3 D^* 96
B-7.4 Filtering of background radiation 97
B-7.5 D^*_{BLIP} 98

B-8. PARAMETER LIMITATIONS 101

B-8.1 Introduction 101
B-8.2 Free carrier absorption limits 101
B-8.3 Quantum efficiency limitations of the SLIP 101
B-8.4 Wavelength range of the SLIP 102
B-8.5 Temperature limitations 102
B-8.6 Material limitations 104
B-8.7 E_F—E_{cw} limitations 105
B-8.8 E_{cb}—E_F limitations 105

B-9. THEORETICAL PERFORMANCE OF THE SLIP 107

B-9.1 Introduction 107
B-9.2 Description of the computer runs 107
B-9.3 Results of the computer runs 109
B-9.4 RC time constant of the SLIP 109
B-9.5 Comparison with conventional photoconductors 113

B-10. SUMMARY AND FUTURE RECOMMENDATIONS 116

B-10.1 Summary of the report 116
B-10.2 Future recommendations 117

LIST OF REFERENCES 118

SUBJECT INDEX 129

Page

LIST OF TABLES

Table — Page

A-2.1 $\alpha(x10^2cm^{-1})$ in the OMO waveguide as the frequency of light is varied 14
A-2.2 $\alpha(x10^2cm^{-1})$ in the OMO waveguide as n_1 and n_3 are varied 15
A-2.3 $\alpha(x10^2cm^{-1})$ in the OMO waveguide as n_2 is varied 16

B-3.1 Theoretical free carrier absorption coefficients for different concentrations and photon energies 70

B-5.1 Background current as a function of wavelength 78
B-5.2 ΔE_{te} as a function of temperature and thermionic emission current 79
B-5.3 Tunnel current through a triangular barrier 82

B-6.1 Electron distribution for the Monte Carlo results of Table B-6.2 91
B-6.2 Comparison of the analytical and Monte Carlo efficiencies for an open well 92
B-6.3 Comparison of the analytical and Monte Carlo efficiencies for a partly closed well 95

B-8.1 Temperature dependence on the thermionic emission current 103

B-9.1 Material parameters for the SLIP computer runs 108
B-9.2 Monte Carlo results for photons with 100 μm wavelengths 110
B-9.3 Monte Carlo results for photons with 50 μm wavelengths 111
B-9.4 Monte Carlo results for photons with 25 μm wavelengths 112
B-9.5 Monte Carlo results for photons with 12.5 μm wavelengths 112

LIST OF FIGURES

Figure Page

A-1.1 Tandem cell concept 6
A-1.2 Selective splitting concept using selective mirrors 7
A-1.3 Comparison of multiple cell concepts 8

A-2.1 The low ohmic loss mode 13
A-2.2 Mode with a large absorption due to tunneling 18

A-3.1 The SIS diode 21
A-3.2 A stack of SIS diodes 23
A-3.3 The tunnel(Esaki) diode 24
A-3.4 The IV curve of a tunnel(Esaki) diode 25
A-3.5 The nipi superlattice 27
A-3.6 The type I superlattice 28
A-3.7 The type II superlattice 29
A-3.8 Comparison of the absorption junctions 31

B-1.1 The proposed photoconductor 36
B-1.2 The proposed photoconductor which prevents tunneling 37
B-1.3 Trajectory of an electron excited by a photon with energy E_λ 38
B-1.4 The two modes in the open well case 41
B-1.5 The three modes in the partly closed well case 42

B-2.1 Intrinsic photoconductor 48
B-2.2 Extrinsic photoconductor 49
B-2.3 Graded well SLIP 51
B-2.4 IS-PC 54
B-2.5 Tunneling IS-PC 55
B-2.6 Resonant IS-PC 57
B-2.7 SAM-APD 60
B-2.8 Graded SAM-APD 61

Figure Page
B-2.9 Superlattice APD 63
B-2.10 Multiplication region of the staircase APD 65
B-2.11 Quantum Well APD 66
B-2.12 Graded gap APD 67

B-5.1 Tunneling through a triangular barrier 81
B-5.2 Shape of a barrier that will lower the tunneling rate 83
B-5.3 Tunneling through a trapezoidal barrier 84
B-5.4 Band diagram example of a SLIP during radiation excitation 86

B-6.1 Physical picture of $\eta_{pcw}(\hbar\,\omega)$ 94

B-7.1 D^{*}_{BLIP} for the conventional PC and for the SLIP 99

B-9.1 Theoretical D^{*} for some SLIPs 114
B-9.2 Experimental D^{*} for some conventional photodetectors 115

LIST OF SYMBOLS

α..................absorption coefficient
A..................Richardson constant
A^*..................effective Richardson constant
A_C..................area of the photoconductor
A_D..................area of the contacts of the photoconductor
β_e..................electron ionization coefficient
β_h..................hole ionization coefficient
ξ..................electric field
c..................speed of light
C..................capacitance
Δ_b..................barrier thickness
Δ_t..................effective barrier thickness
ΔB..................bandwidth
ΔE_c..................barrier height in conduction band
ΔE_s..................grading height in barrier
ΔE_{te}..................thermionic emission barrier height
D(E)..................3D density of states
D^*..................D-star
D^*_{BLIP}..................D-star for background limited infrared photodetector(BLIP)
ϵ..................dielectric constant
ϵ_o..................dielectric constant of air
e..................electric charge
E..................electron kinetic energy
E_c..................conduction band energy
E_{cb}..................energy of barrier conduction band at the quantum well interface
E_{cw}..................energy of well conduction band
E_{ez}..................electron energy in the z-direction before excitation
E_F..................Fermi energy
E_{m0}..................minimum detectable light energy

E_{m1} ....minimum detectable light energy with total excitation above the well
E_v ....valence band energy
E_{vb} ....energy of barrier valence band at the quantum well interface
E_{vw} ....energy of well valence band
E_λ ....photon energy
$E_{\lambda z}$ ....photon energy polarized in the z-direction
E_z ....electron kinetic energy in the z direction
E_{zb} ....electron kinetic energy in the z direction in the barrier at the interface
f(E) ....Fermi distribution function
γ_{inc} ....angle between incident light wave and superlattice planes
γ_{max} ....angle of transmission
G ....gain
θ ....phonon temperature
θ_{min} ....inelastic phonon temperature
$\hbar$ ....Planck's constant
I ....current
I_B ....background current
I_d ....dark current
$\overline{I_n^2}$ ....mean square current of the noise terms
I_{op} ....optical current
I_s ....signal current
I_{te} ....thermionic emission current
I_{tn} ....tunnel current
$J_B(\lambda_a)$ ....background current
$J_{op}(\lambda_a)$ ....optical current density at wavelength λ_a
$J_s(\lambda_a)$ ....signal current density at wavelength λ_a
J_{te} ....thermionic emission current density
J_{tn} ....tunnel current density
J_{sT} ....sum of signal current densities
k ....Boltzmann constant
λ ....wavelength of light
λ_s ....optimum wavelength of light in the FCA-SL-PC
μ_n ....electron mobility
m ....electron(or hole) mass
m^* ....effective mass
M_c ....number of valleys
n ....electron concentration
n_r ....index of refraction

N ....carrier concentration
ϕ..................photon flux
P..................power of incoming light
q ....electric charge
R ....resistance
σ..................Drude conductivity
τ ....lifetime
τ_d ....dielectric relaxation time
τ_{esc} ....escape time from the well
τ_r ....relaxation time
T ....temperature
Υ_t ....transmission probability
Υ_{tm} ....maximum transmission probability
U ....potential
v ....velocity of carrier
V ....voltage
ω..................frequency of light
W_λ ....radiant emittance
$W_{\lambda B}$ ....radiant emittance of a blackbody
$W_{\lambda op}$ ....radiant emittance of the light source
W ....intensity of light
η ....efficiency
η_{ow}...............efficiency of the open well case
η_{pcw}..............efficiency of the partly closed well case
η_{mc}...............efficiency of the partly closed well case
for Monte Carlo simulations

SUMMARY

A novel solar cell utilizing guided optical waves and tunnel junctions has been analyzed to determine its feasibility. From this analysis, it appears that the limits imposed upon conventional multiple cell systems also limit this novel solar cell. Due to this limitation, it appears that the relative simplicity of the conventional multiple cell systems over the novel solar cell make the conventional multiple cell systems the more promising candidate for improvement.

In the course of this investigation, it was discovered that some superlattice structures studied could be incorporated into an infrared photodetector. This photoconductor appears to be promising as a high speed, sensitive(high D^*_{BLIP}) detector in the wavelength range from 15 μm to over 100 μm.

INTRODUCTION

This report covers the work performed under grant NAG 3-433, "Solar Energy Conversion Through the Interaction of Plasmons with Tunnel Junctions," during the period from January 1, 1985 to June 30, 1987. Previous work was reported in technical report TR-EE 85-9 published at Purdue University(School of Electrical Engineering) during February 1985[1]. The major conclusions of that report were:

1. Metal-insulator-metal tunnel structures do not contain sufficient asymmetry in their properties to allow efficient conversion of solar energy. Structures required will be either metal-insulator-semiconductor structures or semiconductor-insulator-semiconductor structures.
2. It is useful to take a general view of the guided waves and not confine consideration to surface plasmons.
3. Even if mode conversion between a surface plasmon and a tunnel mode plasmon can be efficiently accomplished, the coupling between the tunnel mode plasmon and tunneling is sufficiently weak that most of the energy is lost in propagation losses and is not converted to useful energy.
4. If the proper materials can be found such that the strong coupling into photon aided tunneling can occur, a cascaded tunnel diode structure may be promising for broadband energy conversion.
5. The tunnel diode has many of the characteristics that one would attribute to an electronically tunable band gap in a conventional solar cell.
6. A stack of tunnel diodes may be a promising way of obtaining more efficient coupling into a guided wave.
7. A critical problem is the determination of whether or not it is possible to obtain strong enough coupling of the photons into the tunneling process to make the energy conversion scheme feasible.
8. As much metal as possible should be removed from the structure.

Personnel performing the work were Prof. R.J. Schwartz and Graduate Research Assistant P.E. Welsh.

Description of the report

This report is divided into two parts. Part A describes the continued analysis of the solar cell - the basic philosophy behind the device, the absorption junction, and the conclusions of the solar cell analysis. From this study, it appears that the limits imposed upon the conventional multiple cell systems also limit the novel solar cell.

However, during the course of the investigation, it was found that some of these structures show promise as high speed, high D^*_{BLIP} photodetectors in the wavelength range from 15 to over 100 μm. Part B of this report describes this photoconductor.

PART A

SOLAR CELL ANALYSIS

A-1 INTRODUCTION

A-1.1 The purpose of part A

A-1.1.1 Conventional solar cell weaknesses and the multiple cell concepts

Conventional solar cells can only collect a limited amount of energy from the sun. Light with energy less than the band gap is lost because no electron-hole pairs are produced. Light with energy greater than the band gap produces electron-hole pairs; yet any energy in excess of the band gap is lost as heat to the lattice. The most straightforward way to overcome this problem is to have several solar cells with different band gaps, each collecting a specific portion of the solar spectrum. The two best known multiple cell configurations are the tandem cell and the spectrum splitting systems[2,3].

These two multiple cell concepts have usually been made up of discrete materials and devices, ie., the solar cells are made up of different materials with different band gaps[2,4].

A-1.1.2 The purpose of part A

The purpose of part A is to analyze a new type of solar cell that attempts to integrate the spectrum splitting concept onto one substrate(See sec. A-1.3). It will be referred to as the multiple effective gap solar cell(MEG-SC).

Section A-1.2 describes the tandem cell concept and the spectrum splitting concept. The limitations on these conventional multiple cell systems are also limitations on the proposed solar cell. Section A-1.3 describes the MEG-SC and its problems.

A-1.2 The conventional tandem cell concept and the conventional spectrum splitting concept[2,3]

The conventional tandem cell and spectrum splitting concepts were designed to collect the energy of the sun over a large portion of the solar spectrum. When losses are assumed negligible, the efficiency in a seven cell system can be twice as large as an ideal conventional solar cell[2,3]. Unfortunately, the losses are not negligible and may seriously degrade the efficiency of the device[2,3].

A-1.2.1 Description of the tandem cell and spectrum splitting concepts

The conventional tandem cell concept is shown in Fig. A-1.1. The light strikes a sequence of solar cells where the first cell the light strikes has the largest band gap and the successive cells have smaller band gaps[2,3]. Every cell should collect the light that has energy between the previous cell's band gap and its band gap. The conventional tandem cell concept is more efficient and has fewer restrictions if the cells are contacted separately[4,5].

The conventional spectrum splitting concept is shown in Fig. A-1.2. The light is separated into components which are then directed into the corresponding solar cell[2,3].

A-1.2.2 The importance of the losses in the conventional multiple cell concepts

The structural losses in the conventional multiple cell concepts are listed below. These losses also exist in the MEG-SC. For this analysis, it is assumed that all the photon generated carriers are collected[2]. The performance of the multiple cell systems degrade even more when the some of the photon generated carriers are not collected[2].

The structural losses (It is assumed all the light greater than the band gap is absorbed) in the conventional tandem cell concepts are[2]: 1) reflection losses, 2) grid losses, and 3) transmission losses. The losses in the conventional spectrum splitting concept are[2]: 1) reflection losses from each cell, 2) grid shadowing from each cell, 3) reflection losses from each mirror, and 4) transmission losses from each mirror.

The effect of these losses is shown in Fig. A-1.3. These results are from Bennett and Olsen. In this figure, the device "collects all photon generated carriers, has infinite shunt resistance, no series resistance and its J_{diode} is due to injection currents only.[2]" Bennett and Olsen labeled the results "ideal system"(no structural losses) instead of "100%", "spectrum splitting" instead of "95%", and "tandem cell" instead of "85.5%". The relationship between these labels is discussed below.

The structural loss for the conventional tandem cell system is[2]

$$S_{\lambda n} = (1-\rho_{\lambda 1})\prod_{i=1}^{n}(1-\gamma_{\lambda i})\tau_{\lambda(i-1)}$$

where $\rho_{\lambda 1}$ is the reflection from the device, $\gamma_{\lambda i}$ is the grid shadowing losses from the ith cell, and τ_{λ_i} is the percentage of transmission through the ith cell where the photon energy is less than the ith cell's band gap energy($\tau_{\lambda 0}$=1). The structural loss for the conventional spectrum splitting system is[2]

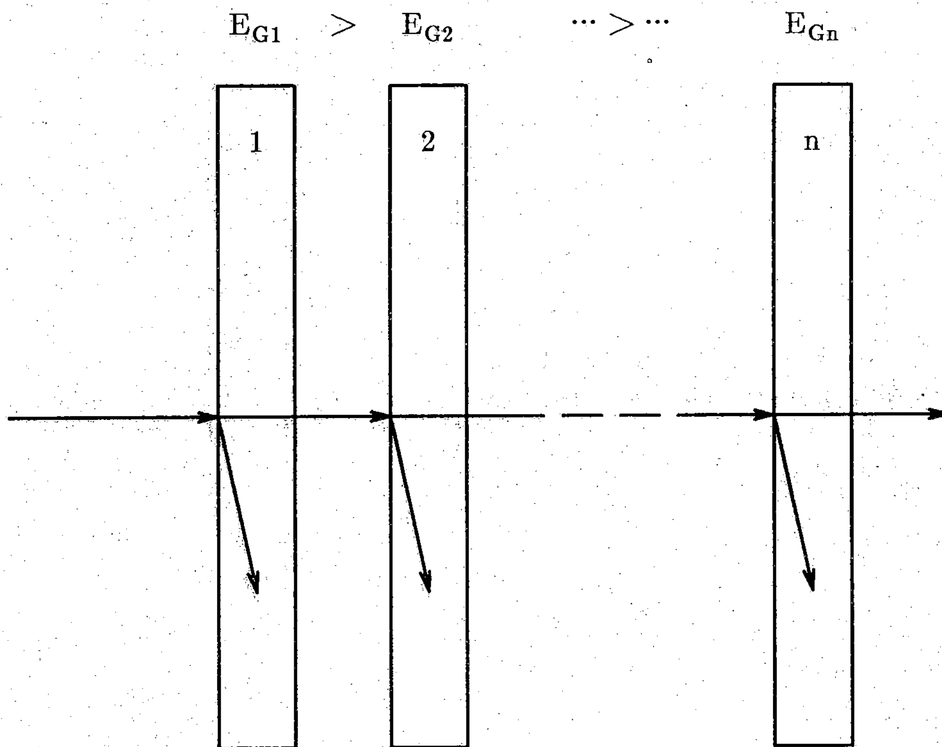

Figure A-1.1 Tandem cell concept(From Bennett and Olsen[2])

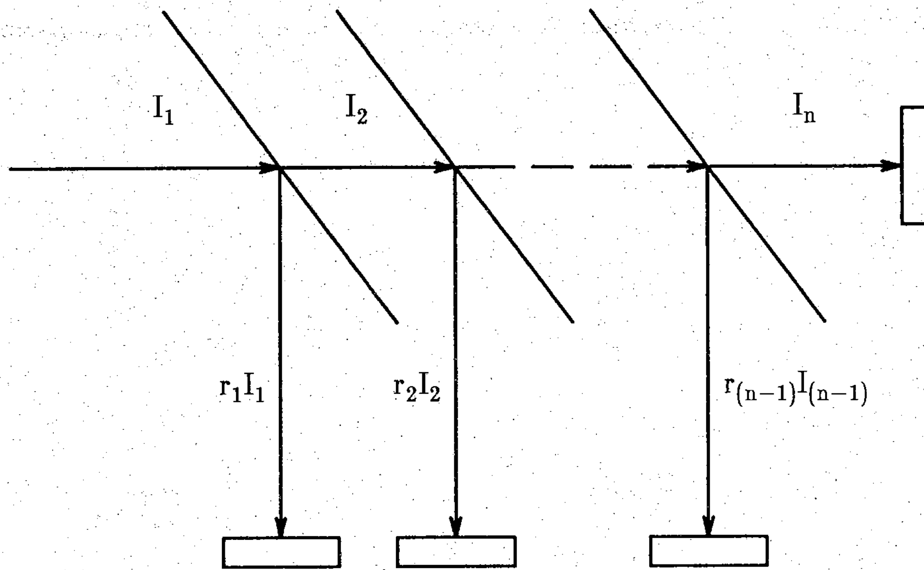

Figure A-1.2 Spectrum splitting concept using selective mirrors(From Bennett and Olsen[2])

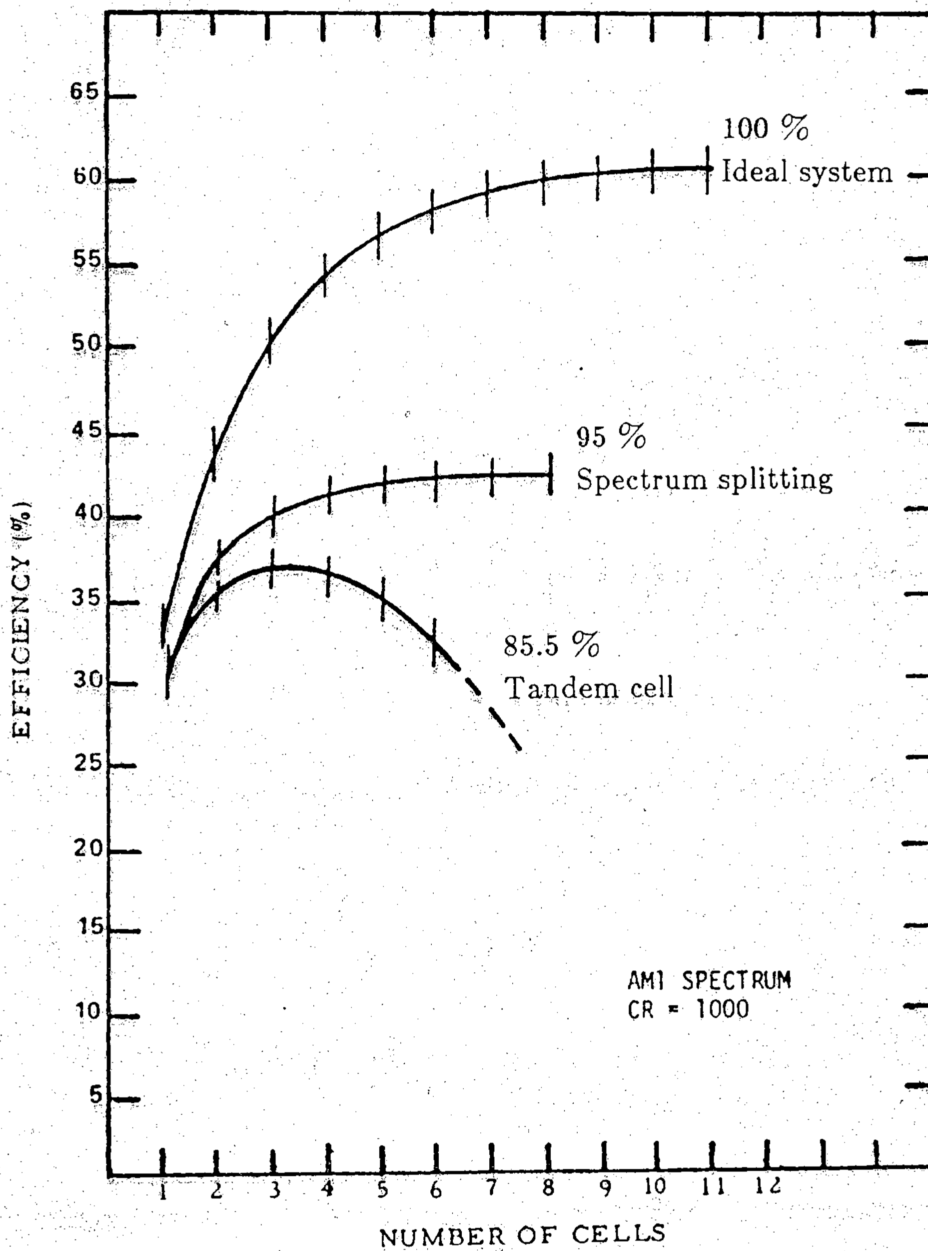

Figure A-1.3 Comparison of multiple cell concepts(From Bennett and Olsen[2])

$$S_{\lambda n} = (1-\rho_{\lambda n})(1-\gamma_{\lambda n})r_{\lambda n}\prod_{i=1}^{n-1}\mu_{\lambda i}$$

where $\rho_{\lambda n}$ is the reflection of the nth cell, $\gamma_{\lambda n}$ is the grid shadowing losses of the nth cell, $r_{\lambda n}$ is the reflection of the nth mirror and $\mu_{\lambda i}$ is the percentage of transmission through the the ith mirror for photons with wavelength λ.

Bennett and Olsen stated that the curves in Fig. A-1.3 are optimum efficiences for the conventional spectrum splitting and tandem cell concepts. Their argument was that the conventional tandem cell concept would be inherently worse than the conventional spectrum splitting concept. Yet, when one examines the previous equations for structural losses, assumes that the only losses are structural losses[2], and considers that the efficiencies for one cell are about the same(ie. $S_{\lambda 1}$ is about the same) for the tandem cell and spectrum splitting curves in Fig. A-1.3, then the shapes of the curves depend upon the losses per cell, not upon the system concept. For instance, the curves in Fig. A-1.3 are calculated using the equation[2],

$$S_{\lambda n} = S_{\lambda 1}(.95)^{n-1}$$

for the conventional spectrum splitting concept and

$$S_{\lambda n} = S_{\lambda 1}(.95)^{n-1}(.90)^{n-1} = S_{\lambda 1}(.855)^{n-1}$$

for the conventional tandem cell concept where $S_{\lambda 1}$ is about the same in either concept. Hence the label 95% and 85.5% which were added to Fig. A-1.3.

The importance of this result is that the shapes of the curves depend not upon the system concept, but the losses. If 85.5 percent of the light passes through each solar cell(tandem cell concept) or mirror(spectrum splitting concept), then the device efficiency reaches a maximum with only 3 cells for either concept. With higher losses, the system degrades even further. Since efficiency, not the type of system, is important, these problems also exist for the devices proposed in this report. In addition, the problems in the conventional spectrum splitting and tandem cell concepts seem relatively simple to surmount compared to the coupling, collection, and contact problems of the proposed device(See sec. A-1.3 and chap. A-4).

A-1.3 Operation of the multiple effective gap solar cell(MEG-SC) and associated problems

A-1.3.1 Description and operation

The MEG-SC is made up of four parts[6,7]. The first part is a thin layer of metal on a substrate which acts as a parallel plane waveguide. The second part is a spectrum splitter which at this time has not been designed. The third part is a coupler that couples the electric field into the tunnel diodes. This coupler has not been designed. The fourth part is the tunnel diode[8] which transforms the light energy into useful electrical energy. These parts are now described in a little more detail.

The light is coupled into the parallel plane waveguide which produces an electric field that travels down the waveguide in the form of surface plasmons. One only has to consider the dielectric constant of the metal and solve for the propagation in a waveguide(See chap. A-2). Surface plasmons were first proposed as an integral part of the device. Problems with surface plasmons arise as a result of free carrier absorption[9](See sec. A-2.1) which is intraband absorption and must be avoided[4](See sec. A-2.2). A practical device would most likely minimize the amount of metal in the structure(See chap. A-2).

Once the light is coupled into the device, the spectrum splitter would have to separate the light into components. There are two ways to split the spectrum. The first is to use mirrors or some analogous operation that separates one portion from the total, then separates another portion, etc. One possible way to do this is schematically shown in Fig. A-1.2(Anderson proposed this type of procedure[6,7]). Considering the results presented in sec. A-1.2.2 and the probable efficiencies of this process, it appears that this type of procedure is not very promising. A better method might be to separate the light into components all at once - as in a prism. Then the transmission losses would occur only in the prism, not in a number of mirrors(spectrum splitting) or solar cells(tandem cell) where the losses propagate(See sec. A-1.2). Unfortunately, incorporating a prism(or some analogous concept) appears to be more difficult than incorporating mirrors(or some analogous concept).

After the light is separated, it must be coupled into the diode. The problem with the coupler is how to concentrate the electric field into the very thin tunneling oxide. A suitable device for this purpose is not available at this time.

The fourth part of the scheme was originally to be an MIS tunnel diode. The tunnel diodes were to extract the energy from the light by absorbing light through tunneling(See [1,6,7,8] for a description of the tunnel diode operation). For absorption to take place, the light must propagate along the tunnel junction(See sec.

A-3.1). As shown in [1], tunnel diodes with a metal layer do not appear feasible. Other devices appear to be more advantageous than the MIS tunnel diodes. These devices will be referred to as absorption junctions and are described in chap. A-3.

A-1.3.2 Problems

The MEG-SC utilizes optics that are very complicated, most likely requiring the ability to epitaxially grow in two dimensions and even then its fabrication would not be trivial. The main problems with any MEG-SC are: 1) The limits on the conventional tandem cell concept(ie. number of cells needed) are also limits on the MEG-SC if both have the same structural losses. 2) It will be difficult to couple the light into the device. 3) It will be very difficult to separate the light into components without large losses. 4) It will be difficult to couple the propagating wave into the tunnel junctions. 5) It appears that the free carrier absorption in metals will be excessive(See chap. A-2).

A-2 REVIEW OF THE PREVIOUS TECHNICAL REPORT[1]

A-2.1 Introduction

The previous report raised two important points[1]. First, surface plasmons are implicitly determined by the dielectric constant of the metal. This dielectric constant may be calculated using the Drude theory of metals. From the Drude theory, one can calculate the Drude optical absorption[10] which is the classical form of free carrier absorption[9].

Although the first report did not state the direct relationship between surface plasmons and free carrier absorption, it was implicitly assumed in the calculation of the absorption of the waveguide modes. The importance of this absorption is described in sec. A-2.2.

The second important point of the report was that the tunneling absorption is too small. Even when one calculates the losses for a very low Ohmic loss mode and compares it to the absorption due to tunneling of a completely different mode with a relatively large amount of tunneling, the Ohmic losses of the first mode still exceed the absorption due to tunneling of the second mode.

A-2.2 A problem with metal layers in the solar cell

In the previous report[1], an absorption coefficient due to losses was compared to an absorption coefficient due to tunneling. The absorption due to tunneling was seven orders of magnitude smaller than the absorption due to losses for both cases considered. In the modes considered, though, one of the semi-infinite layers was metallic. In this section, the absorption due to losses will be considered where only one thin layer is metallic while the other layers are insulators.

The data to calculate the absorption due to Ohmic losses can also be found in [1]. This data is for the oxide-metal-oxide structure(See Fig. A-2.1) and is presented in tables A-2.1 to A-2.3. In table A-2.1, the frequency of light is varied from 4.26×10^{14}(1.76 eV) to 7.86×10^{14}(3.25 eV). The index of refraction of the semi-infinite oxide layers(n_1 and n_3) equals 1.5 and the metal film(with thickness d and index of refraction n_2) is silver[11]. In table A-2.2, the index of refraction of the oxide layers is varied. The frequency of light is 4.86×10^{14}(2.01 eV). In table A-2.3, the material in the metal film is varied. The index of refraction of the semi-infinite oxide layers is 1.5 and the frequency of light is 4.86×10^{14}(2.01 eV).

Examination of these absorption values shows that as the index of refraction of the oxide in the semi-infinite layers increases, the absorption increases. Hence, the

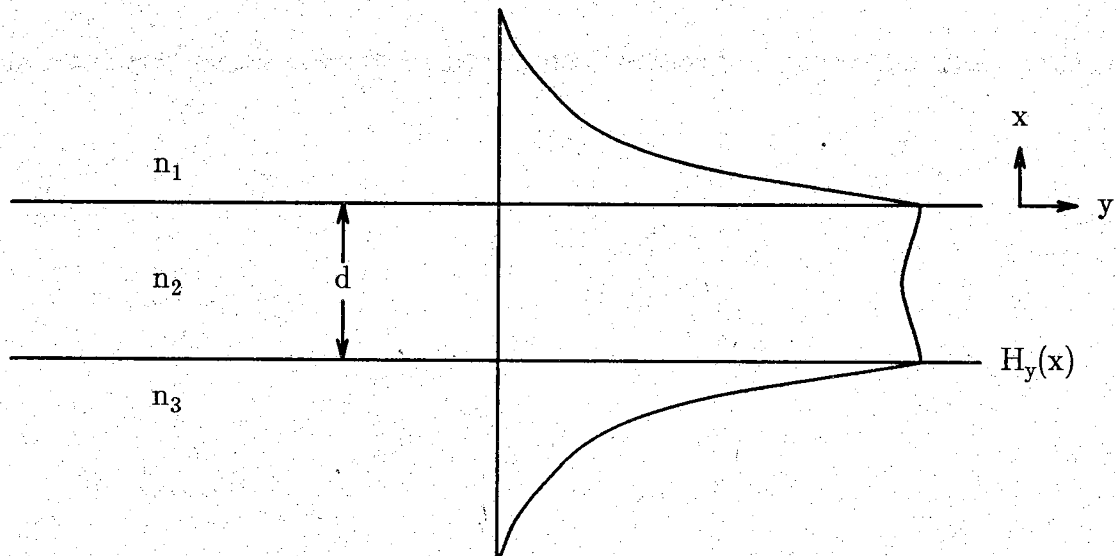

Figure A-2.1 The low ohmic loss mode

Table A-2.1
$\alpha(\mathrm{x}10^2\mathrm{cm}^{-1})$ in the OMO waveguide
as the frequency of light is varied.

		d(Å)				
freq(Hz)	n_2	180.	200.	300.	400.	500.
426.x10^{14}	.04 -j4.838	.046	.060	.16	.32	.49
486.x10^{14}	.06 -j4.152	.156	.200	.51	.97	1.49
547.x10^{14}	.06 -j3.586	.334	.422	1.06	1.93	2.92
604.x10^{14}	.05 -j3.093	.587	.741	1.80	3.24	4.82
665.x10^{14}	.04 -j2.657	1.03	1.29	3.11	5.60	8.30
725.x10^{14}	.05 -j2.275	2.93	3.69	9.07	16.7	25.1
786.x10^{14}	.05 -j1.864	8.39	10.8	30.1	64.0	108.

Table A-2.2

α(x10^2cm^{-1}) in the OMO waveguide as n_1 and n_3 are varied.

	d(Å)				
n_1,n_3	180.	200.	300.	400.	500.
1.0	.0250	.0332	.0986	.203	.330
1.5	.155	.200	.516	.972	1.49
2.0	.647	.816	1.97	3.50	5.09
2.5	2.17	2.71	6.48	11.2	15.7
3.0	6.48	8.28	21.1	37.1	50.5
3.5	19.6	26.3	86.5	168.	213.
4.0	777.	1290.	3140.	2830.	2650.

Table A-2.3

$\alpha(\mathrm{x}10^2\mathrm{cm}^{-1})$ in the OMO waveguide as n_2 is varied.

		d(Å)				
metal	n_2	180.	200.	300.	400.	500.
Ag	.06 -j 4.152	.156	.200	.516	.972	1.49
Au	.21 -j 3.272	1.04	1.30	3.18	5.96	9.34
Ca	.29 -j 7.94	.284	.374	.913	1.39	1.72
Cs	.326-j 4.01	.910	1.16	2.99	5.64	8.66
K	.067-j24.0	.0143	.0152	.0166	.0167	.0168
Mg	.43 -j12.0	.298	.367	.651	.790	.844
Na	.048-j 2.5	.573	.716	1.71	3.19	5.12
Rb	.135-j10.0	.110	.140	.292	.392	.442

oxide-metal-oxide($n_{ox}=1.5$) layers will have lower Ohmic losses than a four layer device where one of the semi-infinite layers is a semiconductor($n_{ox}<n_{semi}$) and the electric field directed across the oxide doesn't change signs(The mode where the electric field directed across the oxide changes sign in the oxide is not of interest). In addition, the semiconductor will probably have to be heavily doped, which will increase the free carrier absorption in the waveguide.

With this in mind, examination of table A-2.3 shows that the lowest absorption coefficient is 1.43 cm^{-1} for potassium(K) for a 180 Å thick metal. This is the value to be compared in the next section. We will ignore the obvious problems associated with using potassium in such a structure.

A-2.3 Problem with tunneling through an oxide

In [1], the highest absorption coefficient due to tunneling was calculated as .01 cm^{-1}. In this case, all the energy was concentrated in a thin oxide(See Fig. A-2.2) while the cases discussed in sec. A-2.2 involved fields that were spread out over a very large distances. Since the absorption due to Ohmic losses in the low loss cases are still larger than this absorption coefficient due to tunneling, one conclusion of the report was that metals cannot be used in the proposed solar cell[1]

A-2.4 Important conclusions of the previous report

There were three basic conclusions in the previous report. 1) The problem should more generally be looked at as one of trying to couple the light into the device. Coupling the light into surface plasmons is one way to accomplish this but it's not the only way.

This leads to the second conclusion. 2) The metals needed to produce surface plasmons may do an adequate job of coupling the light into the device, but the surface plasmons also produce excessive losses. As shown in sec. A-2.2, most, if not all metals, have serious losses in even the most optimal examples. At photon energies less than 2.00 eV and for very thin metals(less than 200 Å), potassium might be viable, but it appears unlikely because of the third conclusion.

3) The MIM and MIS tunnel diodes don't seem to be the ideal junctions to collect photon energy because the absorption due to tunneling is too small.

Junctions other than the MIM and MIS tunnel diodes are considered in chap. A-3. These junctions should have higher absorption coefficients and do not incorporate metals.

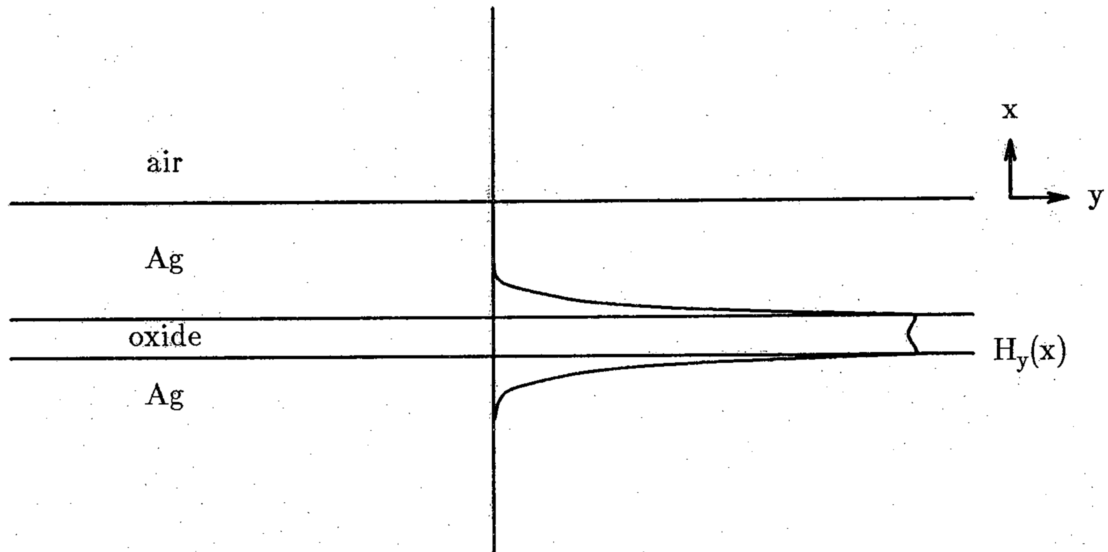

Figure A-2.2 Mode with a large absorption due to tunneling

A-3 POSSIBLE ABSORPTION JUNCTIONS

A-3.1 Introduction

The absorption junction is defined as the location where the conversion of light to useful electrical energy takes place. The absorption coefficient of light in a material is proportional to the amount of spatial overlap between the initial and final states[12,13]. In a conventional solar cell, these initial and final states are spatially centered at the same location. This phenomenon will be referred to as "spatially direct absorption". In all the cases presented in this chapter, the absorption is not spatially direct, but occurs at a junction between two different materials(The absorption is essentially inelastic tunneling[13]). This phenomenon will be referred to as "spatially indirect absorption".

One important point must be made about spatially indirect absorption. For the absorption to occur, the electric field of the light must be polarized in the same direction that the electron is to be excited(the direction along the initial and final states). Since the propagation of light is perpendicular to the polarization[14], the light must propagate parallel to the absorption junctions. Consequently, any solar cell using some type of effective gap will have to incorporate a waveguide and will have the accompanying problems of a waveguide. In addition, not all of the light will be polarized in the proper direction; it will not be trivial to properly polarize the light.

At the absorption junctions considered in this chapter, the initial state is located in the valence band on one side of the junction and the final state is located in the conduction band on the other side. The spatially indirect absorption coefficient is smaller than the spatially direct absorption coefficient. This spatial separation also means that the energy gap between the initial and final states(defined as the "effective gap") can depend on the electric field. This effective gap can change because the valence band levels(which can be quantum levels in a quantum well) on one side of the junction may change in energy relative to the conduction band levels on the other side of the junction. Hence, the effective gap is a result of the spatially indirect absorption. This electric field dependent effective gap should allow a single type of tunnel junction to have a continuum of "gaps" and hence, serve the purpose of many different materials with different gaps which must be used in a conventional multiple cell system.

There are three types of junctions considered as absorption junctions: 1) the semiconductor-insulator-semiconductor(SIS) junction, 2) the pn junction, and 3) the heterojunction. Sections A-3.2 to A-3.5 describe the absorption processes and the

associated problems of the absorption junctions and how they may be stacked to be incorporated in a solar cell. In sec. A-3.2, the SIS junction is the absorption junction and the corresponding stacked device is a stack of SIS diodes. In sec. A-3.3, the pn junction is the absorption junction and the corresponding stacked device is the nipi(or doping) superlattice. In sec. A-3.4, the heterojunction is the absorption junction and the corresponding stacked device is the type I compositional superlattice. In sec. A-3.5, the heterojunction is the absorption junction and the corresponding stacked device is the type II compositional superlattice.

Section A-3.6 compares three of these absorption junctions and shows that the type II compositional superlattice appears to have the highest spatially indirect absorption and the nipi superlattice has the second highest spatially indirect absorption.

There are three problems with these absorption junctions. First, as stated earlier in this section, solar cells incorporating spatially indirect absorption will also encounter waveguide and polarization problems(These two problems are hereafter referred to as coupling problems). Second, the spatially indirect absorption coefficient is less than the spatially direct absorption(Due to the relationship between the overlap of the initial and final electron states). As shown in sec. A-1.2, a MEG-SC would have the same efficiency problems as the tandem cell and splitting spectrum concepts and if the absorption is smaller, the MEG-SC should be less efficient. Third, the effective band gap must have a wide range of values. A reasonable range of energy gaps would be 2 eV(from .5 eV to 2.5 eV). This range would be difficult to obtain with any of the absorption junctions above. A more reasonable effective gap range for a single material group would be .5 eV. Inevitably, the material parameters of the junction would have to be changed four times to cover the complete range of 2 eV. If the material parameters are going to change, then it would be just as easy to build a conventional tandem cell system with AlGaAs-InGaAs materials and to use spatially direct absorption.

A-3.2 Semiconductor-Insulator-Semiconductor(SIS) diodes - stacked SIS diodes

The SIS diode absorption junction was proposed to replace the MIS and the MIM diode. In the MIS and the MIM diodes, the absorption due to tunneling was smaller than the absorption due to Ohmic losses(See chap. A-2). From this result, it was determined that the metal in the device should be minimized or eliminated and subsequently, the SIS diode was the logical candidate for inquiry[1].

The three absorption processes of interest are presented in Fig. A-3.1. Absorption process 1 is the contributing process for photovoltaic action. Processes 2

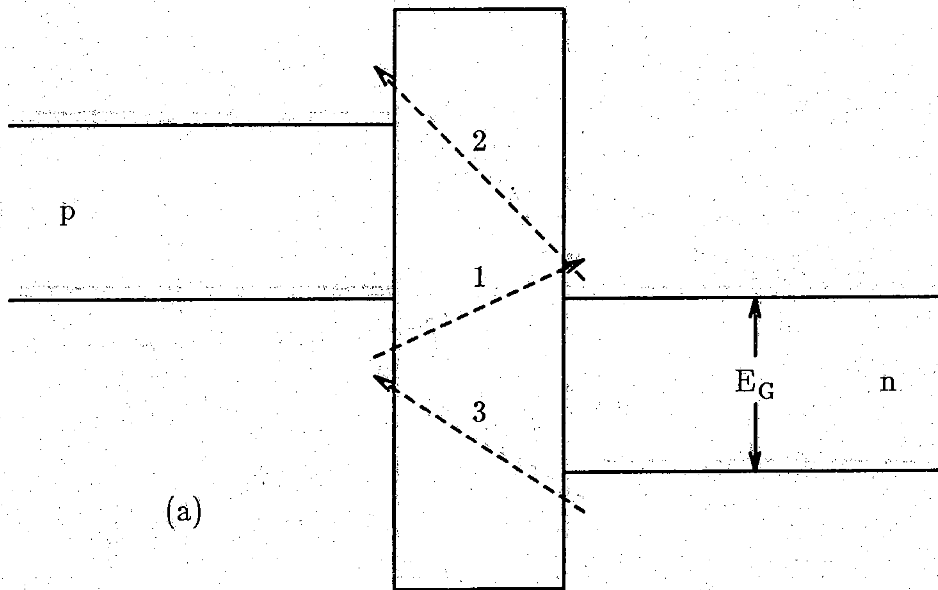

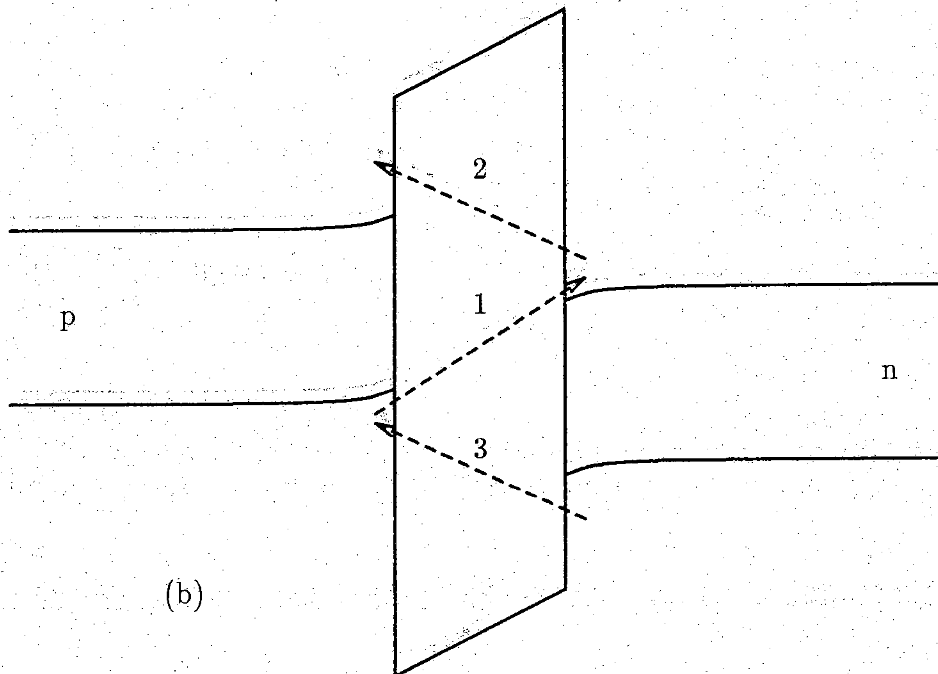

Figure A-3.1 The SIS diode

and 3 can be considered as losses because the current direction is opposite to process 1. Ideally, this device could collect and convert into electricity all photons with energy less than 1/2 of the band gap of the semiconductor. This can be shown as follows. The ideal equilibrium condition for this device occurs if the p-type valence band is lined up with the n-type conduction band(See Fig. A-3.1a). Photons with energy less than the effective gap should be absorbed via process 1, assuming no interface states. As photons are absorbed, the diode biases so that the n-type conduction band moves upward with respect to the p-type valence band(See Fig. A-3.1b). As the n-type layer moves upward, there will come a point when processes 2 and 3 will offset process 1. Processes 2 and 3 will approximately equal process 1 when the junction is biased to about one half of the band gap. Thus the open circuit voltage will be $\simeq E_g/2q$.

For a tandem structure, the SIS diodes would be stacked on each other. As stated before, the light would propagate parallel to the planes of the junctions. One stacked device with SIS junctions is shown in Fig. A-3.2.

The are four problems with this device that hinder its use in the MEG-SC. 1) As we shall see, the absorption coefficient designated by process 1 is extremely small. This is due to the fact that the insulator retards the absorption process. If the insulator is made thinner, then process 1 increases, but all the other processes also increase. In addition, other types of absorption junctions have higher spatially indirect absorption. 2) Light with energy greater than the band gap is lost; the wide band gap materials used would most likely be AlAs(2.16) or GaP(2.25)[15]. 3) If the p-type valence band and the n-type conduction band are to line up, then semiconductors need to be found that can be degenerately doped. Unfortunately, it is difficult to dope wide gap semiconductors n-type. 4) It would not be trivial to grow oxide on semiconductor on oxide, etc. These problems effectively eliminate the SIS from consideration as an absorption junction.

A-3.3 pn junctions - nipi(or doping) superlattices

The two absorption and/or tunneling processes for this absorber are shown in Fig. A-3.3. The absorption process that would be useful for photovoltaic action is process 1. This absorption is much greater than the SIS diode, but there is one significant drawback. The fact that an electron can traverse from the n-type to the p-type(process 2) shows the major weakness of the tunnel(Esaki) diode when used as a solar cell. This problem shows up on the IV curve of the tunnel(Esaki) diode(See Fig. A-3.4)[13]. There is an excess current produced by electrons tunneling from the n region to the p region through impurity levels[13]. This will adversely affect the fill factor. To produce a large enough absorption, the layers need to be highly doped.

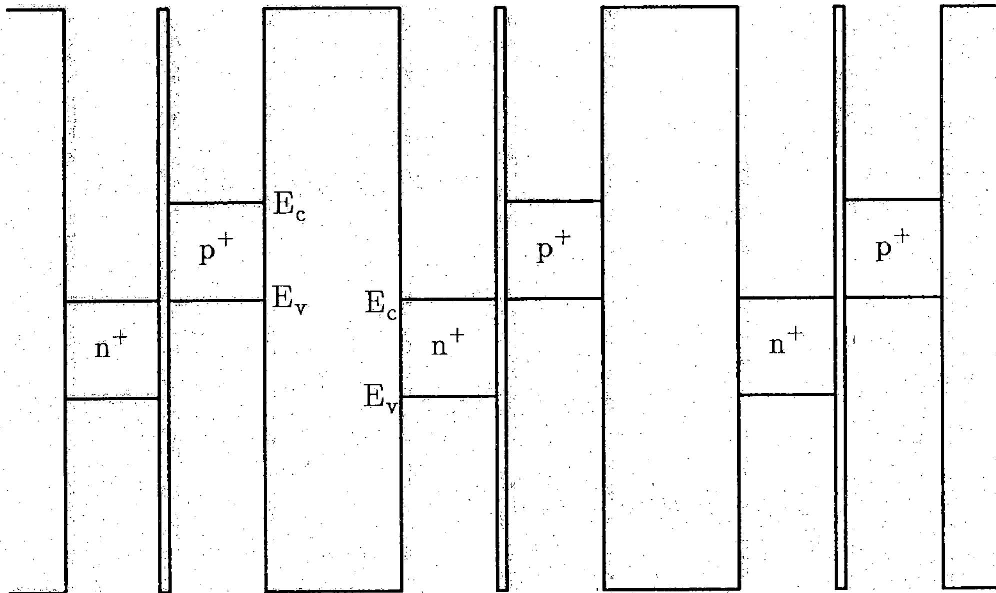

Figure A-3.2 A stack of SIS diodes

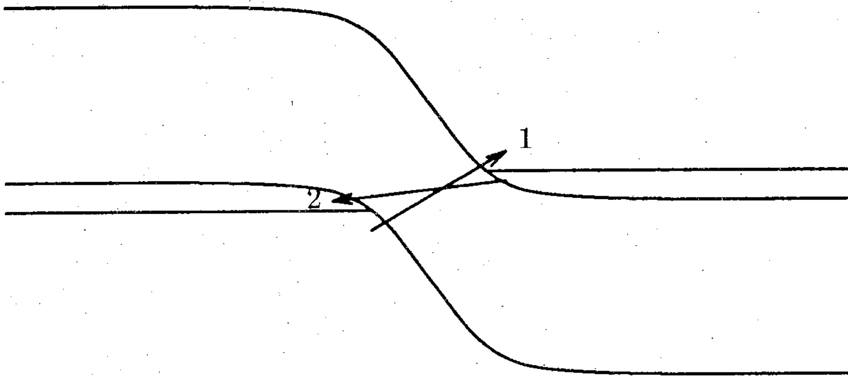

Figure A-3.3 The tunnel(Esaki) diode

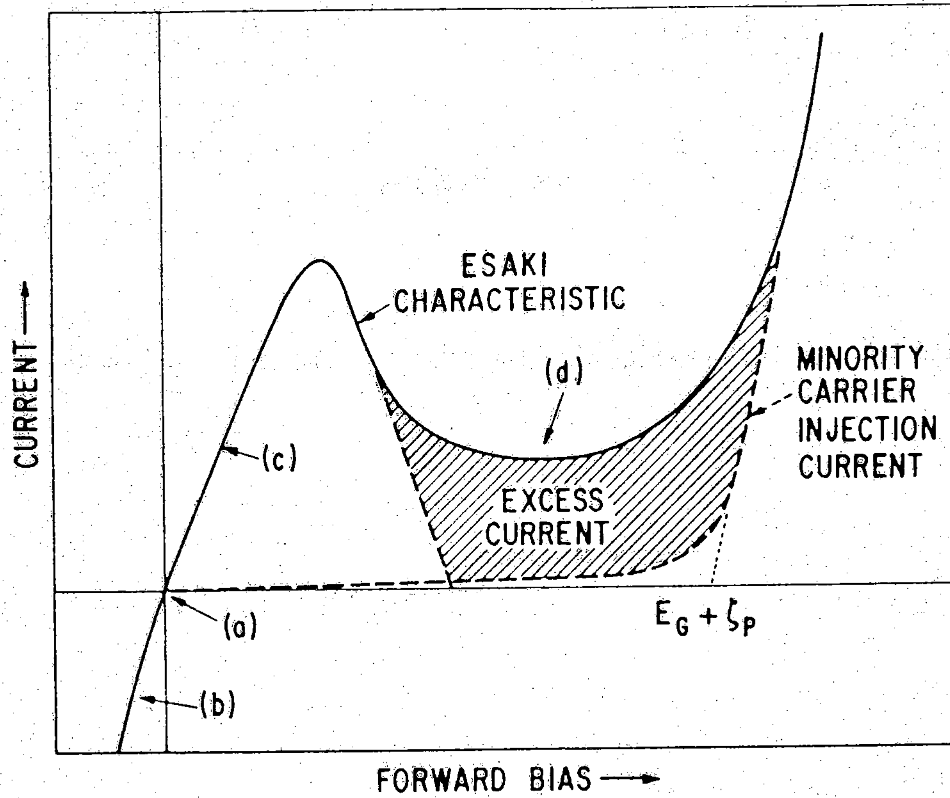

Figure A-3.4 The IV curve of a tunnel(Esaki) diode(From Duke[13])

This reveals a problem with all these devices. How does one get a high absorption coefficient and still avoid the reverse current flow?

The corresponding stacked device of the pn junction is the nipi superlattice[16,17]. The absorption processes of the nipi superlattice are shown in Fig. A-3.5. Doehler et al.[17] have calculated the absorption below the band gap. The problem is that the effective gap range(See sec. A-3.1) is too small(less than .1 eV[17], so one would need 20 different semiconductors to cover a 2 eV range) because the doping is not high enough[17]. In the future, it may be possible to make a larger effective gap range, but even so, the type II superlattice appears to provide better absorption junctions.

A-3.4 Heterojunction - type I Superlattice

The heterojunction is defined as a junction between two different materials. In this section, these materials are two different semiconductors. To examine the absorption processes, consider the type I superlattice[16], which is shown in Fig. A-3.6. This superlattice has not been considered in detail, but is presented to show some of the problems involved. This superlattice is not feasible because the spatially direct absorption of transition 1(from one quantum level to another) is much more likely than the spatially indirect absorption of tunneling transition 2. For spatially direct absorption, it would be better just to use a conventional tandem cell system.

A-3.5 Heterojunction - type II Superlattice

As in the previous section, the absorption junction is a heterojunction. Consider the corresponding stacked device - the type II superlattice[16]. The absorption processes for the type II superlattice are shown in Fig. A-3.7. This structure has the highest spatially indirect absorption coefficient of the four absorption junctions considered[18,19].

The problems with this configuration are that it requires: 1) materials which cover the complete effective gap range(This is a very serious limitation) and 2) a high quality epitaxial growth, thick enough to collect the light(These may be incompatible requirements).

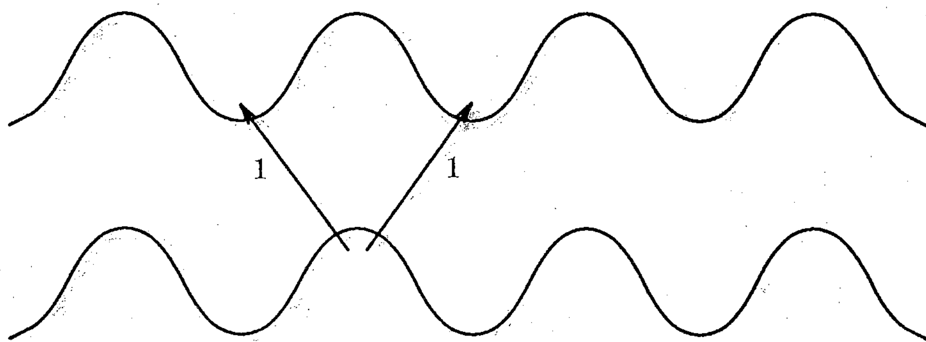

Figure A-3.5 The nipi superlattice

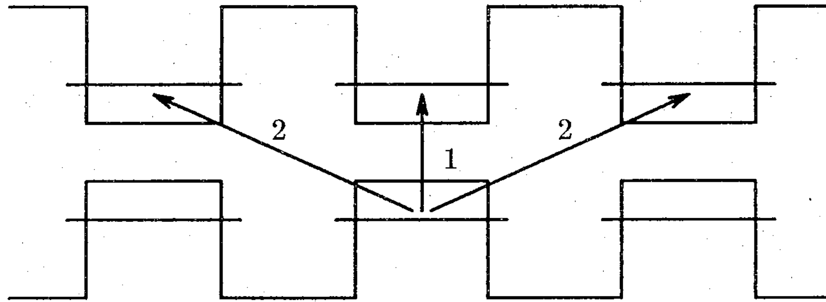

Figure A-3.6 The type I superlattice

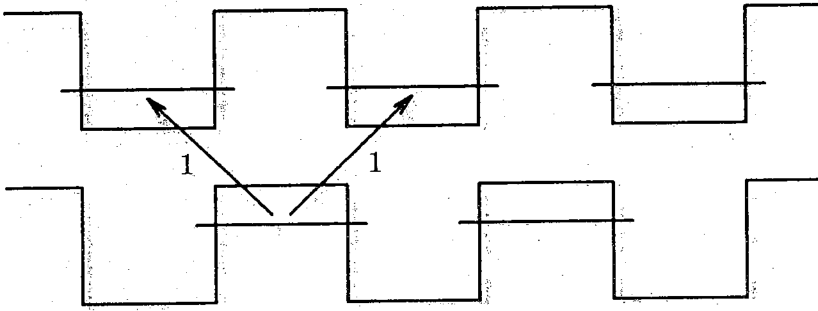

Figure A-3.7 The type II superlattice

A-3.6 Comparison of the various absorption junctions

This section will show that the type II superlattice is the best alternative and the nipi superlattice is the second best.

Keeping in mind that absorption is related to the overlap of the wavefunctions(See sec. A-3.1), it is easy to see that absorption in the device of Fig. A-3.8b is greater than absorption in the device of Fig. A-3.8a. If the band gaps outside the region where the band slopes(hereafter labeled the depletion region) are increased to the band gap in the depletion region, then the result is the band diagram in Fig. A-3.8c. Assuming the depletion region is wide enough, then the absorption will be about equal for the devices of Fig. A-3.8b and A-3.8c. Again assuming the depletion region in Fig. A-3.8c is wide enough, then the absorption for the diagram in Fig. A-3.8d should be greater than the absorption for the diagram in Fig. A-3.8c.

The main point of this discussion is that the SIS diode will not be useful. If one compares the results of Doehler et al.[17] and Chang et al.[19], it is easy to see at this time that the type II superlattice has much greater absorption than the nipi superlattice.

A-3.7 Conclusion

The type II superlattice has the highest spatially indirect absorption and the nipi superlattice has the second highest spatially indirect absorption. These spatially indirect absorption coefficients are still smaller than the spatially direct absorption coefficients[17,19] in a conventional solar cell or a conventional tandem cell system.

For either the nipi or the type II superlattice, there are five problems. 1) The free carrier absorption problems described in chap. A-2 could also be a problem in the heavily doped layers of the absorption junctions. 2) As discussed at the end of sec. A-3.1, coupling problems will exist in solar cells incorporating spatially indirect absorption. 3) Like the tunnel(Esaki) diode, there will most likely be carrier back flow problems at the absorption junction. 4) It will be difficult to find a set of materials that will cover a complete effective gap range of 2 eV(See sec. A-3.1). 5) Assuming that there are four effective gap ranges(which is an optimistic number) that make up the complete effective gap range(See sec. A-3.1), then these four waveguide configurations must be stacked end on end. The loss problems in a conventional tandem cell system would be much easier to overcome than the loss problems of four adjacent waveguides.

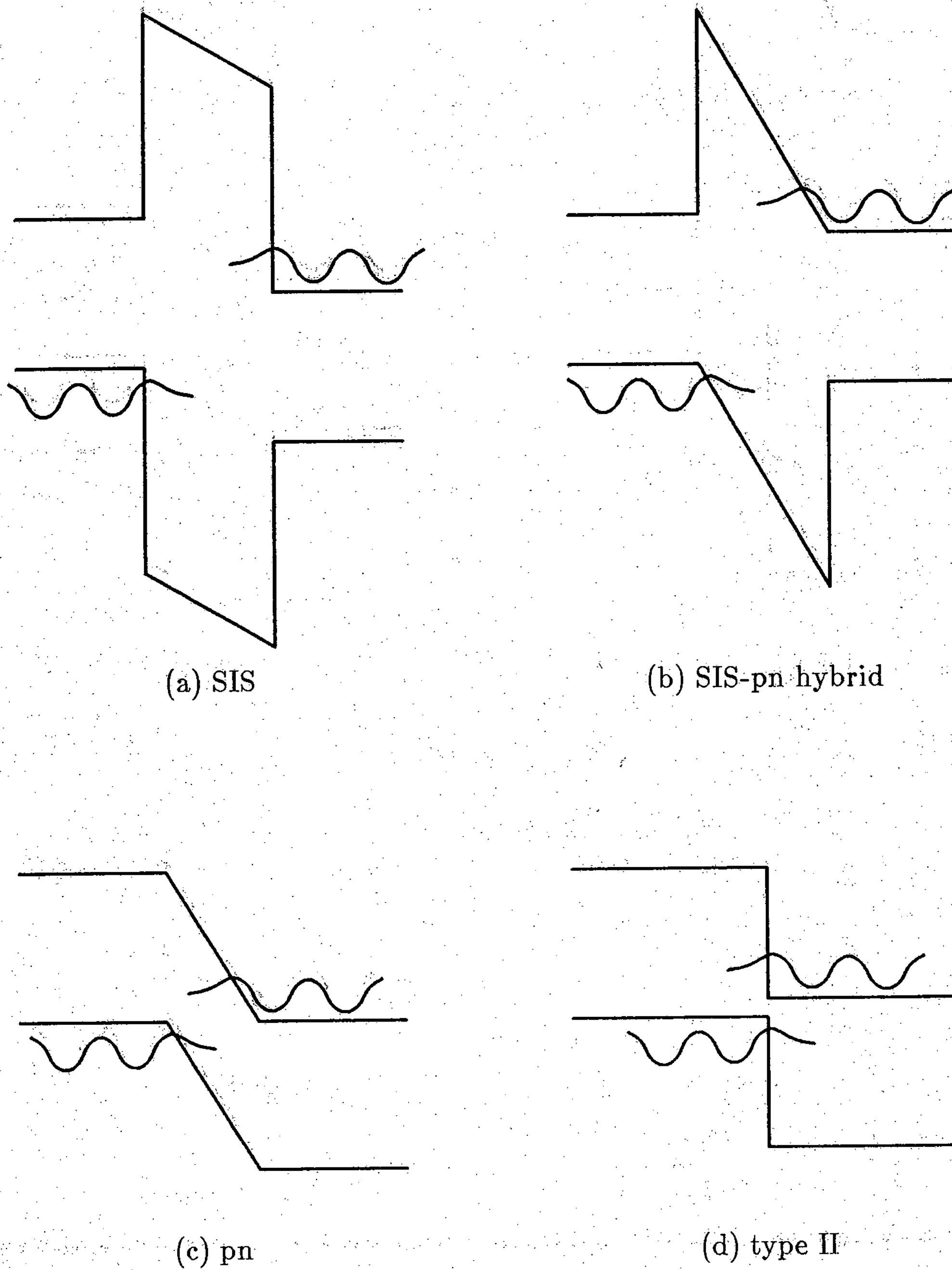

Figure A-3.8 Comparison of the absorption junctions

A-4 CONCLUSIONS

There are many problems associated with the solar cells investigated in this report. Contact, coupling, collection, growth and materials are the major problem areas. There is one major limitation though, that outweighs all of these problems.

This limitation is that structural losses and other losses severely degrade the overall efficiency of a multiple cell device[2](See sec. A-1.2). This same problem exists in both the conventional multiple cell systems(See sec. A-1.2) and the solar cell studied in this report.

In conclusion, conventional multiple cell concepts(See sec. A-1.2) appear to be superior to the proposed solar cell because: 1) the structural losses of the conventional multiple cell concepts can be minimized more quickly and easily in the short run, 2) the structural losses of the conventional multiple cell concepts can most likely be made smaller in the long run, and 3) the collection efficiency of conventional multiple cell concepts(percentage of photon generated carriers collected[2]) should exceed that of the proposed solar cell. While these three points are not necessarily hard and fast for all possible multiple cell systems, the structural loss problem(See sec. A-1.2) combined with a non-ideal collection efficiency loom as very large obstacles in making any multiple cell system.

PART B

PHOTOCONDUCTOR ANALYSIS

B-1. OPERATION OF THE PHOTOCONDUCTOR

B-1.1 Introduction

Three types of photodetectors are predominant today - pin photodiodes, avalanche photodiodes(APDs) and photoconductors(PCs)[20,21,22]. For wavelengths longer than 7 μm, though, conventional photodetectors degrade in performance because of serious device materials problems(See sec. B-1.2). The superlattice intraband-absorption photoconductor(SLIP), described in sec. B-1.3, is proposed as one alternative for the detection of wavelengths greater than 7 μm.

Section B-1.2 describes the problems with conventional detectors at long wavelengths. Section B-1.3 describes how the SLIP operates. Section B-1.4 presents the important physical relationships for the SLIP. Section B-1.5 presents the advantages and disadvantages of the SLIP over conventional photodetectors.

B-1.2 Problems encountered by conventional photodetectors at long wavelengths

The pin photodiode, the APD and the intrinsic photoconductor operate through band to band absorption. When a photon is absorbed, an electron is excited to the conduction band, leaving a hole in the valence band. Two carriers(an electron and a hole) participate in this process. In the extrinsic photoconductor, on the other hand, the radiation excites the electron in an n-type PC(or hole in a p-type PC) from a donor(acceptor) site into the conduction(valence) band. Assuming there is no impurity hopping, this is a one carrier process.

The major problem for two carrier photodetectors at long wavelengths is finding a suitable material with a small band gap. For two carrier detectors, the band gap must be small enough for a long wavelength photon to cause a band to band transition. For wavelengths longer than 7 μm, there are only three materials that are seriously considered for two carrier photodetectors - $Hg_{1-x}Cd_xTe$, $Pb_{1-x}Sn_xSe$, and $Pb_{1-x}Sn_xTe$[21,23]. The lead salts, $Pb_{1-x}Sn_xSe$ and $Pb_{1-x}Sn_xTe$, have serious high frequency limits[21,23] and are only considered because $Hg_{1-x}Cd_xTe$ is an unstable material[21,23].

Because of these serious material problems, the extrinsic photoconductor is the device most commonly used at wavelengths "beyond a few microns"[24] or at this time, approximately 15 μm([25,26,27] - The exact value of this wavelength depends on the geometry of the device, whether the device is used by itself or in an array, and what is acceptable as a yield[25,26]). The one carrier characteristic of the extrinsic photoconductor means that the troublesome narrow gap semiconductor of the two

carrier detector is replaced with a wider gap semiconductor with more desirable material parameters. Unfortunately, several unavoidable disadvantages exist in conventional extrinsic photoconductors(See sec. B-2.2).

The SLIP, described in the next section, and the graded well SLIP and the other novel one carrier devices in sec. B-2.2 are alternative photoconductors that attempt to avoid the narrow band gap problems of two carrier photodetectors and the inherent problems of the extrinsic photoconductor.

B-1.3 Description of the superlattice intraband-absorption photoconductor(SLIP)

The SLIP has the capability of detecting wavelengths from 7 μm(1400 cm^{-1}) to longer than 100 μm(100 cm^{-1}). The 7 μm limit is determined by the fact that stable intrinsic photoconductors can be fabricated to detect wavelengths shorter than 7 μm. The long wavelength limit is determined by the quality of the growth of the material. The SLIP incorporates a superlattice made up of quantum wells and barriers(See Fig. B-1.1 and Fig. B-1.2). The wells contain a large density of free carriers(either through doping in the well or by modulation doping) and the barriers have a minimal density of free carriers. Consequently, the applied electric field will be much larger in the barriers than in the quantum wells. The absorption process is due to the free carriers in the well(intraband-absorption or free carrier absorption). Hence the term SLIP.

The SLIP in Fig. B-1.1 may have a large tunnel current from the well to the conduction band of the barrier because of the triangle shaped barrier(See sec. B-5.5). The band diagram in Fig. B-1.2 takes this tunneling problem into account(See sec. B-5.5 for a detailed description of this barrier). The shape of the valence band is not important in this device because the band gap is greater than the energy of the infrared light and the device is operated at low temperatures. This report describes the situation with n-type wells as shown in Figs. B-1.1 and B-1.2, but an analogous argument could be used for p-type wells with similar results.

In operation, the detector is biased(See Fig. B-1.2b). The radiation can propagate perpendicular to the layers(See sec. B-4.2), parallel to the layers(See sec. B-4.4), or a combination of both these cases(See sec. B-4.3). For any direction of propagation, the photon enters the detector and excites an electron in the well through free carrier absorption(See Fig. B-1.3. $E_{\lambda z}$ is the energy the excited electron has gained in the direction perpendicular to the layers(considered the z-direction). Assuming the scattering is elastic, the total energy gained is E_{λ}, the photon energy, which equals the sum of the excited energies in all three directions). After n collisions(where n can be 0) with phonons, impurities or other carriers, the excited

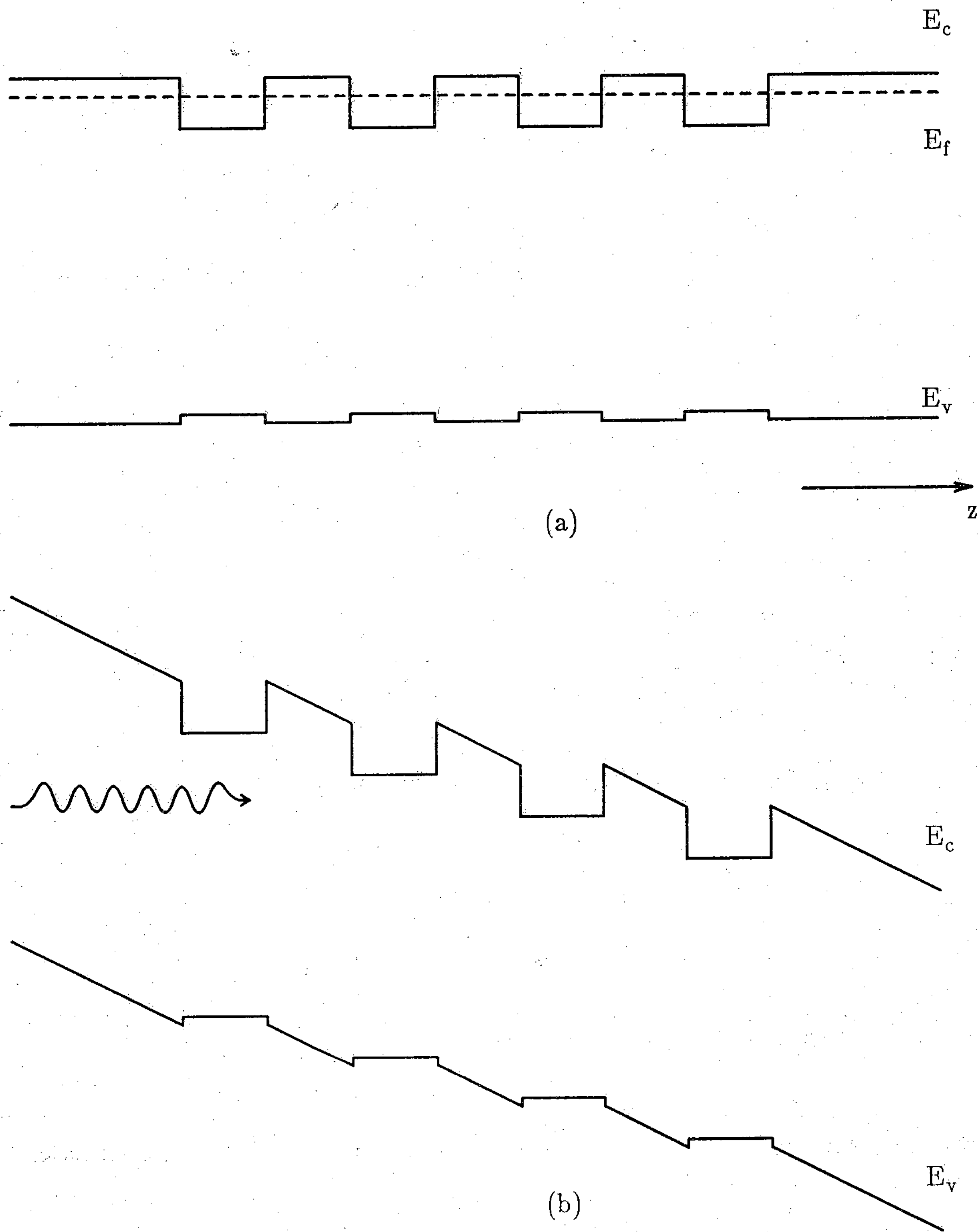

Figure B-1.1 The proposed photoconductor. (a) Unbiased. (b) Biased.

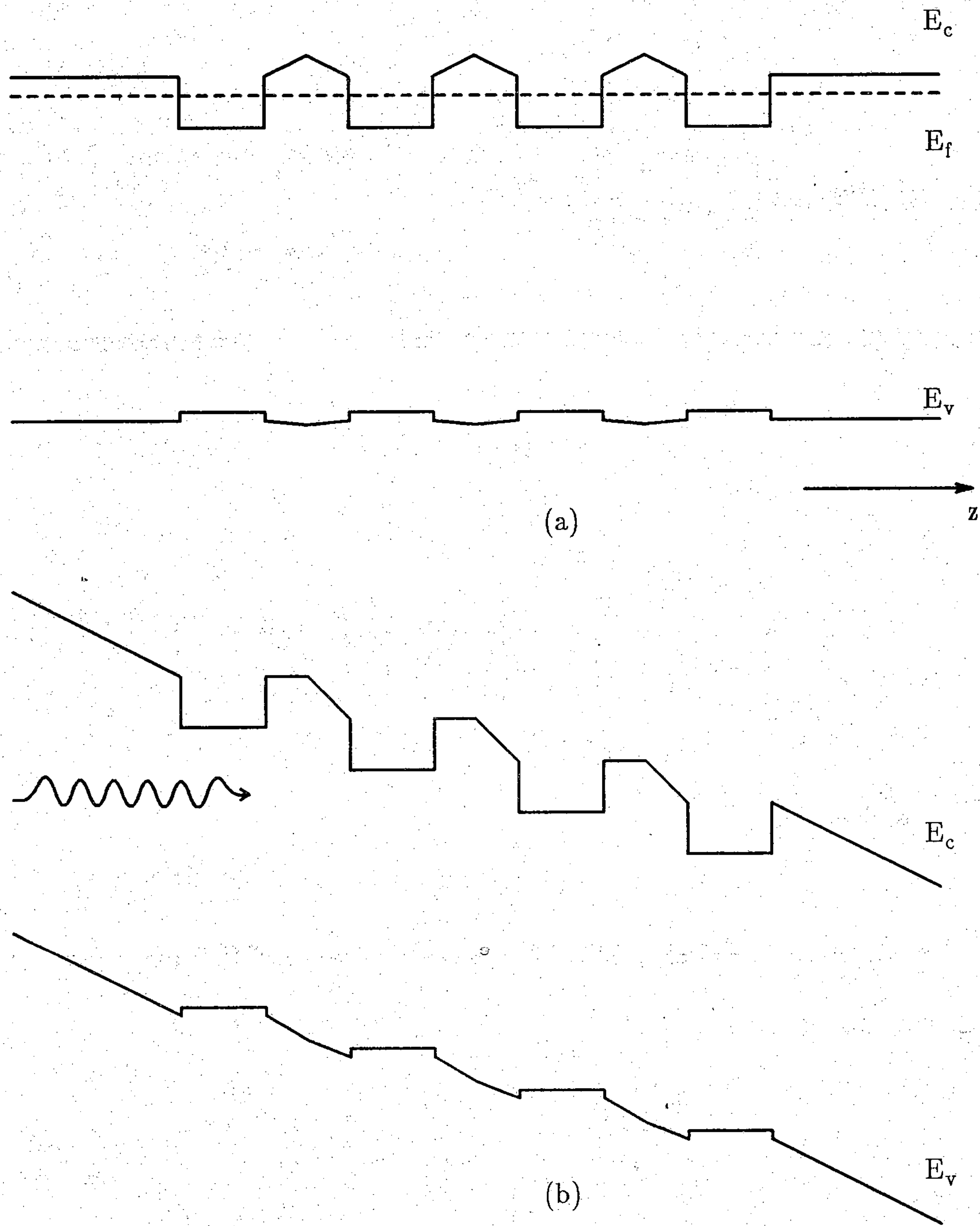

Figure B-1.2 The proposed photoconductor which prevents tunneling. (a) Unbiased. (b) Biased.

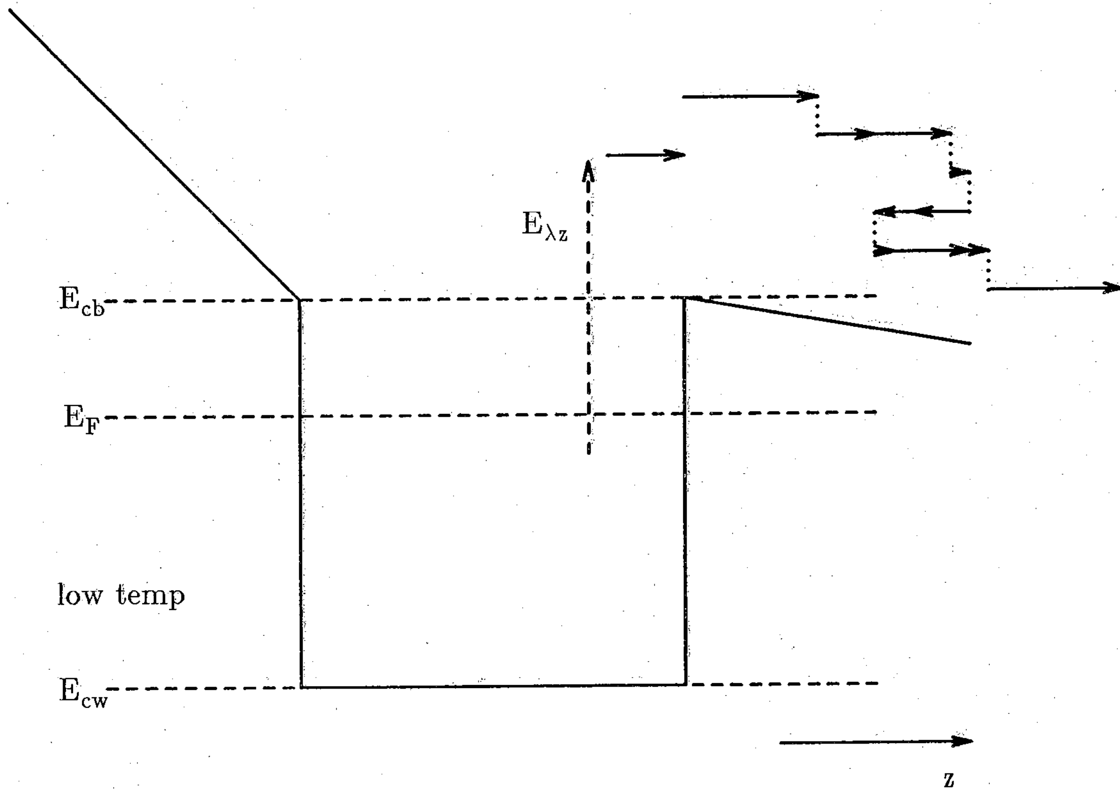

Figure B-1.3 Trajectory of an electron excited by a photon with energy E_λ

electron will either obtain enough energy in the z-direction to escape out of the well or fall back into the well. The quantum efficiency[22] is defined as the percentage of excited electrons that escape out of the well(See sec. B-6.1). Once the electron has escaped from the well, it traverses the device until it falls into another well or reaches the contact(the anode). For each electron that reaches the anode(of a photoconductor with Ohmic contacts), an electron is injected through the other contact(the cathode). The gain is related to the number of times the electron passes through the device until it falls into a well[22].

The design of the SLIP is simple and it appears that an AlGaAs superlattice with p-type GaAs wells will be a feasible material. The GaAs p-type density of states is about as small as one can get and still get a reasonable efficiency. A more desirable material would be a large density of states material, either p-type or n-type.

The detector operates like an extrinsic photoconductor, where the analog of the donor levels is the total free carrier energy levels less than the barrier energy level(The carrier cannot escape out of the well without excitation) and the analog of the conduction band is the total free carrier energy levels above the barrier energy level.

B-1.4 Important physical relationships for the SLIP

There are four important physical relationships that must be considered in the SLIP. First, the free carrier absorption coefficient must be large enough for the SLIP to work. Second, $E_{cb}-E_F$(See Fig. B-1.3) determines the temperature of operation and partly determines the efficiency of the device. Third, E_F-E_{cw}(See Fig. B-1.3) partly determines the efficiency of the device. Fourth, impact ionization appears to be an obstacle to the operation of the SLIP.

B-1.4.1 Free carrier absorption

For free carrier absorption, the electron is excited in the same direction as the polarization direction of the radiation[28], which is perpendicular to the direction of radiation propagation[14].

The free carrier absorption coefficient in the SLIP should approximately equal or exceed $10^4 cm^{-1}$. For an absorption coefficient of $10^4 cm^{-1}$, most of the radiation can be absorbed in a micron thick device. In the SLIP, this means that the sum of all the well widths must equal one micron. For a well width of 200 Å, this means the device must contain 50 wells.

There are few experimental measurements of free carrier absorption at high concentrations and long wavelengths for p-type GaAs. In this situation, theoretically, the absorption coefficient should exceed $10^4 cm^{-1}$ but some experimental results indicate absorption coefficients less than $10^4 cm^{-1}$(See sec. B-3.1). There is a difference of opinion as to whether these experimental absorption coefficients were measured accurately(See sec. B-3.1). This discrepancy in the results is important, because the SLIP will work much better for the high theoretical coefficients than for the lower reported coefficients.

B-1.4.2 E_{cb}—E_F

There are two different limits on E_{cb}—E_F(See Fig. B-1.3). One involves the open well case(See secs. B-6.2 and B-6.3) shown in Fig. B-1.4 and the other involves the partly closed well case(See secs. B-6.2 and B-6.4) shown in Fig. B-1.5. For the open well case, E_{cb}—E_F is greater than the optical and intervalley phonon energies(See sec. B-6.2). For the partly closed well case, E_{cb}—E_F is less than the optical and intervalley phonon energies(See sec. B-6.2).

Section B-1.4.2.1 describes the open well case. Section B-1.4.2.2 describes the partly closed well case. Section B-1.4.2.3 shows how the temperature of operation and the quantum efficiency are related to these cases. Section B-1.4.2.4 presents what others have done with respect to these cases.

B-1.4.2.1 Open well case

In the open well case(See secs. B-6.2 and B-6.3), the electron can easily drop back into the well. Hence, it is very important to excite the electron out of the well before a collision of any kind occurs. Consequently, the electron must be excited in the direction perpendicular to the layers. In turn, the direction the radiation is polarized is very important.

Figure B-1.4 shows the two modes of radiation propagation that are possible in the open well case. For the oblique incidence case, only the radiation polarized in the plane of incidence(See secs. B-4.1 and B-4.3) can be detected. For the parallel incidence case(See secs. B-4.1 and B-4.4), the detector acts as a waveguide and only the TM and TEM modes can be detected(See sec. B-4.4).

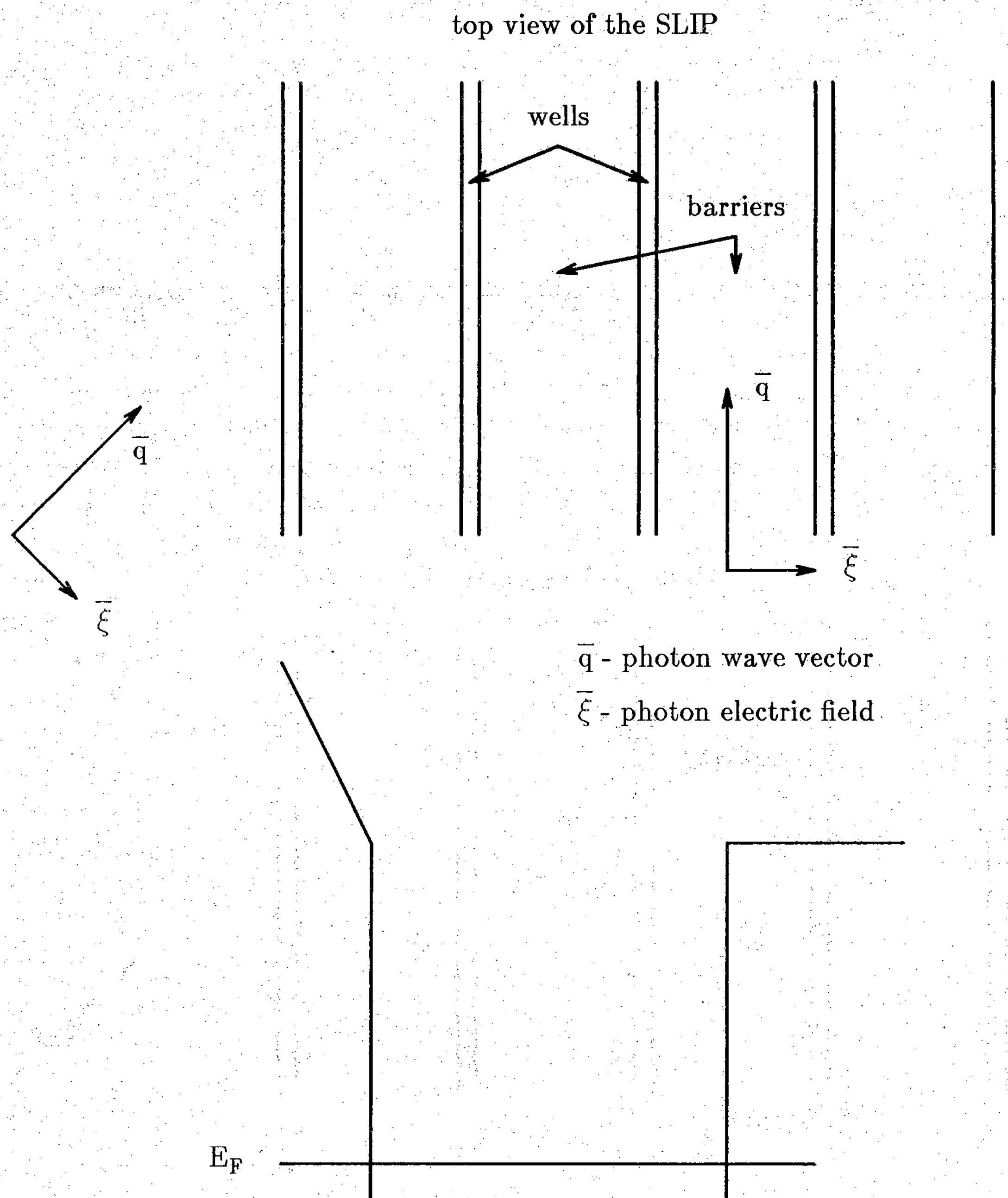

Figure B-1.4 The two modes in the open well case

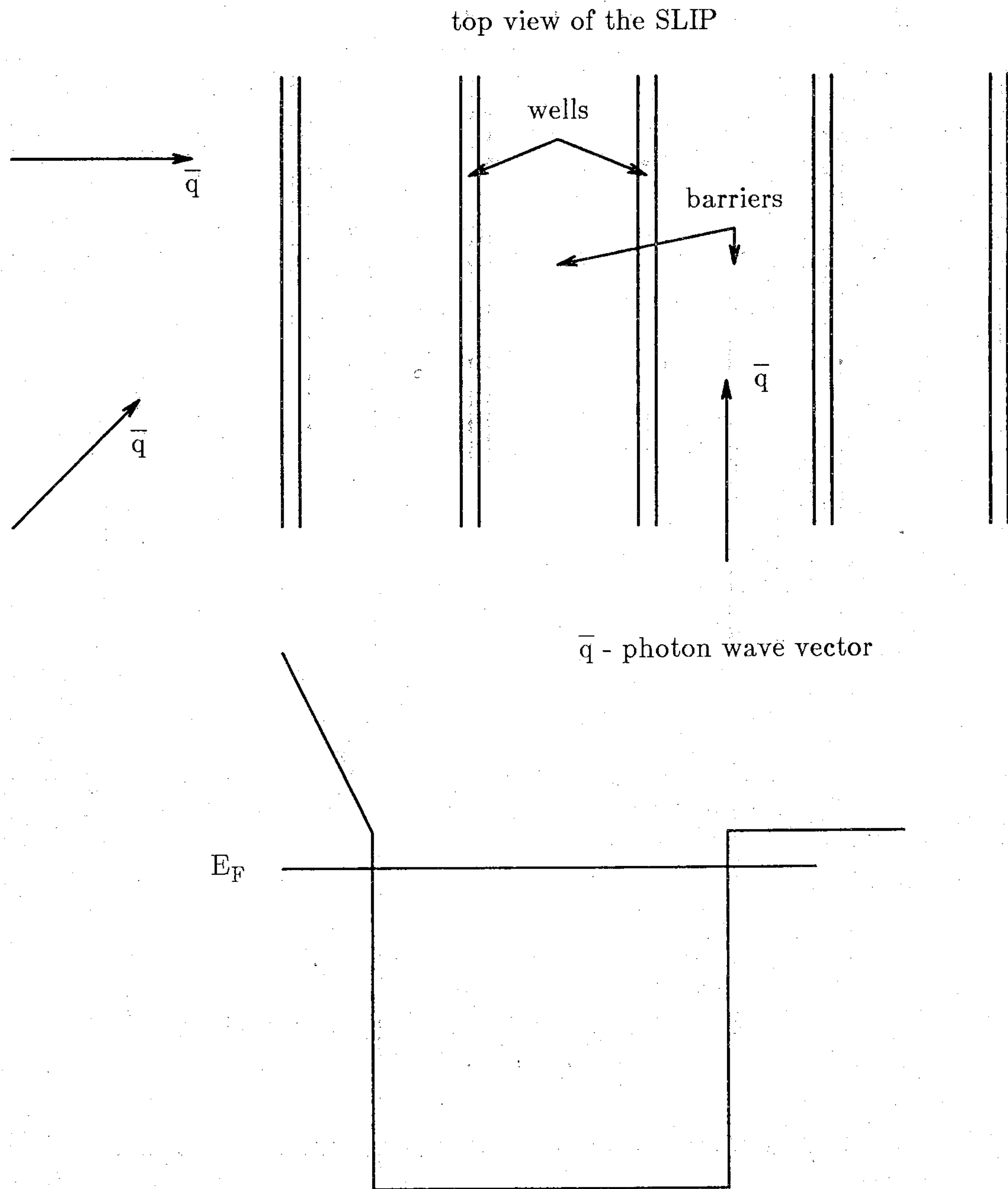

Figure B-1.5 The three modes in the partly closed well case

B-1.4.2.2 Partly closed well case

In the partly closed well case(See secs. B-6.2 and B-6.4), since most of the states in the well are occupied, the electron will not fall back into the well easily. Consequently, collisions can occur and the directions of polarization and radiation propagation are not important.

Three modes are possible in Fig. B-1.5. There can either be perpendicular incidence, oblique incidence, or parallel incidence of the radiation(See sec. B-4.1). The electric field vector of the incident radiation waves in Fig. B-1.5 is not shown because the polarization is not important in the partly closed well case.

For the partly closed well case to be physically realizable, there is one important physical requirement. The time the electron must stay above the well is about 10 psec.(See sec. B-9.3). This is much longer than the energy relaxation time, but if $E_{cb}-E_F$ is less than any of the intervalley or optical phonon energies, this might be physically realizable(See sec. B-6.2 and [29]).

The bulk of this report deals with the partly closed well-perpendicular incidence mode.

B-1.4.2.3 Temperature and quantum efficiency

Due to the relationship between $E_{cb}-E_F$ and the thermionic emission current(See sec. B-5.4), the operating temperature will be around 10 K for the partly closed well case(See sec. B-8.5) but should be higher for the open well case(See sec. B-8.5).

The quantum efficiency can approach 100 percent for the partly closed well case with any direction of radiation incidence, depending upon the wavelength detected(See sec. B-9.3). The quantum efficiency of the open well case should be lower, but in theory could be large if there are few collisions before the electron escapes from the well and the radiation is polarized in the proper direction.

B-1.4.2.4 What others have done

The open well-parallel incidence mode for the SLIP has already been considered but the experimental data has not been promising(See sec. B-2.2.1 and [30]). The authors[30] state that the electrons are excited out of the well. There are two important design parameters that are not mentioned in [30] that make it questionable as to whether the electrons are excited out of the well. First, the value of $E_{cb}-E_F$ is not given. Second, the fact that the very low density of states in the n-type GaAs wells may be a serious problem is not mentioned(See sec. B-1.4.3). These

parameters must be considered for the SLIP to work.

The open well-perpendicular incidence mode(This is the "missing" mode in Fig. B-1.4) has been discussed[31]. Absorption(not photoconductivity) was calculated. For parallel incidence of radiation, the author[31] is more interested in intersubband absorption(See sec. B-2.2.2) than free carrier absorption. This intersubband absorption is the absorption process in the remaining superlattice photoconductors which have been proposed(See sec. B-2.2).

B-1.4.3 $E_F - E_{cw}$

The boundary conditions(See sec. B-6.3) determine that the energy in the direction perpendicular to the layers must exceed the barrier energy level(Assuming the effective masses in the wells and the barriers are the same). Consequently, the barrier height, $\Delta E_c = E_{cb} - E_{cw}$(See Fig. B-1.3), should be as small as possible. This will make it easier for the electron to surmount the barrier(See secs. B-6.3 and B-8.7).

The barrier height can be lowered by decreasing $E_F - E_{cw}$. This can be done by using a material with a higher density of states in the well. This is a major limitation when using n-type GaAs, which has an extremely small density of states. p-type GaAs has a larger density of states.

B-1.4.4 Impact ionization

Impact ionization in an n-type extrinsic photoconductor is caused by electrons in the conduction band(excited by the electric field) that gain enough energy to excite electrons at the donor energy level. These donor electrons are excited to the conduction band by collisions. For extrinsic infrared photoconductors, the electric field which will cause this can be as small as 100 V/cm, depending upon the dopant, the dopant concentration and the semiconductor[32].

This impact ionization problem will most likely also exist in the SLIP. Consequently, it is possible that the SLIP might have to operate at low electric fields especially if one considers a photoconductor with Ohmic contacts(See the next paragraph). If this is the case, this device would be most promising as a high speed detector because the gain would be less than one. This low field requirement could be a serious limitation.

Although impact ionization cannot be tolerated in photoconductors with Ohmic contacts, it can possibly be advantageous in photoconductors with blocking contacts[33]. One possible mode of operation would involve placing the SLIP in an array with CCDs or CIDs[21,34,35]. Then if the temperature is low enough, the

impact ionization might be advantageous. For instance, in a very similar photoconductor(See sec. B-2.2.3), impact ionization is presented as an advantage. For either of these photoconductors, the temperature must be much lower than conventional intrinsic photoconductors.

In this report, it will be assumed that impact ionization is negligible. If one wants to take advantage of impact ionization(as in the previous paragraph), then the gain described in chapters B-5 and B-7 must be adjusted accordingly.

B-1.5 Advantages and disadvantages of the SLIP

The SLIP should have several advantages over conventional infrared photodetectors. 1) The device has a simple design and uses materials with desirable, well known material properties. 2) The absorption coefficient could be as high as $10^4 cm^{-1}$ in the SLIP. 3) D^*_{BLIP} of the SLIP is approximately the same as D^*_{BLIP} of the conventional photoconductor in the wavelength range between 15 and 25 microns and is better for wavelengths longer than 25 microns(See sec. B-7.5). 4) SLIPs can be built to detect any wavelength from 7 μm to more than 100 μm(See sec. B-8.4). 5) Absorption due to phonons can filter out some of the background noise(See sec. B-7.4). 6) The response time in the SLIP should be as fast as an extrinsic photoconductor. 7) Impact ionization could be an asset in an array and there is even a possibility the excess noise may be as small as in a photomultiplier(See sec. B-2.3).

There are several disadvantages for the SLIP. 1) The electron can easily fall back into the well. Hence the gain will most likely be small(unless a high enough electric field is applied, which will probably cause impact ionization) and the temperature of operation will be lower than intrinsic photoconductors and about the same as extrinsic photoconductors(See [36] and sec. B-8.5). 2) D^*_{BLIP} of the SLIP is smaller than D^*_{BLIP} of the conventional photoconductor in the wavelength range between 7 and 15 microns(See sec. B-7.5). 3) The device is a photoconductor, which is more noisy than a photodiode. This is not a serious problem because the narrow gap materials needed for photodiodes have serious limitations(See sec. B-1.2). 4) The low field limit set by impact ionization could be a problem. If used in an array, this impact ionization might be advantageous, but the array would have to be operated at a low temperature(See sec. B-1.4.4). 5) The SLIP will be difficult to fabricate. For the partly closed well case, the error in barrier height may have to be less than 1/2 of the inelastic phonon energy(See sec. B-6.2). If one considers the barrier shape in Fig. B-1.2, it may be possible to overcome this problem because one has half of the barrier where one can get the proper barrier height(See Fig. B-1.2b). For instance, if the error in growth is 5 meV in the conduction band, then the device can be grown such that on average, the conduction band is 5 meV below the desired thermionic

emission barrier height. Then there will most likely be someplace in the barrier which matches the proper barrier height. In any case, the SLIP should be easier to fabricate than any of the photoconductors using intersubband absorption(See sec. B-2.2) designed to detect the same wavelength. 6) Carriers can be rearranged in the wells such that space charge forms. This space charge formation degrades the performance of the device. There are two ways to minimize this problem. First, the barrier shape in Fig. B-1.2 aids in minimizing the space charge formation(See sec. B-5.5). Second, a CCD or CID array[21,34,35] should minimize this because the applied voltage across the detector element varies and the space charge can be neutralized by the adjacent detector elements(for instance, the elements in a CCD array). 7) Phonon absorption could be larger than free carrier absorption. This would only be true for certain wavelengths and can be avoided by using a different partial fraction of Al in the epitaxial layers.

B-2. SURVEY OF THE COMPETING PHOTODETECTORS

B-2.1 Three alternatives for photodetection

This chapter surveys the literature on proposed devices designed to compete with conventional photodetectors. These novel devices are not described in depth. Only the basic physical processes are described. The pertinent experimental results are listed(if there are any) and possible problems and advantages are presented. A set of references accompanies each section.

The pin photodiode has the best combination of low noise and a large bandwidth[20]. Due to these inherent advantages and its simple design, the pin photodiode is the most common of the three[20]. At long wavelengths though, the pin photodiode has some serious limits because of the narrow gap materials problems.

There have been several novel one carrier photoconductors that, like the SLIP, attempt to replace the conventional photoconductors. These novel photoconductors are presented in sec. B-2.2.

Most publications have been on novel devices to replace the APD. This is due to the avalanching and the associated problems of excess noise. The small band gap requirement for long wavelengths limits these new devices to wavelengths less than 7 microns unless there is an improvement in HgCdTe fabrication. The important problems, considerations and alternative devices are presented in sec. B-2.3.

Section B-2.4 lists the novel devices which are most promising.

B-2.2 Conventional and novel photoconductors

The intrinsic photoconductor(See Fig. B-2.1) has a number of advantages over the extrinsic(See Fig. B-2.2) photoconductor[21,22]. The primary advantage is that the absorption coefficient for the intrinsic photoconductor is greater than 10^4 cm^{-1} while for the extrinsic photoconductor, it is approximately 10^2 cm^{-1}[21]. Other related advantages are: 1) It can be operated at a higher temperature[36,21,22] and 2) it has a higher quantum efficiency[22]. However, the intrinsic photoconductor has one major limitation at long wavelengths. It is difficult to build one with a narrow band gap.

The SLIP and the novel photoconductors presented below are in essence extrinsic photoconductors(except the two carrier effective mass filter PC). The main advantage of the proposed devices is the same as the extrinsic photoconductor - they avoid the need for band to band absorption. The main advantage of these devices over the extrinsic photoconductor is absorption. The absorption coefficients in these

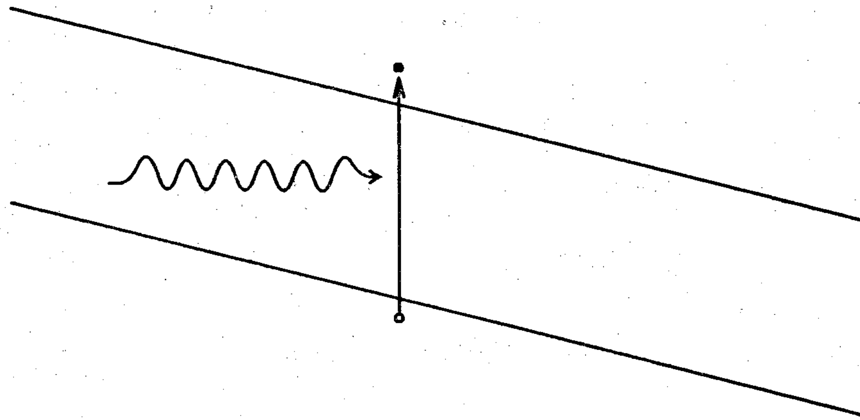

Figure B-2.1 Intrinsic photoconductor

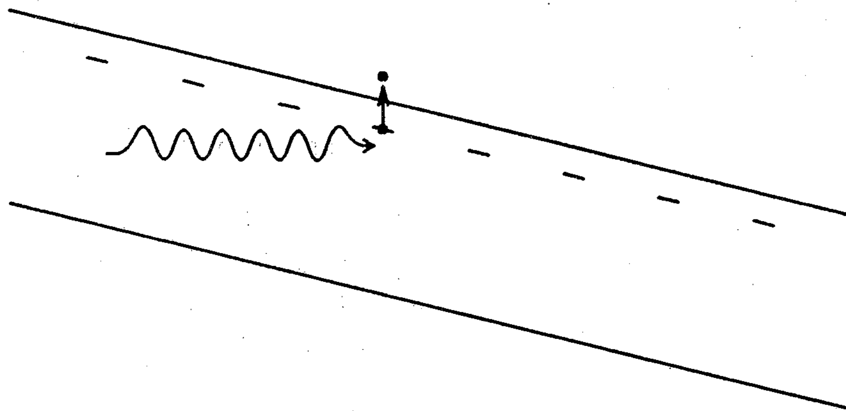

Figure B-2.2 Extrinsic photoconductor

devices have been proposed to be from 10^4 cm^{-1} to 10^6 cm^{-1}. Hence, they could have the absorption advantage of the intrinsic photoconductor and the one carrier advantage of the extrinsic photoconductor.

The eight proposed photoconductors are briefly described in secs. B-2.2.1 to B-2.2.8. The noise in all these devices is the same as in a conventional photoconductor.

B-2.2.1 Graded well SLIP[29-31,37-39]

This device was first proposed and experimentally verified in 1983[30,37]. It is operated in the same manner as the SLIP. Important differences are: 1) The authors[30,37] don't consider the importance of the Fermi level position with respect to the barrier height energy level. 2) They consider it imperative that the well have a built-in electric field(See Fig. B-2.3). 3) The barriers and the wells are doped. Also, since E_F is much lower than E_{cb}, tunneling is not considered much of a problem.

The experimental results[30,37] are not very promising. The response time is 1 sec.. The blackbody source used in these experiments was at 2700 C, which is very large. The radiation from this source between 1 and 10 μm would produce a radiation current density of 14.8 A/cm^2 assuming a quantum efficiency of 1. The actual radiation current density at 1.3 V in [37] is .0222 A/cm^2. For the dark current to be this small at 77 K, the Fermi level would have to be at least .1 eV below E_{cb}. If one assumes a gain of 10,000[30] and compares the current densities, the efficiency is 1.5 x 10^{-5}%. For the experiment, the direction of propagation of radiation was parallel to the layers and the barrier was made up of $Al_{.3}Ga_{.7}As$.

The authors assumed that the electrons were excited out of the well, but considering the long response time and the position of the Fermi level, the electrons might have been excited out of the deep dopant levels in the barrier layers[40] and subsequently trapped in the wells.

B-2.2.2 Intersubband photoconductor(IS-PC)

B-2.2.2.1 Intersubband absorption[29,31,38,41-45]

Intersubband absorption occurs without involving a phonon. It is a direct transition between two energy levels. These energy levels are formed in the direction perpendicular to the superlattice and are analogous to the energy levels in a potential well. One requirement for this type of transition is that the radiation must be polarized in the same direction as these energy levels.

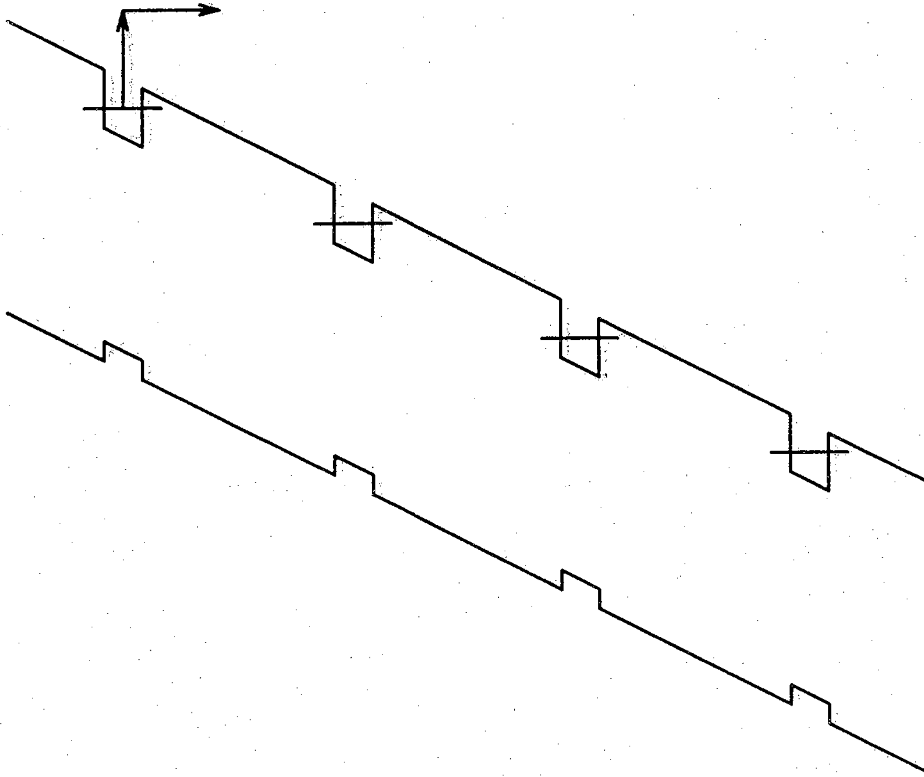

Figure B-2.3   Graded well SLIP

In a 1D potential well along the z-direction, the electron can only exist at certain energies in the z-direction. The same is true for a superlattice or any variation of the quantum well. Ideally, these energy levels are discrete and only exist at a specific value of energy. Due to interactions with other particles though, these levels broaden. In turn, the density of states decreases as the width of the energy level increases.

A photon is absorbed by exciting an electron from an initial energy level to a final energy level. The absorption coefficient is related to the density of states in these levels. For all the variations of the IS-PC presented below, their proponents argue that there is little broadening of the energy levels, which produces a large density of states, which causes a large absorption.

Consider a superlattice with a large thickness, at flat band condition(The static electric field perpendicular to the layers equals zero). In the well, the line broadens due to interaction with carriers[41] and the fact that it can tunnel to other wells[46]. Hence as the final energy level increases, the interaction between the wells increases and the width of the levels increases[44,46]. The absorption decreases as the energy in the well is increased (See Fig. 3 in [44]).

For the levels above the well, the width of the level is determined by how far it can extend to the end of the device. As the energy level is raised above the wells, the width of the level increases. In turn, the resonant absorption will decrease as the energy increases[44].

The special case occurs when the energy of the electron is just above the well and approaches the energy value of the conduction band of the barrier layers. If the width and the depth of the well are of the proper dimensions[31,44], then it is possible to have a level at that energy and only that energy. Hence, one would have a delta function for the density of states and the absorption would be infinite. Collisions broaden this level so it's not infinite[31,41-45] but the absorption could, in theory, be very large.

This is the argument for resonant absorption. This argument is only correct for superlattices at the flat band condition. When an electric field is applied, the levels broaden[31] and the absorption will decrease.

Some people have suggested this could work for a single quantum well(See secs. B-2.2.6 and B-2.2.7). For flat band conditions and infinite barrier layers, this would be the same situation as the superlattice, but as the field is applied or the barrier is made thinner, the levels will subsequently widen. The problem with an applied electric field would be the same as the superlattice at high electric fields because the superlattice becomes a set of noncoherent quantum wells. At low electric fields though, the levels should widen more for the quantum well device.

B-2.2.2.2 Intersubband photoconductor(IS-PC)[29,31,38,39,43-45]

The IS-PC was first proposed in 1983[38]. The final energy level is just above the well for this device(See Fig. B-2.4). The corresponding absorption process was introduced in 1973[43]. No experimental results have been published. The direction of the propagation of radiation is very important for these intersubband processes[31,43-45].

These transitions are largest when the radiation propagates parallel to the layers[31]. The device is operated in the same way that the SLIP is operated. There are three differences from the SLIP. 1) The absorption is due to intersubband absorption. 2) The radiation must be partially polarized in the direction perpendicular to the layers to cause this intersubband absorption. 3) The location of the Fermi level with respect to the barrier height energy level is not mentioned as being important.

B-2.2.3 Tunneling IS-PC[33,47-51]

The tunneling IS-PC was first proposed and experimentally tested in 1987[50]. It operates under the same principle as the IS-PC except that the final energy level is still in the well. The excited electron tunnels through the barrier(See Fig. B-2.5). Another factor is that the dopant concentration in the well is 10^{18} cm^{-3} and the barriers are undoped[33,50,51].

The device was operated at 15 K. The radiation entered the detector at an oblique angle to the layers(See sec. B-4.3). The efficiency is about 25%[33,51]. This efficiency demonstrates that there is promise for this type of device.

Impact ionization has been shown to occur in this type of device[33]. The authors apparently believe this is an advantage because in this paper, the gain is incorporated into the quantum efficiency(The efficiency becomes 84%[33]). Impact ionization is only an advantage in this device for two reasons. First, the temperature is so low that the dark current, even with impact ionization, is not large. Second, there must be some type of blocking contact(as in a CCD array[34,35]) that prevents injection of electrons from the cathode.

B-2.2.4 Resonant IS-PC[52]

The resonant IS-PC was first described in 1986[52]. No experimental results have been published.

This device is similar to the tunneling IS-PC except instead of tunneling into the conduction band of the adjacent barrier, the electron in the resonant IS-PC tunnels

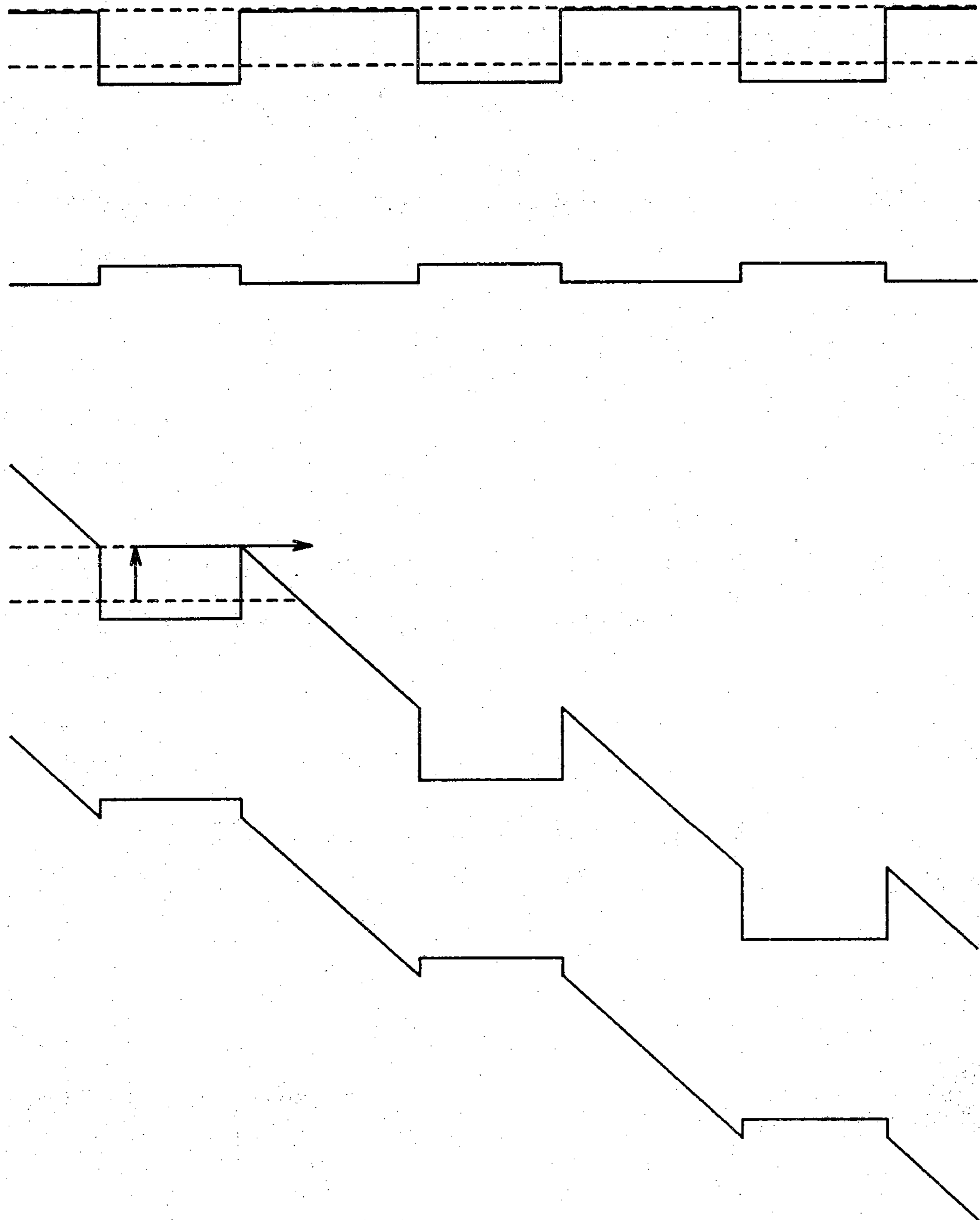

Figure B-2.4 IS-PC

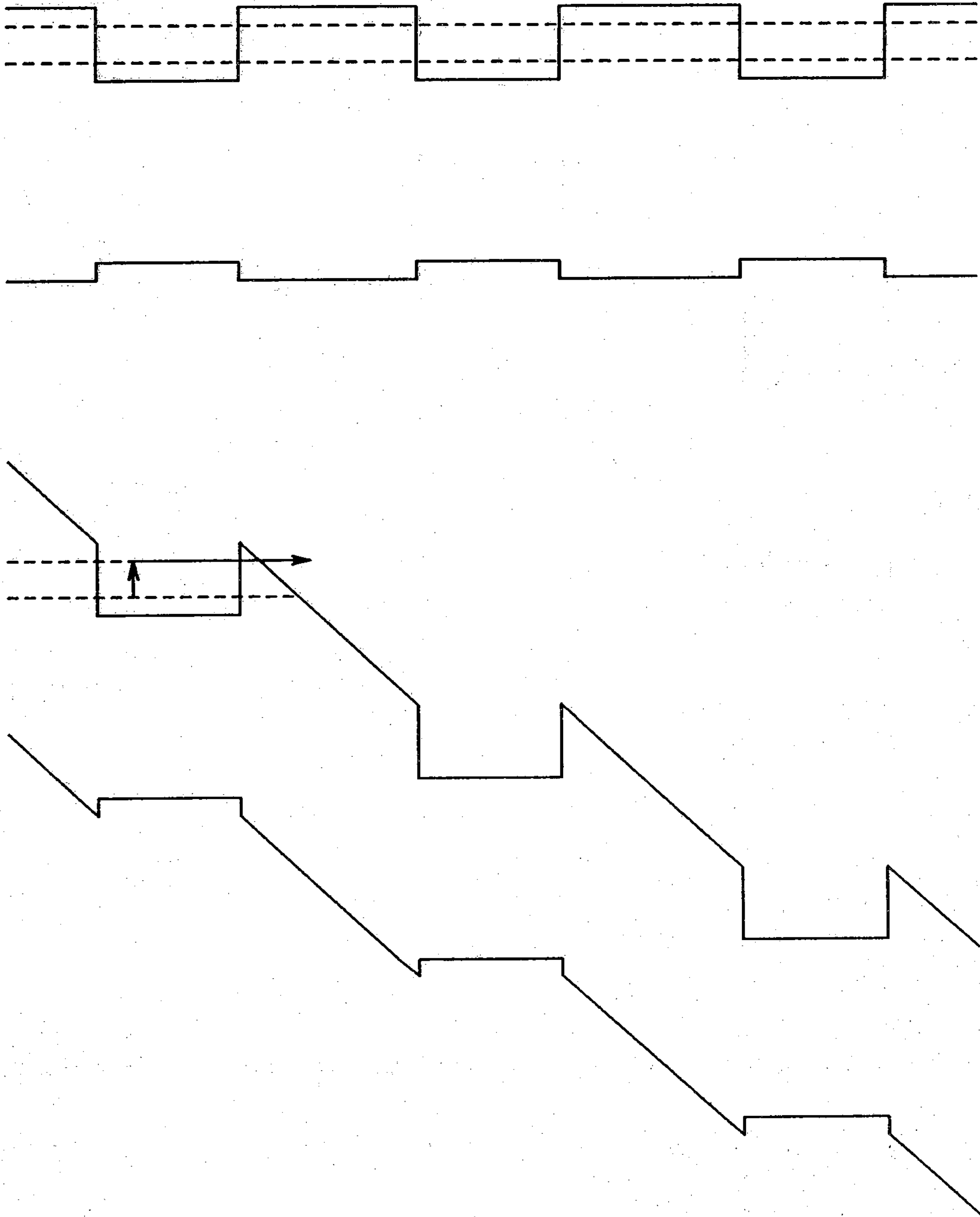

Figure B-2.5 Tunneling IS-PC

from a quantum level in one well to another quantum level in the adjacent well(See Fig. B-2.6). There are two problems with this type of device. 1) In every well, the electron must settle to the second level and tunnel before settling to the lowest level. Since the lowest level has a larger number of states, this may lower the gain drastically. 2) The electric field in the photoconductor depends upon the radiation intensity. This changing electric field appears to be a large obstacle in aligning the quantum levels to cause resonant tunneling.

B-2.2.5 Effective mass filter IS-PC[52-55]

This device was first proposed and experimentally tested in 1985[53]. It does appear to be a very viable photoconductor, except that the absorption is band to band. Which in turn means that one must deal with HgCdTe at sufficiently long wavelengths.

The device is a superlattice with direct band to band absorption. The initial electron state is in the valence band well and the final electron state is in the conduction band well. If the electron has a much smaller effective mass than the hole, then it is possible to choose a correct barrier width and electric field such that the electrons are not localized in the wells and easily pass through the barriers and the holes are localized in the wells and do not pass through the barriers. This would be analogous to an intrinsic photoconductor with no sweepout effects.

B-2.2.6 Quantum well IS-PC[56-58]

The first variation of this device was proposed in 1984[56]. The most recent variation was presented in 1986[58]. No experimental results have been published. This device operates in the same manner as the IS-PC except, instead of a superlattice, there is one quantum well.

The main assumption in these papers is that the absorption is calculated using a flat band situation. When a field is applied, the levels will become wider. At wavelengths with a calculated high absorption, this will pose a problem because the levels are assumed to be very narrow. If one lowers these absorption peaks, the quantum efficiency will be approximately 20 %, at best, for concentrations of 10^{18} cm^{-3}[58].

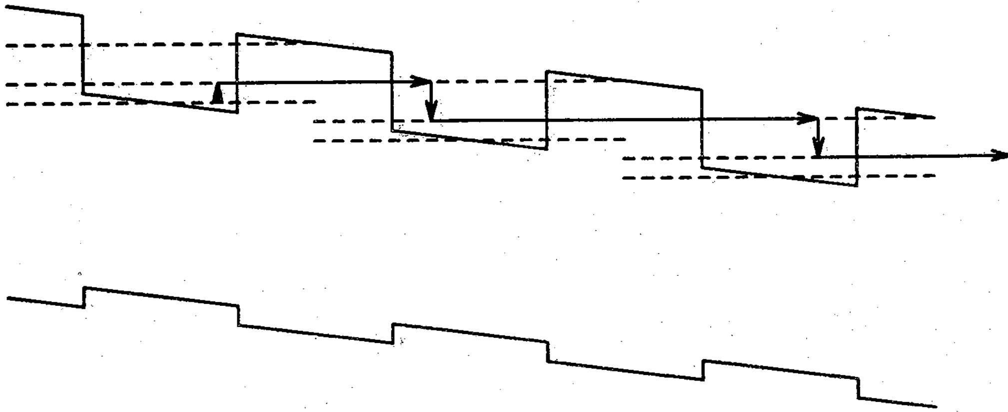

Figure B-2.6 Resonant IS-PC

B-2.2.7 Grating IS-PC[59]

This device was first proposed in 1985[59]. No experimental data has been published to date. The device is a variation of the quantum well IS-PC. The only difference is that in a quantum well IS-PC, the quantum well has barriers on both sides and the contacts are placed on the ends of these barriers. In the grating IS-PC, a grating is inserted at one of these contact-barrier interfaces. The purpose of this grating is to redirect the radiation so that more of the electric field is directed perpendicular to the quantum well layers which will increase the probability of collisionless escape(See sec. B-1.3).

The authors[59] do not state an absorption coefficient. If it is large, the problem of the level widening as the electric field is applied would be a major problem. The competing absorption process of the grating could very easily negate a smaller absorption coefficient[59].

B-2.2.8 Sampling IR detector[60-65]

This device must be used for low radiation intensity detection[60]. This requirement signifies that this device will not be a serious contender when it comes to optical communications or detection with a normal amount of background radiation or signal radiation. In addition, the efficiency is only about 4.5%[64] which is much less than the tunneling IS-PC[33,51].

B-2.3 Conventional and novel avalanche photodiodes(APDs)

There are four important physical requirements that should be met for an APD designed to detect light longer than 7 μm. First, a narrow gap semiconductor must be fabricated. Second, one disadvantage with the conventional APD is that for long wavelengths, Zener tunneling[66,67] becomes a problem. As the band gap decreases, the tunneling current becomes too large and the conventional APD is no longer a viable device. The devices presented in this section represent attempts to overcome this obstacle. Third, to make the response time as fast as possible, the absorption should take place in a region that has an electric field. Diffusion makes the response time too sluggish[24,68]. Fourth, to make the noise as small as possible, the electron's rate of ionization β_e should be much larger or smaller than the hole's rate of ionization β_h[69-71]. For instance the ionization ratio, β_e/β_h, is approximately thirty five for silicon[72]. All of the novel devices try to approach or better this ionization ratio.

The increase in the rms noise current caused by avalanching is always greater than the increase of the signal current. This extra increase in noise is related to the excess noise factor[69,73]. If other noise terms, which also includes any amplifier noise, are greater than this avalanching noise, then the signal can be increased while the overall noise stays the same[20,68,73]. This increase is beneficial until the avalanching noise becomes comparable to all other noise terms.

There has been a study[73] that compares the excess noise factors of the photomultiplier, the APD and a group of novel photodiodes. The authors concur with a previous conclusion[74] that the novel photodiodes would always have lower excess noise factors than APDs with the same ionization ratios. If the ionization ratio is infinite and multiplication occurred at every stage, then it would have a minimum excess noise factor of 1. It is pointed out though that as the ionization ratio approaches one and the number of multiplication stages increases, the excess noise factor increases accordingly.

B-2.3.1 Separate absorption and multiplication region APD(SAM-APD)[75-86]

This device was first proposed and experimentally tested in 1979[75]. Of all the novel devices, this is the one that has been considered most seriously. As stated before, the main problem with an APD with a thin gap is that the Zener current is too large. The SAM-APD is divided into two regions. A narrow band gap absorption region that has an electric field small enough to prevent avalanching and a wide band gap multiplication(or avalanche) region where the electric field is large enough to cause avalanching. An idealized band diagram of this device is presented in Fig. B-2.7. A more realistic band diagram is presented in [82] and the corresponding electric field is in [84]. The problem with the abrupt junction is that the notch(See Fig. B-2.7) traps electrons(holes in [82]) which lowers the bandwidth.

There have been several suggested improvements of the SAM-APD. One has been to grade the junction[79]. An ideal graded SAM-APD is shown in Fig. B-2.8(See [79] for a more realistic band diagram). This would solve the electron(hole in [79]) trapping problem. Other suggestions have been to use a doping spike to better control the electric fields in the absorption and multiplication regions[81] and to grade the gap by using a superlattice[83].

Another new device with the same operating principles has been presented in [86]. Instead of holes, one considers the ionized donor states as being the holes. The time response is about a μsec. This detector is very promising for one simple reason. It is a wide band gap, two carrier detector for long wavelengths.

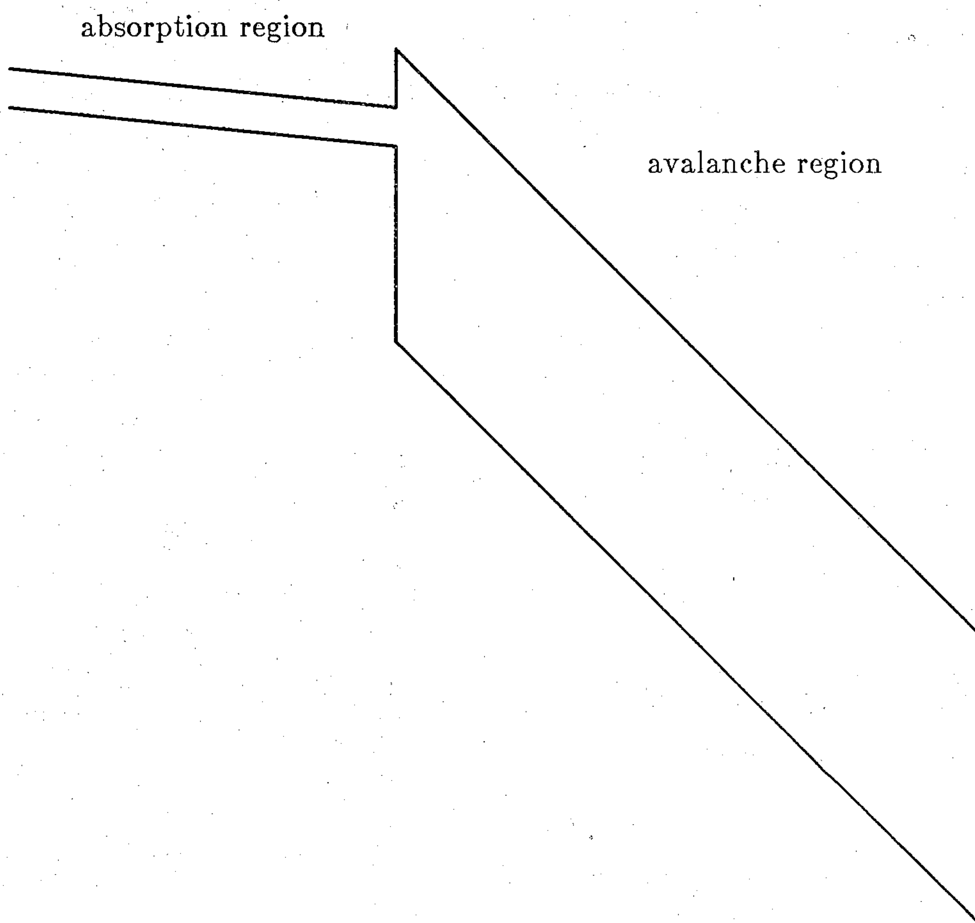

Figure B-2.7 SAM-APD

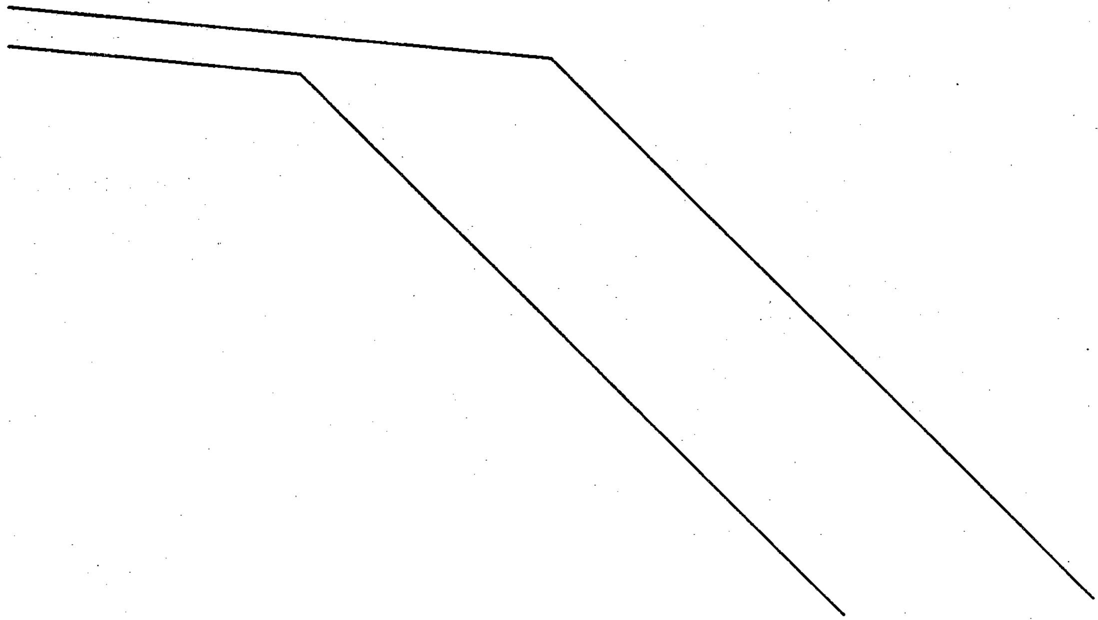

Figure B-2.8 Graded SAM-APD

These devices are being seriously considered, but there are three problems at present. First, the slow response due to hole trapping at the abrupt junction[79]. Second, it is hard to fabricate the graded junction SAM-APD without having large leakage currents[20]. Third, the ionization ratio in most of the III-V materials is about equal to 1 which causes noise problems(See sec. B-2.3 or [69]). The devices presented in secs. B-2.3.2 to B-2.3.7 try to increase this ionization ratio. In fact, the devices presented in secs. B-2.3.2 to B-2.3.7 are SAM-APDs with more exotic avalanche regions.

The noise in these devices would be the same as the conventional APDs with similar ionization ratios.

B-2.3.2 Superlattice APD[74,87-94]

This device was first proposed in 1980[87]. The first experimental results were presented in 1982[88]. The first theoretical calculation of ionization rates was presented in 1985[90].

Most papers describing this device don't discuss where the absorption is taking place. Some papers show absorption in the flat band region[90,92,94]. This would greatly lower the response time due to diffusion and is avoided in conventional APDs(See sec. B-2.3 and [24,68]). This type of diffusion limited superlattice APD is shown in Fig. B-2.9.

A practical device would be something like the SAM-APD with the multiplication region being the superlattice APD(See Fig. B-2.7). A major problem occurs with this configuration though. To get impact ionization, an electric field larger than 100,000 V/cm is needed in the avalanche region[88].

In [88], it is assumed that the electrons are not trapped in the well because the average electron energy in the electric field is greater than the conduction band height. One way to overcome this trapping problem is presented in [89]. The material must be of high quality because of the large number of heterointerfaces and the large electric field[88].

The excess noise factor of this device will be better than the conventional APDs[73,74].

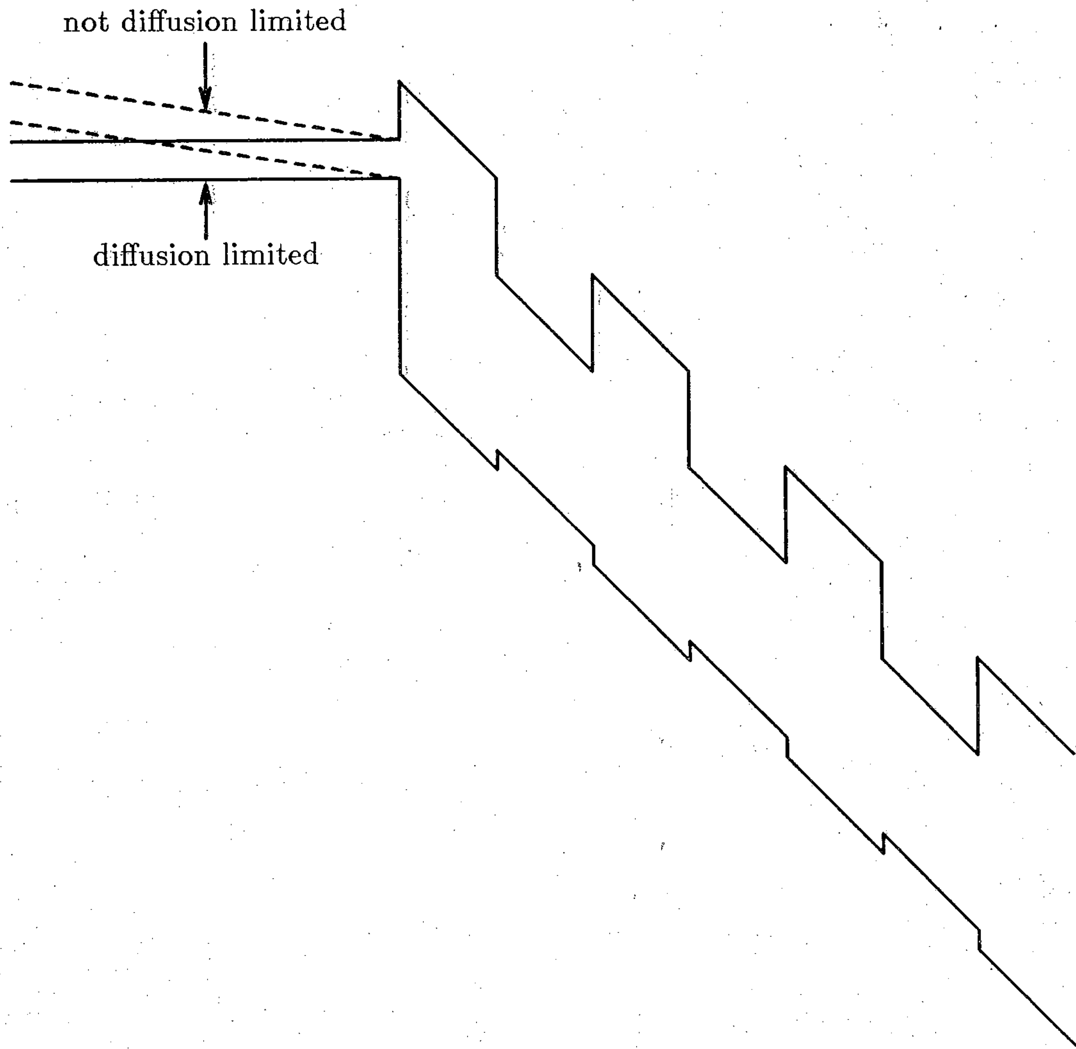

Figure B-2.9 Superlattice APD

B-2.3.3 Staircase APD[74,92,94-96]

This is an alternative to the superlattice APD. It was first proposed in 1982[95]. No experimental results have been presented at this time[20].

The multiplication region of the device is shown in Fig. B-2.10. A modification of this design is shown in [74]. The ionization ratio should increase because the electron has a high kinetic energy when it enters the narrow band gap region. The electric field is much smaller than the superlattice APD - around 10,000 V/cm[96].

The reason for no results may be the difficulty in grading the gap for such a large conduction band difference. One proposed material composition requires a conduction band change of .8 eV(the ionization energy) in a layer thickness of 3000 Å[96]. These requirements may be too difficult to achieve. A similar problem occurs for the graded SAM-APD[20].

The excess noise factor is the same as the superlattice APD[73,74].

B-2.3.4 Quantum well APD[94,97-101]

The quantum well APD was first proposed in 1982[97]. No experimental results have been published. Other than the SAM-APD papers, this is the first paper[97] that explicitly considers the separation of the absorption and avalanche regions.

This device is the same as the superlattice APD except that the doping profile is adjusted in the barriers to increase the electric field at certain points(See Fig. B-2.11).

The excess noise factor is the same as the superlattice APD[73,74].

B-2.3.5 Graded Gap APD[74,102]

The graded gap APD was first proposed and experimentally tested in 1982[102]. A representation of the graded gap APD is shown in Fig. B-2.12.

As can be seen in Fig. B-2.12, the effective electric field in the device is larger for the electron than the hole. If only one layer is used, the gain would be around 5 at best[102]. Matching this device to a compatible absorption region would be much more difficult than the SAM-APD(See Fig. B-2.12)

The excess noise factor is the same as the conventional APD[73,74].

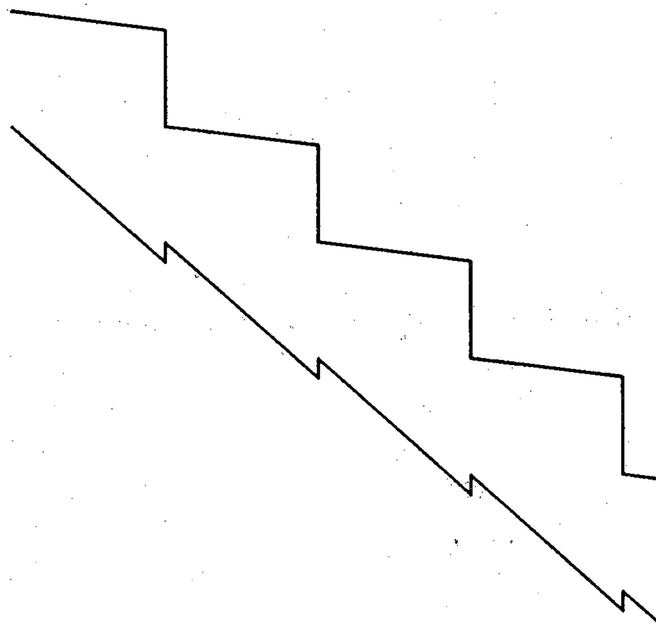

Figure B-2.10 Multiplication region of the staircase APD

Figure B-2.11 Quantum well APD

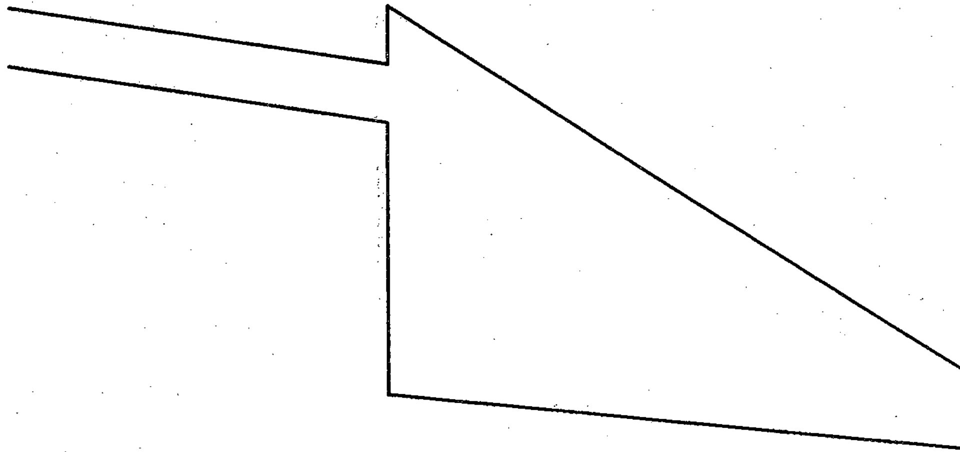

Figure B-2.12 Graded gap APD

B-2.3.6 Resonant tunneling superlattice APD(RTS-APD)[103,104]

The RTS-APD was first proposed in 1987[103]. It operates by aligning quantum levels in adjacent wells such that resonant tunneling can occur. This is a spin off of another novel APD[104]. No experimental results have been published.

This paper[103] explicitly discusses absorption in the flat band region and diffusion currents. The band diagram is shown in [103]. For the device to be competitive, one would have to have an electric field in the absorbing region.

The RST-APD is proposed as an alternative to the SAM-APD. This is due to the slower response caused by the trapped charge at the notch of the abrupt junction. It seems that there could possibly be similar trapping problems in the valence band of the RST-APD. In addition, the voltage in conventional photodiodes and APDs change when the radiation varies. It seems reasonable to assume the voltage in the RTS-APD will also change. This change in voltage appears to be a large obstacle in aligning the quantum levels to cause resonant tunneling. These problems appear to be more difficult to solve than the grading problems of the SAM-APD.

The excess noise factor is the same as the superlattice APD[73,74].

B-2.3.7 Channeling APD[74,105-107]

The channeling APD was first proposed in 1982[105]. No experimental results on the device have been published.

As shown in [105], this device is very complicated. The major problem with this device is that for wavelengths of interest, one needs small band gap. With such a small band gap and a high electric field needed for ionization, Zener tunneling would be a serious obstacle.

The excess noise factor is the same as the conventional APD[73,74].

B-2.4 Conclusion

Of the novel devices presented in this chapter, only a few are promising. The novel one carrier photoconductors are more promising at long wavelengths because of the small band gap problems in the novel APDs.

For one carrier detectors, the IS-PC and the tunneling IS-PC are the most promising.

The most promising two carrier detectors are presented in secs. B-2.3.1 to B-2.3.5 and the effective mass filter PC in B-2.2.5.

B-3. FREE CARRIER ABSORPTION

B-3.1 Experimental free carrier absorption results

In this chapter only bulk free carrier absorption coefficients will be discussed. The intersubband absorption process is neglected because there have been no experimental results presented for excitation above the well(See sec. B-2.2.2). The 2D effect on the free carrier absorption coefficients will also be neglected at this time. There are two justifications for this assumption. First, the case considered in this report is perpendicular incidence[31,108] where the electrons are excited parallel to the layers. Second, the possible 2D effects on the carrier concentration appear to decrease as the effective mass increases and a large effective mass(or density of states) is desired because it increases the quantum efficiency of the SLIP(See sec. B-1.4.3).

The absorption of radiation will take place in the well. If the absorption coefficient is 10^4cm^{-1} and the well thickness is 200 Å, then 50 wells will be needed in the device. Of course, the wells can be made wider, which in turn decreases the number of wells, but this will lower the quantum efficiency because the excited electron is more likely to drop back into the well before it escapes(See sec. B-1.3).

B-3.2 Free carrier absorption limits

In this section, the absorption coefficient, α, is presented for p-type GaAs because AlGaAs superlattices can be easily fabricated and can be doped more strongly p-type than n-type when grown in an MBE system[109]. In addition, the density of states is larger in the valence band in GaAs. As will be seen, p-type GaAs is a feasible material for the SLIP. There is room to improve by considering other materials with a higher density of states. On the other hand, n-type GaAs will not work because of the small density of states.

There is a scarcity of free carrier absorption data on p-type GaAs. Most people find free carrier absorption a detriment, and hence there is no apparent interest in free carrier absorption by itself. One of the first things that must be accomplished before fabricating this device is to measure free carrier absorption in p-type GaAs.

Since there is a scarcity of data in the literature, there will be two limits considered, an upper limit when α is comparable to the theoretical free carrier absorption(See table B-3.1) and a lower limit when one considers that the experimental α equals one tenth of the theoretical α. The absorption values in table B-3.1 are approximately the silicon theoretical values. It is assumed that the free carrier absorption coefficients are about the same in p-type GaAs and p-type Si. The

Table B-3.1
Theoretical free carrier absorption coefficients
for different concentrations and photon energies

n	$E_F - E_{cw}$	α (cm^{-1})			
(cm^{-3})	(eV)	(E_λ=.1eV)	(.05eV)	(.025eV)	(.0125eV)
1.e17	.0017	-	-	-	1.9e3
5.e17	.0051	-	-	-	9.6e3
8.e17	.0070	-	-	-	1.5e4
9.e17	.0075	-	-	-	1.7e4
1.e18	.0081	-	-	4.8e3	1.9e4
2.e18	.0128	-	-	9.6e3	3.8e4
3.e18	.0168	-	-	1.4e4	5.8e4
4.e18	.0204	-	4.8e3	1.9e4	7.7e4
5.e18	.0236	-	6.0e3	2.4e4	9.6e4
6.e18	.0267	-	7.2e3	2.9e4	1.2e5
7.e18	.0295	-	8.4e3	3.4e4	1.3e5
8.e18	.0323	-	9.6e3	3.8e4	1.5e5
9.e18	.0349	-	1.1e4	4.3e4	1.7e5
1.e19	.0375	3.0e3	1.2e4	4.8e4	1.9e5
2.e19	.0596	6.0e3	2.4e4	9.6e4	3.8e5
3.e19	.0780	9.0e3	3.6e4	1.4e5	5.8e5
4.e19	.0956	1.2e4	4.8e4	1.9e5	7.7e5
5.e19	.1097	1.5e4	6.0e4	2.4e5	9.6e5

lower limit is considered because of the data presented for high carrier concentrations and long wavelengths in Si[110]. It appears that the free carrier absorption coefficients in [110](and in turn, the lower limit) are too pessimistic[9,111-113] because of possible errors in the transmission measurements(These errors in [110] are addressed directly in [111]).

In table B-3.1, $E_F - E_{cw}$(See Fig. B-1.3. For p-type semiconductors, one would calculate $E_{vw} - E_F$) is calculated using an effective mass of .45 m_o(It is assumed the mass doesn't vary significantly if the semiconductor is degenerately doped[114-118]).

Table B-3.1 can be generated for any material. The important thing is not whether it is p-type or n-type, but the mass and the density of states. Since this proposal mainly uses the notation of an n-type material, the $E_F - E_{cw}$ notation will be used in place of $E_{vw} - E_F$.

The important relationship is how α relates to $E_F - E_{cw}$. The larger the density of states, the smaller $E_F - E_{cw}$, the better the device(See sec. B-1.4.3).

B-3.3 Classical calculation of free carrier absorption

The classical calculation of free carrier absorption can be found using the Drude conductivity[10]

$$\sigma = \frac{Ne^2\tau_r}{m^* \omega^2 \tau_r^2 4\pi\epsilon_o}$$

where τ_r is the relaxation time, m^* is the effective mass of the carrier, and $4\pi\epsilon_o$ in the denominator is needed for MKS units.

The absorption is found by using the relation[15]

$$\alpha = \frac{4\pi}{n_r c}\sigma = \frac{4\pi Ne^2}{m^* n_r c \omega^2 \tau_r 4\pi\epsilon_o}$$

where n_r is the index of refraction and c is the speed of light.

Using the relationship,

$$\omega = \frac{2\pi c}{\lambda}$$

then[119]

$$\alpha = \frac{Ne^2\lambda^2}{4\pi^2 n_r c^3 \epsilon_o m^* \tau_r} .$$

In the limit of low frequencies and elastic scattering mechanisms, the absorption can be approximated using this Drude theory[9,10].

B-3.4 Quantum calculation of free carrier absorption

The calculation has been carried out by Meyer[28], Dumke[120], Seeger[121], Jenson[122], and Nag[123].

Meyer describes how the ellipsoidal masses would be entered in the calculation. Dumke relates the quantum calculation to the classical calculation. Seeger has the best form when one wants to consider different scattering processes. Nag presents a comprehensive review.

A quick summary of the quantum free carrier absorption is not presented here because it is too complicated to summarize quickly. Since it is a second order process, one must integrate over the initial and final states. This process has been described by Dumke and is not repeated here.

The other reason quantum mechanical free carrier absorption is not presented is because we are interested in actual absorption and as shown in sec. B-3.2, there is a difference of opinion as to whether the theoretical calculations hold at high densities and long wavelengths.

B-4. PROPAGATION OF RADIATION

B-4.1. Three cases of incidence

There are three ways the radiation can enter the device - perpendicular incidence, oblique incidence and parallel incidence. The radiation propagates perpendicular to the layers, oblique to the layers or parallel to the layers for the three cases, respectively.

At this time, the two cases most likely to be used would be the perpendicular and oblique incidence cases. These are discussed in secs. B-4.2 and B-4.3 respectively. The main advantage of these two cases is that it is relatively simple to couple the radiation into the device. The reflection coefficient[124] can be minimized by merely adding an antireflective coating. Consequently, this planar configuration is simpler to make, and has other related advantages[125].

The parallel incidence case has several problems that are described in sec. B-4.4. The reflection coefficient(which is related to coupling) is much harder to minimize because of the long wavelengths to be detected[126].

B-4.2. Perpendicular incidence

The main problem with perpendicular incidence is that the polarization of radiation(which is perpendicular to the radiation direction) is parallel to the layers[31]. The electrons are excited in the direction of polarization[28,127,128], which means that for the electrons to cross the barrier, there must be at least one collision to readjust the direction of the electron with an increase of energy in the direction perpendicular to the layers(See sec. B-6.2).

Perpendicular incidence would be possible only if a partly closed well(See secs. B-6.2 and B-6.4) can be fabricated. This requirement of a partly closed well means that the operating temperature must be below 10 K(See sec. B-8.5).

B-4.3. Oblique incidence

This case has been considered in the IS-PC devices in sec. B-2.2.

If the partly closed well cannot be fabricated or if a higher temperature is desired, then the oblique incidence case must be considered. This is because the electron can be partially excited in the perpendicular direction and one doesn't need a collision for the electron to escape from the well. Since a collision is not needed, the open well case can be used(See secs. B-6.2 and B-6.3).

In the open well case, as much of the polarization of the electric field as possible should be in the perpendicular direction. Consequently, 1) only radiation with the electric field in the plane of incidence[124] is useful and 2) the larger the angle between the perpendicular direction of the layers and the propagation direction, the higher the probability of escape.

B-4.4. Parallel incidence

In this case, the superlattice acts as a parallel plate waveguide. There are three modes in a parallel plate waveguide - TE, TM and TEM. In reality, the TEM mode is a special case of the TM modes[129] and hereafter will be lumped with them.

If one is considering the open well case, the TM modes are important because the TE modes have no electric field in the perpendicular direction[124,129].

The smaller the mode number, the more the electric field points in the perpendicular direction[124,129]. Hence, the TEM mode would be the best because the mode number is zero[129].

Coupling the radiation into the waveguide is a major problem. First, the modes will have to be TM modes and second, it appears that the longer the wavelength, the more difficult this coupling may become[126]. The simpler oblique incidence case would probably be preferable to this case.

B-5. CALCULATION OF THE CURRENT IN THE SLIP

B-5.1 Description of the current terms

This chapter describes the current flow in the device. This is of interest because noise and in turn, D^* depend on the current.

There are three current terms in a photodetector. First, the object or signal that the photodetector should detect produces the signal current. Second, the radiation from the background produces background current. Third, the current flowing through the detector when no radiation is present is the dark current. This dark current is produced by thermal generation in the device or tunneling of the carriers into the conduction or valence band.

B-5.2 Calculation of the signal current

B-5.2.1 Signal current for a conventional photodetector

The total intensity radiated from a source is W where[130]

$$W = \int_{\lambda=0}^{\lambda=\infty} W_\lambda(\lambda_a) d\lambda_a$$

where $W_\lambda(\lambda_a)$ is the radiant emittance of the source. $W_\lambda(\lambda_a)\Delta\lambda$ can be thought of as the intensity from the source in a range $\Delta\lambda$ at λ_a.

The photon flux(the number of photons per second per area) from a source that strikes a detector in a wavelength range $\Delta\lambda$ at λ_a, is

$$\phi(\lambda_a,\Delta\lambda) = \frac{W_\lambda(\lambda_a)\Delta\lambda}{E_\lambda(\lambda_a)} = \frac{P(\lambda_a,\Delta\lambda)}{A_D\, E_\lambda(\lambda_a)}$$

where

$$E_\lambda(\lambda_a) = \frac{\hbar\, c}{\lambda_a}$$

and is the photon energy, P is the power of the incoming radiation, η is the quantum

efficiency[22], and A_D is the detector area(The area the radiation strikes).

The optical current is(assuming all the radiation is absorbed)

$$J_{op}(\lambda_a) = q\phi_{op}(\lambda_a)\eta(\lambda_a)\,\frac{A_D}{A_C}$$

where A_C is the area of the contacts. For background limited infrared detection(where the background radiation is the major source of noise), the $\frac{A_D}{A_C}$ term cancels out when considering D^*(See chap. B-7).

$J_{op}(\lambda_a)$ should not be confused with the actual signal current which is

$$J_s(\lambda_a) = G\ J_{op}(\lambda_a) = q\ G\ \phi_{op}(\lambda_a)\eta(\lambda_a)\,\frac{A_D}{A_C}$$

where G is the gain.

$J_s(\lambda_a)$ is the actual signal current that is detected. $J_{op}(\lambda_a)$ has no physical significance except that it is the signal current when the gain equals 1.

To calculate the total signal current,

$$J_{sT} = q\frac{A_D}{A_C}\ G\int\frac{W_{\lambda op}(\lambda_a)\eta(\lambda_a)}{E_\lambda(\lambda_a)}d\lambda_a\ .$$

B-5.2.2 Signal current for the SLIP

For the SLIP, the radiation will most likely propagate through the contact area or $A_C = A_D$. This relationship will be assumed for the rest of the report.

The current produced in the SLIP by the incoming radiation is

$$J_s(\lambda_a) = q\sum_{i=1}^{i_m}\int_{z_{wl(i)}}^{z_{wr(i)}}\eta(z,\lambda_a)\alpha(z,\lambda_a)\phi(z,\lambda_a)G(z,\lambda_a)dz$$

where $\frac{d\phi(z,\lambda_a)}{dz} = \alpha(z,\lambda_a)\phi(z,\lambda_a)$, $\alpha(z,\lambda_a)$ is the absorption coefficient, i_m is the

number of wells, $z_{wl(i)}$ is the left boundary of the ith well and $z_{wr(i)}$ is the right boundary of the ith well.

Now assume that $n_e(z-z_{wl(i)})$ (number of electrons in the well), $\eta(z-z_{wl(i)},\lambda_a)$ and $G(z-z_{wl(i)},\lambda_a)$ are the same for all wells so

$$J_s(\lambda_a) = q\ \phi(z_o) \int_{z_{wl(1)}}^{z_{wr(1)}} \eta(z,\lambda_a)\ G(z,\lambda_a)\ \alpha(z,\lambda_a) e^{\alpha i_m[z-z_{wl(1)}]} i_m dz$$

where the integral can be over any well and $\alpha=\alpha(z,\lambda_a)$.

If one can assume that $G(z,\lambda_a)$ and $\eta(z,\lambda_a)$ are constant values in the well, then

$$J_s(\lambda_a) = q\ \phi(z_o)\eta(\lambda_a)\ G(\lambda_a)(1-e^{-\alpha i_m(z_{wr(1)}-z_{wl(1)})})$$

or

$$J_s(\lambda_a) = q\frac{P(\lambda_a,\Delta\lambda)}{A_D\ E_\lambda(\lambda_a)}G(\lambda_a)\eta(\lambda_a)$$

if α is large enough such that $e^{-\alpha i_m(z_{wr(1)}-z_{wl(1)})}$ is negligible.

B-5.3 Calculation of the background current

By analogy with the previous section, the current produced by the background radiation is

$$J_B(\lambda_a) = q\int\frac{W_{\lambda B}(\lambda_a)\eta(\lambda_a)}{E_\lambda(\lambda_a)}d\lambda_a$$

where $W_{\lambda B}$ is the incoming radiant emittance of the background. The hemispherical field of view is taken into account in $W_{\lambda B}$.

Table B-5.1 displays the background current of a background at a temperature of 300 K. This would be the current density for any conventional photodetector with a quantum efficiency of 1. In a conventional photodetector, it is assumed that all the

radiation with energy greater than the band gap(or ionization energy for an extrinsic photoconductor) is absorbed.

Table B-5.1
Background current as a
function of wavelength

wavelength range	$J_B(\eta=1)$ (A/cm^2)
$\lambda \leqq 41.3\mu m$	.535
$\lambda \leqq 20.7\mu m$	.34
$\lambda \leqq 15.7\mu m$	.22
$\lambda \leqq 11.3\mu m$	.106

As in the signal current, the actual background current measured is the gain times J_B.

B-5.4 Calculation of the thermionic emission current

The thermionic emission current[24,131] is calculated using the equation

$$J_{te} = \frac{A^*}{A} 120T^2 \, e^{\frac{-\Delta E_{te}}{kT}}$$

where A is the Richardson constant, A^* is the effective Richardson constant, and

$$\Delta E_{te} = E_{cb} - E_F \ .$$

E_{cb} is the conduction band level for the barrier and E_F is the Fermi level in the well(See Fig. B-1.3).

Rearranging the terms, letting $A^* = A$,

$$\Delta E_{te} = -kT\ln\left(\frac{J}{120T^2}\right) .$$

Using this equation, the values for ΔE_{te} are entered in table B-5.2.

Table B-5.2
ΔE_{te} as a function of temperature and thermionic emission current

$J_{te}(A/cm^2)$	ΔE_{te} (eV)						
	T=4.2K	5K	16K	20K	40K	60K	80K
10^{-1}	.00362	.0044	.0174	.0225	.0499	.0789	.1093
10^{-2}	.00445	.0054	.0206	.0265	.0578	.0909	.1252
10^{-3}	.00528	.0064	.0238	.0304	.0658	.1028	.1411
10^{-4}	.00611	.0074	.0269	.0344	.0737	.1147	.1570
10^{-5}	.00694	.0084	.0301	.0384	.0816	.1266	-
10^{-6}	.00777	.0094	.0333	.0423	.0896	.1385	-
10^{-7}	.00861	.0104	.0365	.0463	.0975	.1504	-
10^{-8}	.00944	.0114	.0397	.0503	.1054	-	-
10^{-9}	.0103	.0124	.0429	.0542	.1134	-	-
10^{-10}	.0111	.0134	.0461	.0582	.1213	-	-

If $A^* \neq 1$, then

$$\Delta E'_{te} = \Delta E_{te} - kT\ln(\frac{1}{A^*}) \ .$$

I_{te} must be multiplied by G to obtain the contribution of thermionic emission to the dark current.

B-5.5 Calculation of the tunnel current

The tunnel current, I_{tn}, is the other contribution to the dark current. The thermionic emission current is caused by electrons passing over the barriers and the tunnel current is caused by electrons passing through the barriers. Since the electrons will tunnel into the barrier conduction band(as opposed to tunneling into another well), the current is also multiplied by the gain to get its contribution to the dark current. Consequently,

$$I_d = G(I_{te} + I_{tn}) \ .$$

B-5.5.1 Triangular barrier

It is assumed that the tunneling current in the SLIP is analogous to the field emission current. Consequently, for a free metal with mass m_e at T$\simeq$ 0K[13,132-134]

$$J_{tn} = \left(\frac{4\pi m_e q}{(2\pi\hbar)^3}\right)\int_{E_{cw}}^{E_F} (E_F - E_z)\, \Upsilon_t(E_z) dE_z$$

where $\Upsilon_t(E_z)$ is the transmission probability at E_z. E_z will be considered to be between E_F and E_{cw}(the conduction band of the well) for low temperatures.

One can calculate a maximum transmission probability Υ_{tm} such that

$$J_{tn} \leqq \frac{4\pi m_e q}{(2\pi\hbar)^3}\, \Upsilon_{tm}\, \frac{(E_F - E_{cw})^2}{2} \quad .$$

Using the WKB approximation[13,24,134],

$$\Upsilon_t(E_z) = \exp\left(-K_1 \int_0^{z'} \sqrt{U(z)-(E_z-E_{cw})}\, dz\right)$$

where z' is the effective barrier width(See Fig. B-5.1), U(z) is the potential of the barrier, and

$$K_1 = 2\frac{\sqrt{2m^*}}{\hbar} \quad .$$

For the barrier in Fig. B-5.1,

$$U(z)-(E_z-E_{cw}) = \Delta E_c - q\xi z-(E_z-E_{cw})$$

and

$$\Upsilon_t(E_z) = \exp\left(-K_1 \frac{2}{3}\, \frac{\Delta_b}{qV}(\Delta E_c-(E_z-E_{cw}))^{3/2}\right)$$

where ξ is the electric field, Δ_b is the barrier thickness between adjacent wells, and V is the potential across the barrier.

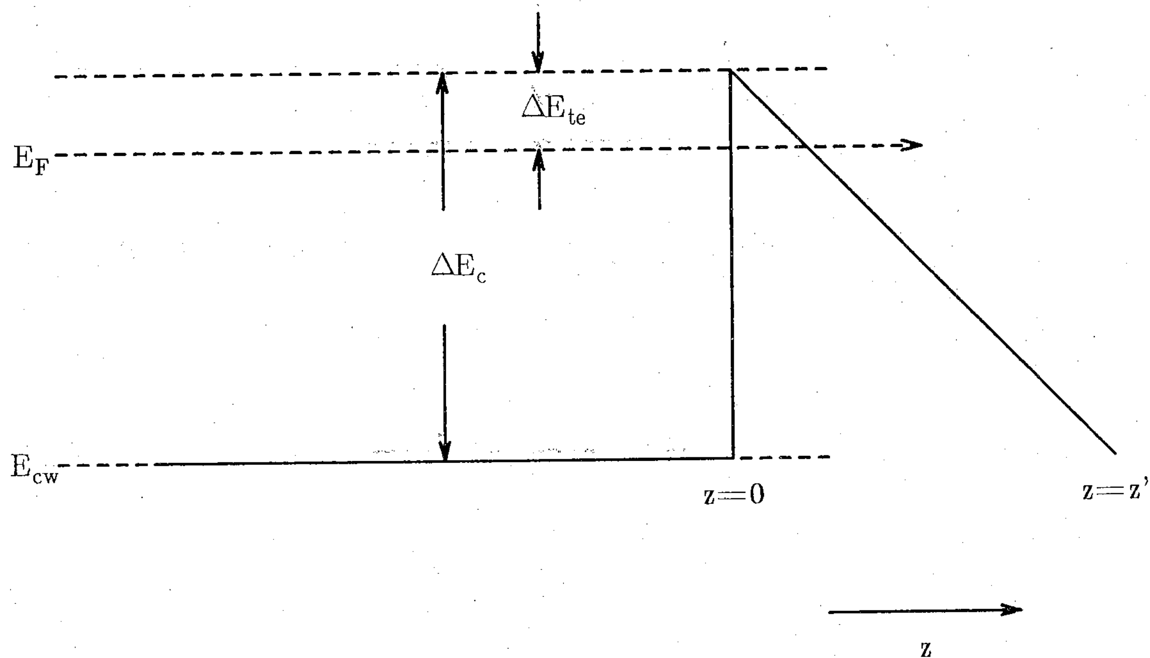

Figure B-5.1 Tunneling through a triangular barrier

For Δ_b=.2μm, qV=q$\xi\Delta_b$=.2eV and ΔE_{te}=.01eV(See Fig. B-5.1),

$$\Upsilon_{tm} = \Upsilon_t(E_F) = e^{-4.58} \simeq .01 \ .$$

Table B-5.3 shows how the approximate tunnel current through a triangular barrier depends on the electric field($E_F - E_{cw}$ = .01 eV).

Table B-5.3
Tunnel current through
a triangular barrier

ξ (V/cm)	qV (eV)	Υ_{tm} (unitless)	$J_{tn} \leqq$ (A/cm^2)
500	.01	$e^{-91.6}$	$6.03\text{x}10^{-33}$
1000	.02	$e^{-45.8}$	$4.69\text{x}10^{-13}$
2000	.04	$e^{-22.9}$	$4.14\text{x}10^{-03}$
10,000	.2	$e^{-4.58}$	$3.74\text{x}10^{05}$

As can be seen, the current is very large for the electric fields greater than 2000 V/cm.

B-5.5.2 Trapezoidal barrier

One way to overcome this problem is to change the shape of the barrier. Consider the barrier shape in Fig. B-5.2. For a barrier width of 2000 Å, an electric field of 10,000 V/cm, and a ΔE_s of .1 eV(See Fig. B-5.2), the effective electric field would be zero in one half of the barrier and an effective field of two times 10,000 V/cm in the other half. This very convenient result is shown in Fig. B-5.3.

As can be seen in Fig. B-5.3, this barrier is shaped like a trapezoid instead of a triangular barrier. The transmission probability for this trapezoid can be approximated as

$$\Upsilon_t(E_z) = \exp(-K_1(\Delta E_c - E_z - E_{cw})^{1/2}\ \Delta_t) \ .$$

For Δ_t=.1μm, qξ=10,000eV/cm, ΔE_{te}=.01eV, and

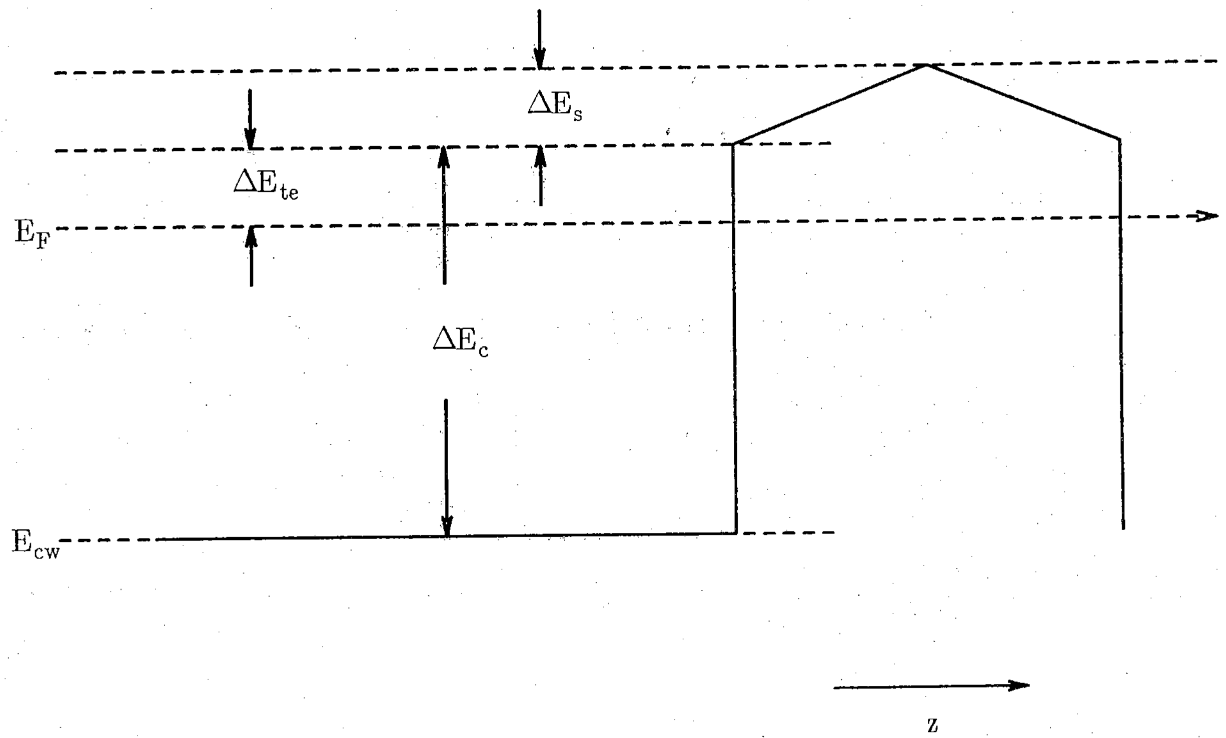

Figure B-5.2 Shape of a barrier that will lower the tunneling rate

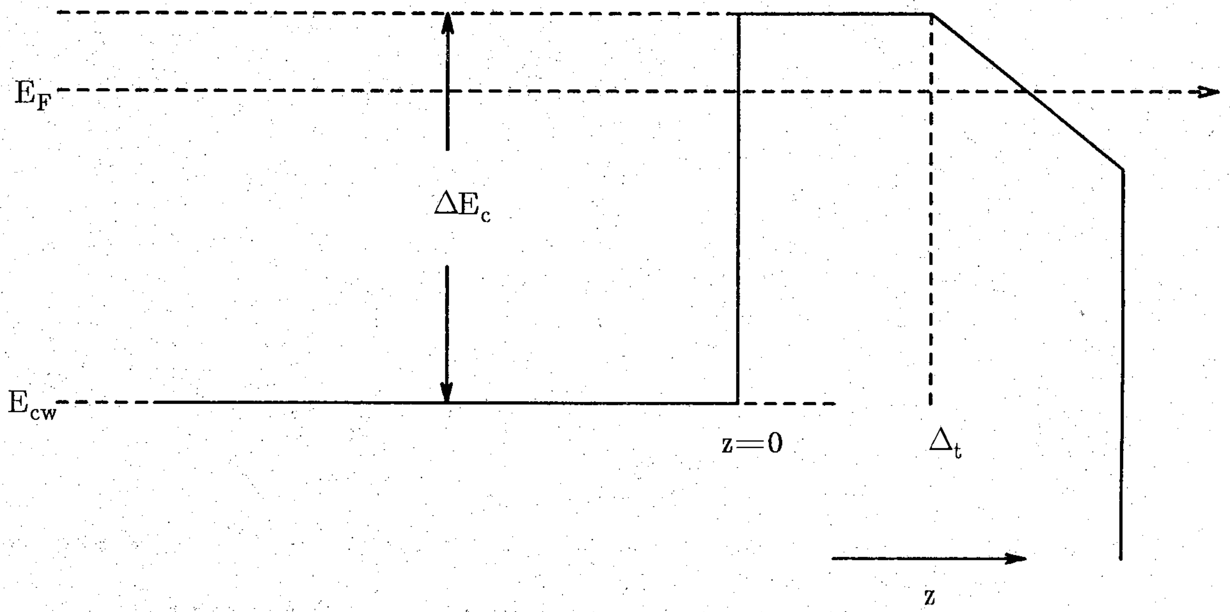

Figure B-5.3 Tunneling through a trapezoidal barrier

$$\Delta E_s \simeq .1\text{eV} ,$$

$$\Upsilon_{tm} = \Upsilon_t(E_F) = e^{-68.9} .$$

J_{tn} can then be calculated for E_F–E_{cw}=.01eV as

$$J_{tn} \leqq 1.75\text{x}10^{-24}\frac{A}{cm^2} .$$

B-5.5.3 Comparison between the triangular barrier and the trapezoidal barrier

From secs. B-5.5.1 and B-5.5.2, it appears that the trapezoidal barrier is better because of the higher electric field that can be applied. Yet if one considers impact ionization[32], the electric field might be limited to 1000 V/cm or less. If the electric field is this small, the tunnel current would be negligible for either type of barrier.

However, there is one other advantage that makes the trapezoidal barrier superior, even at small fields. This advantage can be seen in Fig. B-5.4. It is assumed in Fig. B-5.4 that the radiation is entering the device from the left. As the radiation propagates in the device, the intensity decreases due to the free carrier absorption. Consequently, the closer the well is located to the side at which the radiation enters the device, the larger the excitation rate of the electrons in that well. The positive charge left in the well causes the barrier to bias upward. The shape of the barriers when they are biased upward(See Fig. B-5.4) causes the excited electrons to be more likely to be collected in the wells where this upward biasing is the strongest - in the wells where most of the excitation is taking place. This variation of the recombination rate means that the response in a SLIP using trapezoidal barriers should be faster than a in SLIP using triangular barriers.

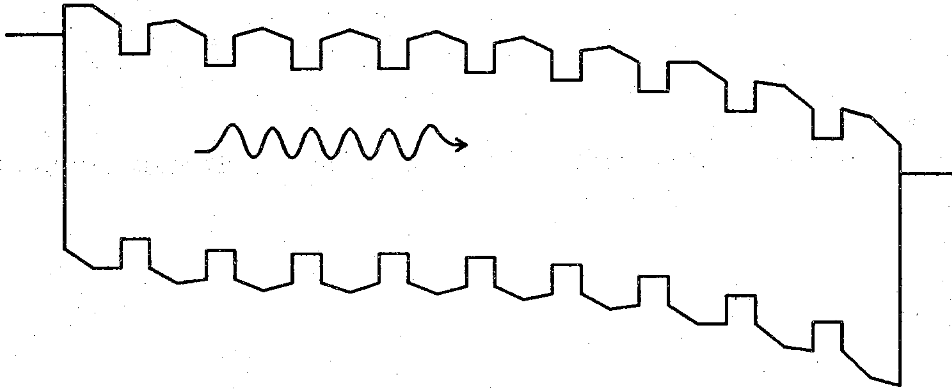

Figure B-5.4 Band diagram example of a SLIP during radiation excitation

B-6. QUANTUM EFFICIENCY

B-6.1 Definition of quantum efficiency in the SLIP

The quantum efficiency is defined as the percentage of excited electrons that surmount the barrier and escape from the well. In this chapter, the quantum efficiency for an n-type well is estimated. A similar argument can be used for holes in a p-type well.

B-6.2 Comparison of quantum efficiencies in open and partly closed wells

In this section, the immense advantage of having a partly closed well of electrons compared to an open well of electrons is demonstrated.

As a simplification, the temperature is assumed to be low enough such that the distribution can be approximated as

$$f(E)=1 \text{ if } E<E_F$$

and

$$f(E)=0 \text{ if } E>E_F \quad .$$

This approximation is made so that the states are full below the Fermi level and are empty above the Fermi level. If this distribution is used, an electron cannot emit a phonon such that the electron's energy after emission is less than E_F.

B-6.2.1 Description of scattering mechanisms

In this section, the importance of the various scattering mechanisms is described. The important scattering mechanisms will be optical phonon scattering, intervalley scattering, acoustic phonon scattering, impurity scattering and carrier-carrier scattering[123,135].

An inelastic phonon is a phonon that inelastically interacts with the electron. Subsequently, the electron gains or loses energy $k\theta$, where k is Boltzmann's constant and θ is in units of degrees Kelvin[136,137]. An inelastic collision is defined as a collision in which the electron loses a relatively large amount of energy. For instance, acoustic phonons have a non-zero energy, but this energy is usually much

smaller than the total electron energy, hence it is assumed to be elastic. In this report, the inelastic phonons are the optical phonons and the intervalley phonons.

If one can neglect scattering with the inelastic phonons, then the only remaining types of scattering would be impurity scattering, acoustic phonon scattering and carrier-carrier scattering.

Impurity scattering becomes more important as the impurity concentration increases. For the free carrier concentrations of interest, impurity scattering should be much greater than acoustic scattering[138]. If the SLIP incorporates modulation doping, one may want to dope the wells just to have impurity scattering in the well.

In addition to the small scattering rate for acoustic phonons, energy loss for acoustic scattering is usually small enough that if this was the only type of scattering, the electron would probably surmount the barrier before it could be trapped.

The electron-electron scattering mean free path is expected to be greater than 10,000 Å for $E-E_F$ less than .1 eV, where E is the total electron energy and E_F is the Fermi level in a metal[139]. As a result, electron-electron scattering is neglected. If anything, it should increase the current because of impact ionization which, as stated in sec. B-1.4.4, could be an advantage or a disadvantage, depending on the application.

B-6.2.2 Definition of open well and partly closed well

A partly closed well is defined by the situation

$$E_{cb} - E_F = \Delta E_{te} < k\theta_{min}$$

where ΔE_{te} is defined in sec. B-5.4 and $k\theta_{min}$ is the smallest energy of the nonnegligible inelastic phonons(See sec. B-6.2.1). Negligible inelastic phonons have such a small scattering probability that it can be assumed that they don't exist.

An open well is defined by the situation

$$E_{cb} - E_F = \Delta E_{te} > k\theta_{min} .$$

B-6.2.3 Physical significance of open well and partly closed well

The difference between the partly closed well and the open well is that in the open well case, the well states that the electron can drop into are unoccupied. Consequently, in the open well case, the electron will always drop into the well when the electron emits an inelastic phonon. In the partly closed well case, there are some well states which are occupied that the electron could drop into if it could emit an inelastic phonon. However, in this case, the electron cannot emit an inelastic phonon. Hence, the electron will only emit a portion of the inelastic phonons that are emitted in the open well case. The value of this portion is related to how close in energy the Fermi level is to the energy level at the top of the well.

Since there is a restriction in the partly closed well case, then there is a lower probability of the excited electron dropping into the well. Due to this lower probability, the quantum efficiency will be higher in the partly closed well case. The quantum efficiency will be higher because in the partly closed well case, there will be energy levels where an inelastic phonon cannot be emitted([29,135] - The low temperature, low field case in [135] is similar to this situation). Hence the electron will continually travel above the well colliding with elastic phonons and impurities until its energy in the direction perpendicular to the superlattice layers is greater than the barrier height ΔE_c(See sec. B-6.5 for the boundary conditions). Since the elastic phonons do have a finite amount of energy, it is a race between the electron surmounting the barrier before a large amount of these "elastic" collisions cause the electron to drop into a well state. Due to the boundary conditions, the smaller the barrier height(ΔE_c), the quicker the electron should surmount the barrier. In addition, the larger the density of states, the smaller this barrier height becomes(See sec. B-8.7).

The idea is to keep the electron's total energy above the barrier as long as possible while at the same time having elastic collisions which keep changing the electrons direction until the electron energy in the z-direction is large enough to surmount the barrier. This basic physical mechanism must exist for the SLIP to work efficiently.

B-6.3 Analysis of quantum efficiency in an open well

In this section, a calculation to determine the percentage of electrons that surmount the barrier in an open well situation is compared to a Monte Carlo program calculation.

The calculation is simple if one makes four assumptions. 1) The electric field in the wells is zero; 2) the bands are parabolic; 3) the electrons are randomly excited in

any direction and 4) there are no collisions before it reaches the barrier.

The energy in the z-direction that the electron has when it surmounts the barrier is labeled E_{zb}. The energy of the photon is E_λ and the barrier height is ΔE_c. The equation becomes

$$E_{zb} = E_\lambda \cos^2\gamma + E_{ez} - \Delta E_c$$

where γ is the angle between the electron k vector due to the absorption and the direction perpendicular to the layers. E_{ez} is the electron energy in the direction perpendicular to the layers before excitation. If one assumes $E_{ez} \ll \Delta E_c$, then

$$E_{zb} = E_\lambda \cos^2\gamma - \Delta E_c \ .$$

The largest angle γ allowed for the electron to cross the barrier occurs when E_{zb} equals zero. Hence,

$$\cos\gamma_{max} = \left(\frac{\Delta E_c}{E_\lambda} \right)^{1/2} .$$

γ_{max} can be thought of as the angle of a cone of passage. The axis of the cone points along the direction perpendicular to the layers. Since there is no electric field in the well(assumption 1), the distribution should be random in direction. Any electrons such that their k vector lies within this cone will surmount the barrier. The smaller the barrier height or the larger the photon energy, the larger the angle.

To find the percentage of electrons that cross the barrier(η_{ow}), one must calculate the ratio of the steradian area of the cone to the steradian area of the sphere.

$$\eta_{ow} = -\frac{1}{4\pi} \int_0^{\gamma_{max}} \int_0^{2\pi} d\phi \, d(\cos\gamma)$$

or

$$\eta_{ow} = 1 - \cos\gamma_{max} = 1 - \left(\frac{\Delta E_c}{E_\lambda} \right)^{1/2}$$

where η_{ow} stands for the quantum efficiency of an open well.

Table B-6.2 compares the equation presented above to the results of a Monte Carlo calculation. The electron distribution for this Monte Carlo calculation is displayed in table B-6.1.

Table B-6.1
Electron distribution for the
Monte Carlo results of Table B-6.2

$E-E_c$ (eV)	distribution (# of electrons)
.001	155
.002	21
.003	2
$\geqq$ .004	0

For this distribution, $E_{ez} \ll \Delta E_c$ and the quantum efficiency values are shown in table B-6.2 as the effective mass is varied.

The main purpose of table B-6.2 is to show that as the mass increases, one cannot make the assumption that there are no collisions before the electron approaches the barrier. This demonstrates that as the mass increases, the rate of collisions increases(This is related to the increase in the density of states).

B-6.4 Analysis of quantum efficiency in a partly closed well

An analytical solution is now presented for the partly closed well. Two assumptions are made for this analysis. 1) It is assumed that the electron will drop into the well if it is in the proper energy range. In other words, the electron will not escape from the well until several collisions have occurred. For large effective masses and photon energies comparable to the barrier height, this is a fairly good assumption(See sec. B-6.3). 2) The inelastic phonons all have the same energy value, $k\theta$.

With these assumptions, the efficiency can be calculated using the following equation.

Table B-6.2
Comparison of the analytical and
Monte Carlo quantum efficiencies for an open well

ΔE_c(eV)	E_λ(eV)	η_{ow}	η - Monte Carlo $m^*=.082m_o$	$m^*=.100m_o$	$m^*=.200m_o$
.0254	.03	7.98	8	7	3
	.04	20.4	17	15	7
	.05	28.7	24	22	12
.0511	.06	7.7	6	6	2.8
	.07	14.6	12	10	4.7
	.08	20.1	16	17	8.1
.0769	.08	2.0	3	2.4	.45
	.09	7.6	7	6	3.1
	.10	12.3	12	10	4.7
.1029	.11	3.3	3	2.2	1.1
	.12	7.4	6	4.6	4.2
	.13	11.0	11	8.9	5.3

$$\eta_{pcw}(E_\lambda) = 1 - \frac{\int_{E_\lambda}^{E_\lambda+E_F} \mathrm{rect}\left[\frac{E-E_F-ik\theta-\frac{E_{cb}-E_F}{2}}{E_{cb}-E_F}\right] D(E-E_\lambda)dE}{\int_{E_{d1}}^{E_F} D(E)dE} - \frac{\int_{E_{d0}}^{E_{cb}} D(E-E_\lambda)dE}{\int_{E_{d1}}^{E_F} D(E)dE}$$

where i is an integer greater than or equal to 1, D(E) is the density of states,

$$\mathrm{rect}\left[\frac{t}{\tau}\right] = 1 \text{ if } \left|\frac{t}{\tau}\right| < 1/2$$

$$\mathrm{rect}\left[\frac{t}{\tau}\right] = 0 \text{ if } \left|\frac{t}{\tau}\right| > 1/2$$

and

$$E_{d1} = E_F - E_\lambda \text{ if } E_\lambda < E_F - E_{cw}$$

$$E_{d1} = E_{cw} \text{ if } E_\lambda > E_F - E_{cw} \ .$$

The last term in the previous integral equation is valid for the situation, $E_\lambda < E_{cb} - E_{cw}$, where

$$E_{d0} = E_F \text{ if } E_\lambda < E_F - E_{cw}$$

$$E_{d0} = E_\lambda + E_{cw} \text{ if } E_\lambda > E_F - E_{cw} \ .$$

The physical description of the integral equation is shown in Fig. B-6.1. There are energy ranges ΔE_{te} wide that are separated $k\theta$ apart. As the distribution function is shifted an amount E_λ(the photon energy) towards the ΔE_{te} energy ranges, any part of the distribution that falls within these energy ranges(the shaded regions in Fig. B-6.1) is assumed to be captured because the electron can emit inelastic phonons until it drops in the well. Outside of these ranges, it is not possible to drop into the well due to inelastic phonon processes alone.

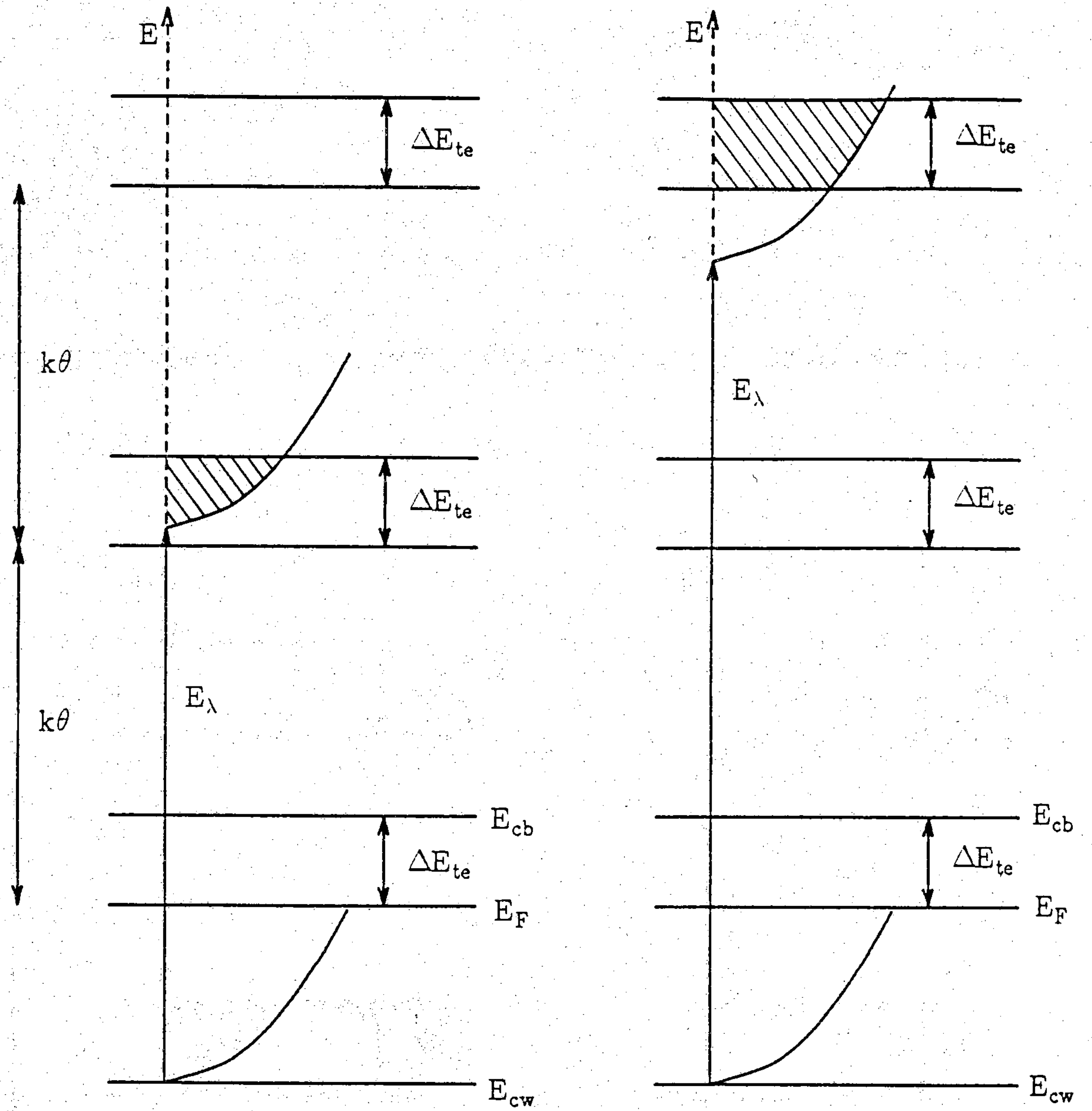

Figure B-6.1 Physical picture of $\eta_{pcw}(\hbar\omega)$

A comparison between the quantum efficiency for the Monte Carlo calculation η_{mc} and the analytical quantum efficiency η_{pcw} is presented in table B-6.3. The physical parameters of the run are listed in table B-9.1 under the run number 25mx1.

Table B-6.3
Comparison of the analytical and Monte Carlo
quantum efficiencies for a partly closed well

	ΔE_{te}=.0101 eV		ΔE_{te}=.02 eV		ΔE_{te}=.0303 eV		ΔE_{te}=.0401 eV	
E_λ(eV)	η_{mc}	η_{pcw}	η_{mc}	η_{pcw}	η_{mc}	η_{pcw}	η_{mc}	η_{pcw}
.01	0	0	0	0	0	0	0	0
.02	33	34	0	0	0	0	0	0
.03	74	78	32	40	0	0	0	0
.04	76	80	53	55	16	18	0	0
.05	57	62	36	36	11	13	1	0
.06	69	71	26	33	8	8	3	0
.07	86	88	57	60	15	17	7	0
.08	68	64	59	51	25	21	4	0
.09	67	64	40	27	22	16	5	0
.10	75	75	47	44	18	2	18	0

For small photon energies, the analytical efficiencies are larger because in the Monte Carlo calculation, it is assumed that any electron that doesn't surmount the barrier after an arbitrary number of collisions will drop into the well.

For large photon energies, γ_{max} gets large enough(See sec. B-6.3) that it takes several phonon emissions for the electron to drop in the well. In other words, assumption 1 presented at the start of this section is not correct, because the photon energy is too large.

The second observation is that as ΔE_{te}(See sec. B-5.4) increases, the quantum efficiency decreases. This happens because a larger percentage of excited electrons are excited to the energy ranges shown in Fig. B-6.1 which in turn means a larger percentage is captured in the wells before escape.

B-7. NOISE AND D^*

B-7.1 Introduction

In this chapter, the determination of D^* for the SLIP is discussed. Since the SLIP is operated in the infrared region, one of the most important noise sources will be due to the background. This and the other noise sources of interest are listed in sec. B-7.2. One of the advantages of the SLIP is the inherent filtering mechanisms in the device. These mechanisms are presented in sec. B-7.4.

B-7.2 Noise terms[68,140,141]

There are five noise terms of interest in an infrared photodetector - Recombination-generation(RG) noise, background noise, shot noise, thermal noise, and amplifier noise[140,68]. Putley[140] considers three more(for extrinsic photoconductors), but these will be neglected at this time.

B-7.3 D^*

D^* depends on the wavelength, the frequency of modulation, and is defined to have a bandwidth of 1 Hz. The wavelength dependence of D^* is discussed in sec. B-7.5. The modulation frequency is related to the response time.

D^* is calculated by finding the Noise Equivalent Power(NEP). NEP is defined as the minimum amount of radiation power incident on the detector needed to obtain a Signal to Noise ratio(S/N) equal to 1[24,68,142,143]. NEP can be obtained as follows[68]

$$I_s = I_{op}G = \sqrt{2(\overline{I_n^2})}$$

and

$$\overline{I_n^2} = 4\,e\,(I_d + I_{op}G + I_BG)\,G\,\Delta B + \frac{4kT\Delta B}{R}$$

where G is the gain, $I_{op}G$ is the current produced by the signal, hereafter known as the signal current or I_s(See sec. B-5.2), I_d is the dark current, I_B is the background current[22], ΔB is the bandwidth, and R is the resistance of the circuit. In the

SLIP(See secs. B-5.4 and B-5.5. I_{tn} is assumed to be negligible),

$$I_d = I_{te}G$$

where I_{te} is defined in sec. B-5.4.

Using the quadratic equation,

$$I_s = 4Ge\Delta B + (16(Ge\Delta B)^2 + 8(eG(I_{te}G + I_BG) + \frac{kT}{R})\Delta B)^{1/2} .$$

If $I_{te}G+I_BG$ is large enough and ΔB is small enough[68], then

$$I_s = \sqrt{8e\ (I_{te} + I_B)(G^2)\ \Delta B} .$$

Hence[68]

$$D^* = \frac{(\frac{e}{E_\lambda})\ \eta \sqrt{A_D}}{\sqrt{4e\ (I_{te} + I_B)}}$$

where E_λ is the energy of the photon and A_D is the area of the detector.

B-7.4 Filtering of background radiation

There are two obvious inherent filtering mechanisms in the SLIP. The first is due to free carrier absorption while the second is due to phonon absorption.

Free carrier absorption has the interesting property that as the wavelength decreases, the absorption also decreases. Most of the blackbody radiation at 300 K occurs at wavelengths around 10 μm. If one designed the SLIP for wavelengths around 50 μm or longer, some of the background noise around 10 μm will be effectively filtered out. For a more in depth description of this phenomenon and how D^* is affected by it, see sec. B-7.5.

The other filtering mechanism is the absorption of radiation due to phonon emission alone. For GaAs, the phonon absorption exceeds $5x10^4 cm^{-1}$[144]. In the barrier layers, the photons could be absorbed by these phonons, effectively filtering

out this wavelength range. Since the phonon energy changes as the composition in AlGaAs changes, there would be some freedom in filtering specific wavelengths. This filtering could take place in AlGaAs from .0354 eV(35 μm, 285 cm^{-1} - for GaAs) to .05 eV (24.8 μm, 403 cm^{-1} - for AlAs)[137]. Other compositions, such as InGaAs, could filter different wavelength ranges.

B-7.5 D^*_{BLIP}

D^*_{BLIP}(Background Limited Infrared Photodetector) is defined as the D^* value when the main source of noise is the background noise. For a background temperature of 300 K, a sufficiently low operating temperature, and a photodetector operating in the wavelength range greater than 3 μm, background noise becomes a major source of noise. In general(See sec. B-7.3),

$$D^*_{BLIP} \propto \frac{\lambda}{\sqrt{I_B}}$$

where it is assumed that the quantum efficiency is one at the wavelength that the detector is designed to collect. This wavelength will be labeled λ_s.

In a conventional detector, the noise is due to all the photons with energies greater than the band gap(for 2 carrier detectors). Since most of the background noise is in the 10 μm range for a background temperature of 300 K, the slope downward of D^*_{BLIP} as the wavelength increases is due to the increase in noise(See Fig. B-7.1). D^* begins to increase when the wavelength is greater than 20 μm because the photon wavelength is increasing. This increase in wavelength is larger than the increase in I_B(See sec. B-5.3).

In the SLIP, all radiation with a wavelength longer than λ_s is collected. This is due to the special relationship that as the wavelength increases, the free carrier absorption coefficient increases. For wavelengths shorter than λ_s, the absorption coefficient decreases. The significance of this is that if λ_s is long enough(ie. greater than 30 μm), then the major portion of background noise at 10 μm can be filtered out.

This tradeoff of high energy background noise for low energy background noise is an advantage until λ_s gets so short that the background noise is collected over the entire spectrum. As can be seen in Fig. B-7.1, the SLIP has a larger D^* than the conventional photoconductor when λ_s is longer than 25 μm and a smaller D^* when λ_s is shorter than 15 μm. A word of caution, though. There are several approximations

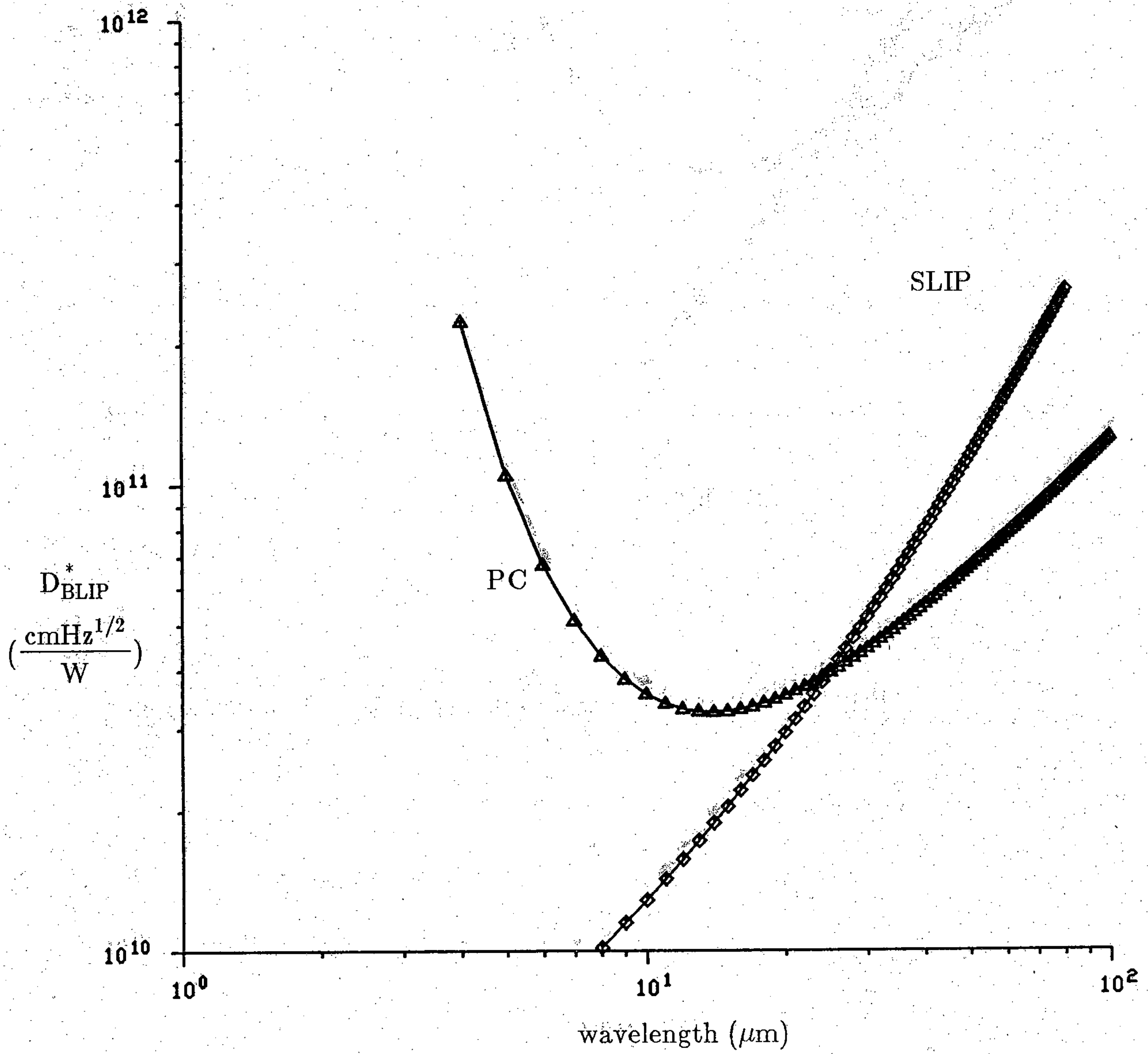

Figure B-7.1 D^*_{BLIP} for the conventional PC and for the SLIP

used in making this figure. For instance, free carrier absorption depends upon the index of refraction and the index of refraction depends upon absorption, so the index of refraction does change. This change is not taken into account in Fig. B-7.1.

B-8. PARAMETER LIMITATIONS

B-8.1 Introduction

In this chapter, the limitations of the SLIP are presented. The following sections predominantly refer to n-type material, conduction bands, and electrons. Similar results are obtained for p-type wells, valence bands and holes.

B-8.2 Free carrier absorption limits

For a description of the limits on free carrier absorption, see sec. B-3.2.

B-8.3 Quantum efficiency limitations of the SLIP

In this section, the wavelength range is determined for an n-type well. A similar argument can be used for p-type wells with the same results.

E_{m0} is the minimum detectable radiation energy and equals $E_{cb} - E_F$(See Fig. B-1.3). This is true if the free carrier absorption is due to an elastic process such as impurity scattering or an essentially elastic process such as acoustic scattering. If the scattering is due to inelastic scattering with an energy $k\theta$, then E_{m0} must be redefined as $E_{cb} - E_F + k\theta$. This appears to be avoidable because at high concentrations, the free carrier absorption due to impurity scattering is much larger than the free carrier absorption due to optical or acoustical phonons[138].

The minimum photon energy needed to excite the least energetic electron out of the well, E_{m1}, would equal the barrier height, $\Delta E_c = E_{cb} - E_{cw}$(See Fig. B-1.3), where E_{cw} is the conduction band level for the quantum well.

$$E_{m1} = E_{m0} + E_F - E_{cw} .$$

$E_F - E_{cw}$ is related to the free carrier concentration in the well. Assuming a parabolic band, the relationship between $E_F - E_{cw}$ and n is(T=0K)

$$n = \frac{4.56\text{x}10^{21}}{\text{cm}^3\ \text{eV}^{3/2}} \left((m_t^*)^2\ m_l^*\right)^{1/2} M_c\ (E_F - E_{cw})^{3/2}$$

where m_t^* and m_l^* are the effective masses(unitless), and M_c is the number(unitless) of valleys.

Free carrier absorption depends on n and approximately on the square of the photon wavelength. There is some disagreement about the validity of these relationships(See [110,111] and sec. B-3.2) at longer wavelengths. The free carrier absorption coefficients in GaAs, InAs, and any other desirable material need to be experimentally confirmed.

With these requirements and relationships,

$$E_{m1} = E_{m0} + \left(\frac{n(\ \alpha \geqq\ 10^4/\mathrm{cm}\ )}{4.56\mathrm{x}10^{21}}\ \frac{1}{((m_t^*)^2\ m_l^*)^{1/2}\ M_c}\right)^{2/3} .$$

This equation determines the minimum photon energy detectable for high efficiencies.

E_{m1} is not necessarily a hard limit. Any energy in between E_{m1} and E_{m0} can be detected. The closer the energy is to E_{m0}, the smaller the quantum efficiency.

B-8.4 Wavelength range of the SLIP

The long wavelength limit is determined by the ability to grow a large number of wells with a small variance. As the error in growth due to the epitaxial process gets smaller, longer wavelengths can be detected.

The short wavelength limit will be determined by the ability to make a wide area photodetector with some consistency[25,26]. Since there appears to be much trouble with HgCdTe at this time[25,26], this wavelength is around 7 μm. At these wavelengths, D^*_{BLIP} is better for the conventional photodetectors (because the SLIP collects background energy greater than AND less than the signal energy(See sec. B-7.5)). Even if one filters out the background noise, the dark current noise(RG noise due to thermal excitations) is expected to be smaller in conventional photodetectors at comparable operating temperatures.

B-8.5 Temperature limitations

To obtain a high quantum efficiency, the energy difference between the barrier conduction band level E_{cb} and the Fermi level E_F must be less than the optical and intervalley phonon energies(See the partly closed well case in sec. B-6.2). The smaller $E_{cb}-E_F = \Delta E_{te}$, the higher the quantum efficiency. Simultaneously, ΔE_{te} must be large enough to prevent the thermionic emission current, I_{te}, from getting too large. If the background radiation isn't filtered out, the thermionic emission current noise will become comparable to the background noise when $J_{te} \simeq\ .1\mathrm{A/cm}^2$(See sec. B-5.3).

If one assumes that the smallest optical or intervalley phonon energy is $k\theta_{min}$, then the temperatures of interest would be where J_{te} is less than or equal to .1 A/cm^2 and ΔE_{te} is less than $k\theta_{min}$.

Table B-8.1 shows how ΔE_{te} varies as one varies the temperature and the thermionic emission current. If one assumes that ΔE_{te} must be less than .02 eV, then the highest possible operation temperature is 18 K.

Table B-8.1
Temperature dependence on the thermionic emission current

J_{te}	ΔE_{te} (eV)						
(A/cm^2)	T=4.2K	5K	10K	12K	14K	18K	20K
10^{-1}	.00362	.0044	.0100	.0125	.0149	.0200	.0225
10^{-2}	.00445	.0054	.0120	.0149	.0178	.0235	.0265
10^{-3}	.00528	.0064	.0140	.0172	.0205	.0271	-
10^{-4}	.00611	.0074	.0160	.0196	.0233	-	-
10^{-5}	.00694	.0084	.0180	.0220	.0260	-	-
10^{-6}	.00777	.0094	.0200	.0244	-	-	-
10^{-7}	.00861	.0104	.0220	.0268	-	-	-
10^{-8}	.00949	.0114	.0240	-	-	-	-
10^{-9}	.0103	.0124	.0260	-	-	-	-
10^{-10}	.0111	.0134	-	-	-	-	-

The main problem of the SLIP is this temperature limitation. In the partly closed well case, for the thermionic emission current to be less than 10^{-6} amps the device must be operated at 10 K or less. This low temperature limit means that the device must be cooled using liquid helium.

One way to overcome this temperature limitation is to propagate the radiation at an oblique angle to the superlattice layers(See sec. B-4.3). Then $E_{cb} - E_F$ could be greater than $k\theta_{min}$, the well becomes an open well and the quantum efficiency will depend on the probability of one collision occuring before the electron escapes from the well(See sec. B-6.3).

A comparison of a conventional extrinsic photoconductor with the two cases of the SLIP(open well and partly closed well cases) yields the following results: 1) For a conventional photodetector, the temperature is limited by E_λ, 2) For propagation in the direction perpendicular to the layers in the SLIP, the temperature is limited by

the smaller of the two energies - $k\theta_{min}$ or E_λ, and 3) For propagation along a direction oblique to the layers in the SLIP, the temperature can be limited by E_λ.

In summary: 1) the SLIP incorporating partly closed wells will have a lower temperature of operation than an extrinsic PC designed to detect the same wavelength, 2) the SLIP incorporating open wells should have the same temperature of operation as an extrinsic PC designed to detect the same wavelength, and 3) if the photon energy, E_λ, is less than the phonon energy, $k\theta_{min}$, the wells are necessarily partly closed AND should have the same temperature of operation as an extrinsic PC designed to detect the same wavelength.

B-8.6 Material limitations

There are 3 types of materials that can make up the well - semiconductors with large electron density, zero gap semiconductors, and metals. The best one to use would be the first type. It is easier to grow semiconductor on semiconductor and the barrier height is easier to adjust than metal or semimetal systems.

The problem with metals is that they tend to be different crystal structures than semiconductors or insulators. Consequently, the superlattices grown are not crystalline. This can cause conduction problems and make the barrier height hard to control. Finding materials that have a barrier height of .01 eV - .03 eV at the metal interface is also a problem.

The zero gap semiconductor(ZGS) has one advantage over the metals - there have been superlattices grown that incorporate them and maintain a crystalline structure[145]. The major problem is to find a wide gap semiconductor or insulator (The gap should be wide enough to prevent direct gap absorption of the background radiation) that lattice matches the ZGS and has a barrier difference of approx. .01 eV. These requirements may be met, but at this time it is much easier to meet them using a more conventional superlattice. Even if these problems are solved in the future, the narrow gap intrinsic photoconductor will probably be much easier to make since the materials in both devices would most likely involve HgCdTe.

The best way to get a crystalline structure, a controllable barrier height and materials that are easy to grow would be to use a semiconductor as the well material. Carriers would be placed in the well by 1) degenerately doping the semiconductor well or 2) doping the barriers and have the electrons fall into the well(modulation doping). One system that must be considered is AlGaAs. p-type dopants in the AlGaAs will probably be used because it's easier to dope AlGaAs p-type than n-type in an MBE system[109,146]. Another reason is the density of states in the valence band is larger than the density of states in the conduction band for GaAs.

B-8.7 $E_F - E_{cw}$ limitations.

Ideally, the density of states should be as large as possible, which minimizes $E_F - E_{cw}$. One major reason that the density of states should be large is because the smaller the density of states, the higher the barrier height - the higher the barrier height, the smaller the maximum cone angle γ_{max}(See sec. B-6.3) - the smaller γ_{max}, the lower the quantum efficiency AND the longer the response time. A small $E_F - E_{cw}$ value appears to be desirable for any wavelength.

With modulation doping, it is difficult to get enough electrons to fall into the well. Only a fraction will reside in the well. The rest would become confined in the barrier. Using the graded barrier shown in Fig. B-1.2, it may be possible to inject a larger portion of the electrons into the barrier.

If the wells are heavily doped semiconductors, then one must consider band gap narrowing and it's associated effects[114-118]. It seems that one can assume k vs. E values similar to an intrinsic case, with the effective mass slightly less than the intrinsic case[115,147]. With these results, the only real limitation to $E_F - E_{cw}$ is the amount of dopant that can be added to the well material in the MBE growth. For instance in GaAs, the maximum amount of n-type dopants is about 10^{18} to $10^{19}cm^{-3}$[146] while for p-type dopants, the maximum amount is about 10^{19} to $10^{20}cm^{-3}$[148]. For these values, $E_{vw} - E_F$ is approximately .02 eV for the p-type well where $p \simeq 2x10^{19}cm^{-3}$ and $E_F - E_{cw}$ is approximately .02 eV for the n-type well where $n \simeq 2x10^{18}cm^{-3}$. Hence, the p-type well in GaAs is a more desirable possibility.

B-8.8 $E_{cb} - E_F$ limitations.

For the partly closed well-perpendicular incidence mode, the main limitation is

$$E_{cb} - E_F \leqq k\theta_{min}$$

where $k\theta_{min}$ is the smallest energy value of the inelastic phonons - intervalley phonons or optical phonons(See sec. B-6.2). The smaller $E_{cb} - E_F$ is compared to $k\theta_{min}$, the higher the quantum efficiency(See sec. B-6.2 and B-6.4). The tradeoff is that the smaller $E_{cb} - E_F$, the larger the dark current(See sec. B-5.4 and sec. B-8.5).

For the open well-oblique incidence mode(assuming the proper polarization(See sec. B-4.3)),

$$E_{cb} - E_F \leqq E_\lambda \cos\gamma_{inc}$$

where γ_{inc} is the angle between the direction of propagation of the incident radiation wave and the plane of the layers. The relationship between the quantum efficiency and $E_{cb}-E_F$ is explained in sec. B-6.3.

B-9. THEORETICAL PERFORMANCE OF THE SLIP

B-9.1 Introduction

This chapter briefly presents a possible set of results for the SLIP. It is assumed there is NO impact ionization. The important device parameters considered are η, D^*, τ, the gain(G), and the RC time constant.

B-9.2 Description of the computer runs

In the SLIP computer runs presented in this section, the absorption coefficients in table B-3.1 are used. The absorption coefficient is chosen to be $10^4 cm^{-1}$. It is assumed that most of the free carrier absorption is due to impurities scattering[138]. The barrier widths are 2000 Å; the well widths are 200 Å. The number of wells used in the program equals 50. The operating temperature is 5 K. The 2D effects are assumed to be negligible on the absorption coefficient because the effective mass is .45 m_o.

The electrons are in the Γ valley(For a definition of the Γ valley, see [24]). The runs are for a single spherical valley material. Intervalley scattering and its associated effects are assumed to be negligible. The inelastic phonon energy, $k\theta$, equals .035 eV.

The direction of radiation propagation in the program was assumed to be isotropic. This assumption is acceptable since the partly closed well is considered in this case(See sec. B-6.2).

In table B-9.1, the run is labeled first with a number, then mn(for minimum) or mx(for maximum). Some runs have an additional number. The first two digit number is the wavelength of radiation and E_λ is the energy of the radiation. Hence, the SLIP is tested at four different wavelengths. mx means that the $10^4 cm^{-1}$ absorption coefficients in table 3.1 are used. mn means that the carrier concentration parameters for the $10^5 cm^{-1}$ absorption coefficients in table 3.1 are used while the actual absorption is assumed to be $10^4 cm^{-1}$. The last number merely distinguishes between mx runs.

For table B-9.1, E_{cb} and E_{cw}(See Fig. B-1.3) can best be described by the equation

$$\Delta E_c = E_{cb} - E_{cw}$$

Table B-9.1
Material parameters for the
SLIP computer runs

run	E_λ(eV)	$E_F - E_{cw}$(eV)	$E_{cb} - E_F$(eV)	ΔE_c(eV)	n(cm^{-3})	J_{te}(A/cm^2)
99mx1	.0125	.005	.007	.0121	5.e17	1.e-5
99mx2	.0125	.008	.005	.0127	9.e17	1.e-3
99mn	.0125	.026	.007	.0330	6.e18	1.e-5
50mx1	.025	.0128	.010	.0229	2.e18	1.e-9
50mx2	.025	.0128	.007	.0203	2.e18	1.e-5
50mn	.025	.0780	.007	.0847	3.e19	1.e-5
25mx1	.05	.0323	.010	.0424	8.e18	1.e-9
25mx2	.05	.0323	.007	.0394	8.e18	1.e-5
25mn	.05	.0780	.007	.0847	3.e19	1.e-5
12mx1	.1	.0780	.010	.0873	3.e19	1.e-8
12mx2	.1	.0780	.007	.0847	3.e19	1.e-5

where ΔE_c is the barrier height of the junction between the well and the barrier. n is the carrier concentration in the well and J_{te} is the thermionic emission current density.

B-9.3 Results of the computer runs

Tables B-9.2 to B-9.5 contain the pertinent results for the SLIP using a Monte Carlo transport program. η is the quantum efficiency of the device(See chap. B-6). D^* is calculated for background limited detection since the thermionic emission currents in table B-9.1 are much smaller than the background current(See sec. B-5.3).

τ_{esc} is the amount of time needed for the electron to escape from the well and reach the adjacent well.

τ is the lifetime of the device. In the SLIP, τ is equal to the mean time between when the electron is excited and the time the electron falls back into another well.

G is the gain of the device. For background limited detectors, gain is only important when considering how to improve the time response, how to increase the signal current, or how to make the charge distribution more uniform during radiation excitation.

The values defined above are calculated from a Monte Carlo program. The number of trials is very small, so the values in tables B-9.2 to B-9.5 are rough approximations. These approximate values could be used as a gauge for either n-type or p-type doping with an effective mass of .45 m_o.

η and in turn D^* are believed to be close to their actual value, assuming that partly closed wells can be fabricated(See sec. B-6.4). η should be fairly independent of the electric field in the barriers. τ, τ_{esc} and G are approximate values because they depend more upon the material parameters. These numbers are not nearly as important though, because they can easily be adjusted by changing the field.

The conclusions from tables B-9.2 to B-9.5 are: 1) For gains greater than 1, the electric field in the barrier(ξ_b) may have to be around 30 kV/cm. 2) The lifetime appears to be around 100 psec.. 3) The quantum efficiencies, even for the mn runs, are better than the results of the tunneling IS-PC(See sec. B-2.2.3).

B-9.4 RC time constant of the SLIP

The dielectric relaxation time is the optimum RC time constant in the SLIP. This optimum RC time constant is calculated in this section.

Table B-9.2
Monte Carlo results for photons
with 100 μm wavelength

run	ξ_b(kV/cm)	η	$D^*(\frac{cmHz^{1/2}}{W})$	τ_{esc}(psec)	τ(psec)	G
99mx1	5	100	7.e11	11	19	.06
99mx1	15	100	7.e11	10	89	.19
99mx1	25	100	7.e11	28	179	.85
99mx1	35	100	7.e11	25	187	2.28
99mx2	5	100	7.e11	22	64	.14
99mx2	15	100	7.e11	27	231	.42
99mx2	25	100	7.e11	31	111	.64
99mx2	35	100	7.e11	23	276	2.68
99mx2	45	100	7.e11	17	179	3.34
99mn	5	36	2.5e11	39	90	.14
99mn	15	32	2.5e11	43	104	.12
99mn	25	36	2.5e11	57	226	.40
99mn	35	32	2.5e11	37	124	.84
99mn	45	32	2.5e11	48	141	1.61

Table B-9.3
Monte Carlo results for photons
with 50 μm wavelength

run	ξ_b(kV/cm)	η	$D^*(\frac{cmHz^{1/2}}{W})$	τ_{esc}(psec)	τ(psec)	G
50mx1	5	100	1.4e11	24	97	.72
50mx1	15	100	1.4e11	26	250	.24
50mx1	25	100	1.4e11	23	116	.32
50mx1	35	100	1.4e11	32	180	1.14
50mx1	45	100	1.4e11	25	152	1.36
50mx2	5	100	1.4e11	24	73	.08
50mx2	15	100	1.4e11	11	183	.27
50mx2	25	100	1.4e11	15	175	.71
50mx2	35	100	1.4e11	23	114	1.72
50mx2	45	100	1.4e11	12	110	1.88
50mn	5	63	8.e10	37	118	.23
50mn	15	58	8.e10	30	97	.27
50mn	25	63	8.e10	47	158	.61
50mn	35	63	8.e10	29	138	2.66

Table B-9.4
Monte Carlo results for photons
with 25 μm wavelength

run	ξ_b(kV/cm)	η	$D^*(\frac{cmHz^{1/2}}{W})$	τ_{esc}(psec)	τ(psec)	G
25mx1	5	56	2.e10	49	86	.08
25mx1	15	58	2.e10	54	111	.11
25mx1	25	57	2.e10	30	82	.33
25mx1	35	61	2.e10	24	110	1.08
25mx1	45	53	2.e10	32	124	1.8
25mx2	5	72	3.e10	34	96	.14
25mx2	15	74	3.e10	32	86	.16
25mx2	25	69	3.e10	31	69	.52
25mx2	35	69	3.e10	27	123	1.32
25mx2	45	72	3.e10	18	118	3.00
25mn	5	65	3.e10	44	135	.32
25mn	15	71	3.e10	21	71	.29
25mn	25	69	3.e10	24	86	.83
25mn	35	69	3.e10	29	139	1.42

Table B-9.5
Monte Carlo results for photons
with 12.5 μm wavelength

run	ξ_b(kV/cm)	η	$D^*(\frac{cmHz^{1/2}}{W})$	τ_{esc}(psec)	τ(psec)	G
12mx1	5	72	1.e10	27	100	.22
12mx1	15	88	1.e10	40	96	.20
12mx1	25	79	1.e10	37	91	.49
12mx1	35	79	1.e10	30	109	1.49
12mx2	5	84	1.e10	32	118	.24
12mx2	15	84	1.e10	24	103	.30
12mx2	25	84	1.e10	35	138	.86
12mx2	35	91	1.e10	18	119	1.93

The relationship between the dielectric relaxation time(τ_d) and the optimum RC time constant is

$$RC = \frac{\rho L}{A}\frac{\epsilon}{L}A = \rho\epsilon = \tau_d$$

where ρ is the resistivity,

$$\rho = \frac{1}{e\mu n}$$

and ϵ is the static dielectric constant.

Typically $n \simeq 10^{10} cm^{-3}$[32]. For GaAs, $\mu \simeq 50{,}000 cm^2/V{-}sec$[27] and $\epsilon = 12\epsilon_o$ [15]. For these numbers[27],

$$RC = 13.2 x 10^3 \text{ psec.}$$

When comparing this optimum RC time constant with the the lifetimes in tables B-9.2 to B-9.5, it can be seen that the device will be limited by the RC time constant, not the lifetime.

B-9.5 Comparison with conventional photoconductors

Approximate D^* values of the runs presented in sec. B-9.3 are shown in Fig. B-9.1(As stated in sec. B-7.5, the D^*_{BLIP} curve for the SLIP is a rough approximation). The corresponding response times for these SLIPs are about 10^{-8} sec.(See sec. B-9.4). Similar curves of conventional photodetectors are shown in Fig. B-9.2 with their corresponding response times.

From these results, assuming that the well can be partially closed, it can be seen that the SLIP can be competitive with conventional photoconductors. The ultimate question is whether the well can be partially closed.

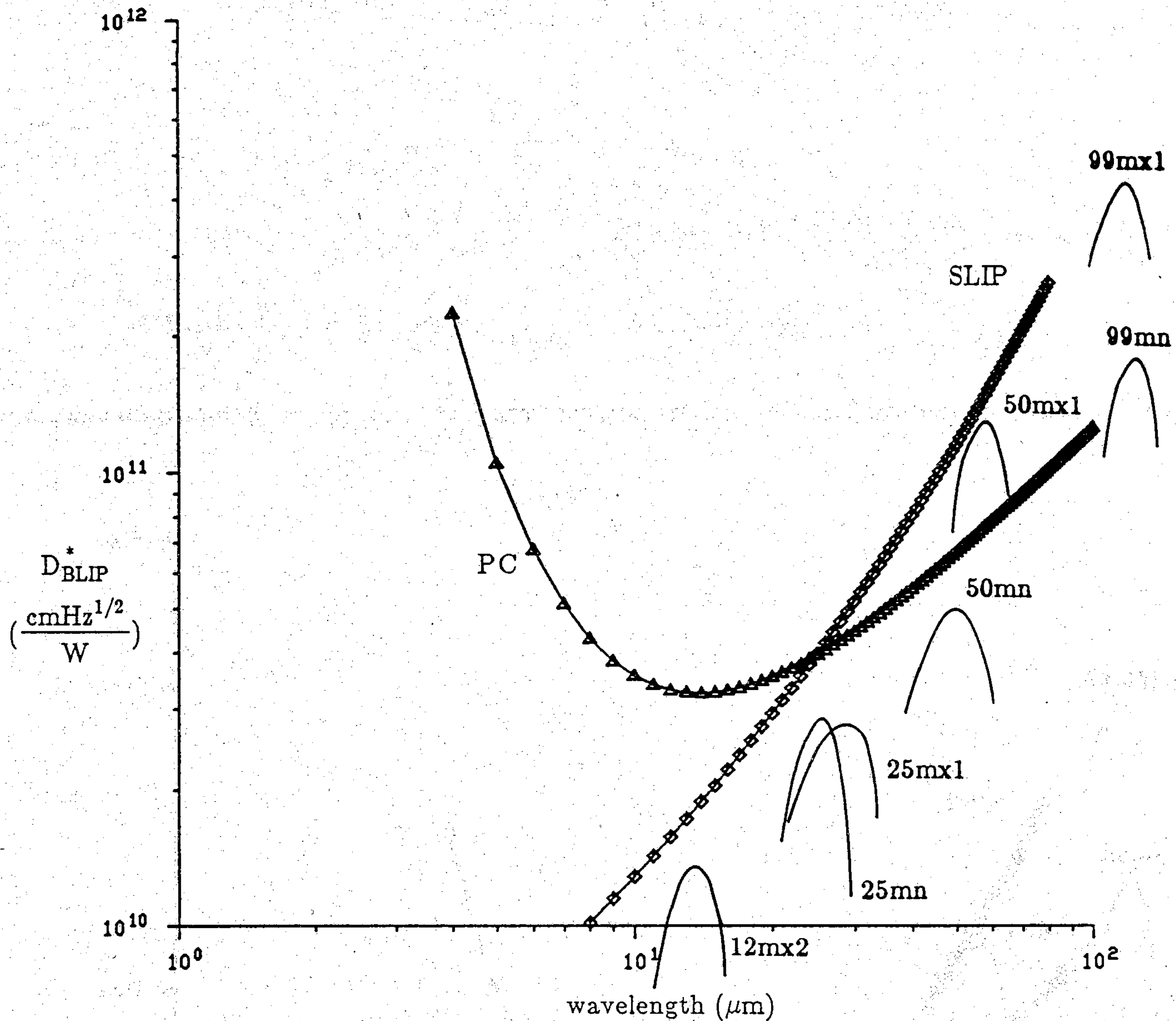

Figure B-9.1 Theoretical D^* for some SLIPs

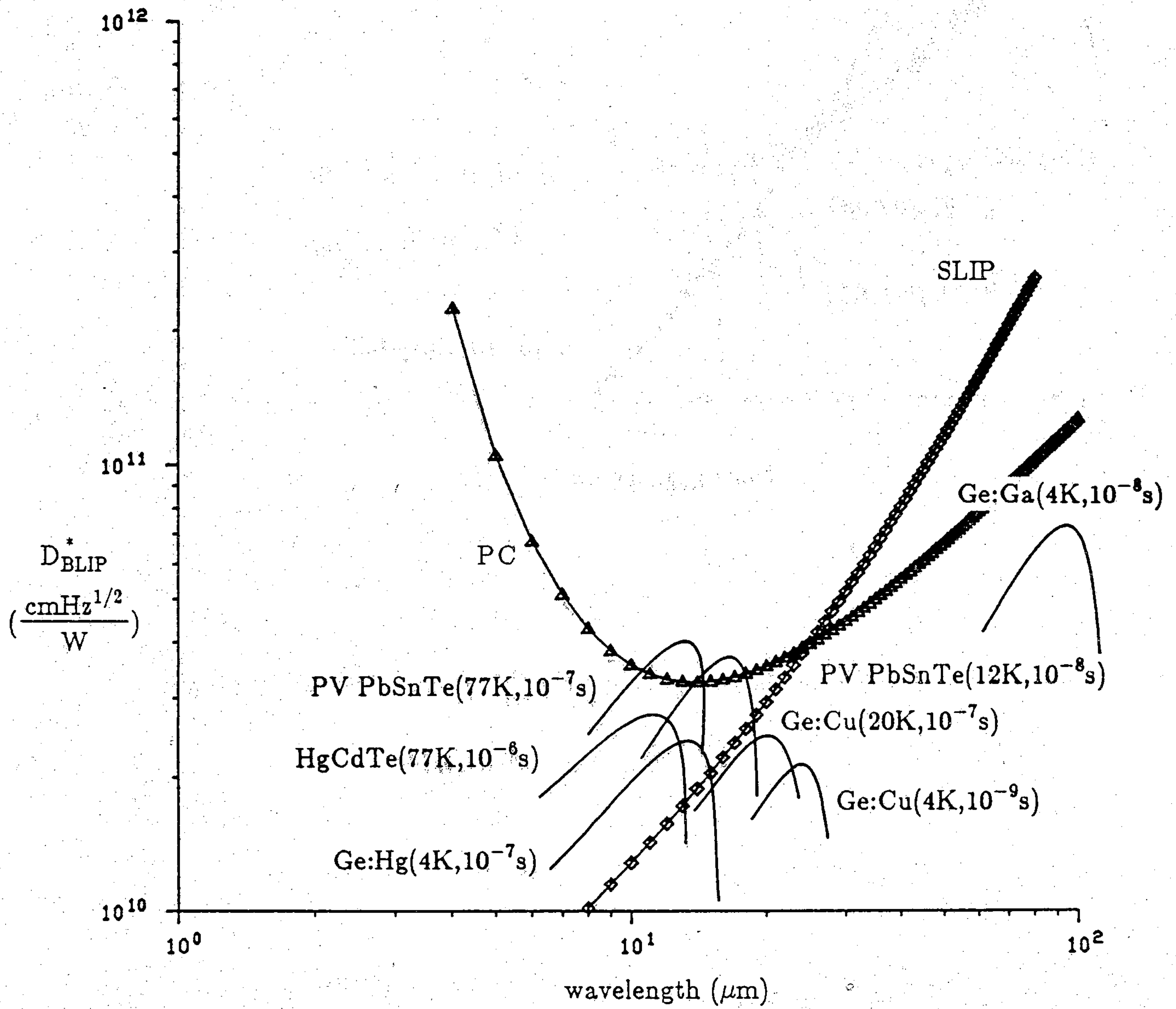

Figure B-9.2 Experimental D^* for some conventional photodetectors

B-10. SUMMARY AND FUTURE RECOMMENDATIONS

B-10.1 Summary of the report

An infrared photoconductor, designated as the SLIP, has been proposed to detect wavelengths from 7 μm to more than 100 μm. There are five modes of operation. The partly closed well case(See sec. B-6.2) has three different modes. All should have high efficiencies. The temperature of operation will have to be around 10 K. The open well case(See sec. B-6.2) has the other two modes. The operating temperature of this mode can be higher than the partly closed well case, but the efficiency should be lower. The design of the device is simple and it appears that an AlGaAs superlattice with p-type GaAs wells should be a feasible material. The GaAs p-type density of states is about as small as one can get and still get a reasonable efficiency. A more desirable material would be a large density of states material, either p-type or n-type.

The SLIP appears to be very competitive against the most promising photoconductors presented in the literature(See chap. B-2).

The SLIP would be best suited to be incorporated into an array. It should have a high absorption coefficient, which means there should be little optical crosstalk[21,34]. It can be made up of materials with stable properties, which means that the array should be uniform in its response(A major weakness in HgCdTe arrays[25,26]). In addition, impact ionization(See sec. B-1.4.4) could very well be an asset in a CID or CCD array and even the excess noise due to impact ionization could possibly be neglected[73,74,39].

There are some problems that must be addressed. First, if the theoretical free carrier absorption coefficients are assumed to be correct, the device should work very well. There may be a discrepancy between the theoretical coefficient and the actual coefficient[110,111]. This discrepancy could mean the difference between a good device, an average device or a device that doesn't work. Second, it is unknown whether a partly closed well can actually be fabricated. More precisely, it is unknown whether the electron can stay above the well long enough to escape from the well before it falls back in the well. If the partly closed well can be fabricated, then the efficiencies could approach 100 percent(See secs. B-6.2 and B-6.4). Third, it appears that the carrier lifetime is small, which means that the gain will be small and the temperature of operation will be equal to or less than the temperature of operation in extrinsic photoconductors.

B-10.2 Future recommendations

At this time, no experimental results have been obtained for the SLIP. The recommendations for future work on the SLIP are: 1) determine if the free carrier absorption coefficients for p-type GaAs at long wavelengths and high carrier concentrations are large enough, 2) determine if a partly closed well can be fabricated, and 3) experimentally examine the open well and/or partly closed well case.

From these three recommendations, it can be determined if p-type GaAs is a feasible material and what material parameters(ie., effective mass, density of states, dispersion relations for the phonons, number of valleys, etc.) are essential for the SLIP to operate. Using these results, it can be determined if other semiconductors would be more suitable than p-type GaAs.

BIBLIOGRAPHY

[1] R.J. Schwartz, S. Datta, and P.E. Welsh, "Report on solar energy conversion through the interaction of plasmons with tunnel junctions," Technical Report TR-EE 85-9, NASA grant NAG 3-433, Purdue University(February 1985).

[2] A. Bennett and L.C. Olsen, "Analysis of multiple-cell concentrator/photovoltaic systems," 13th Photovoltaic Specialists Conference, pp. 868-873(1978).

[3] M.A. Green, *Solar cells,* Prentice-Hall, Inc., Englewood Cliffs, NJ, pp. 213-219(1982).

[4] J.M. Gee, R.Y. Loo, G.S. Kamath, and R.C. Knechli, "A GaAs/silicon mechanically-stacked, multijunction solar cells," 18th Photovoltaic Specialists Conference, pp. 546-551(1985).

[5] I. Chambouleyron and F. Alvarez, "Conversion efficiency of multiple-gap solar cells under different irradiation conditions," 18th Photovoltaic Specialists Conference, pp. 533-538(1985).

[6] L.M. Anderson, "Solar energy converter using surface plasma waves," US Patent No. 4,482,778(13 November 1984)

[7] L.M. Anderson, "A new strategy for efficient solar energy conversion: parallel-processing with surface plasmons," 16th Photovoltaic Specialists Conference, pp. 371-377(1982).

[8] L.M. Anderson, "Inelastic tunnel diodes," US Patent No. 4,482,779(13 November 1984)

[9] B. Jenson, "The infrared absorption spectrum of n-type GaAs," Physica Status Solidi B, vol. 86, pp. 291-301(1978).

[10] W.A. Harrison, *Solid State Theory,* Dover, New York(1979).

[11] P.B. Johnson and R.W. Christy, "Optical constants of the noble metals," Physical Review B, vol. 6, pp. 4370-4379(1972).

[12] L.I. Schiff, *Quantum Mechanics,* 3rd ed., McGraw Hill, New York(1971).

[13] C.B. Duke, "Tunneling in solids," *Solid State Physics, suppl. 10,* Academic Press, New York(1969).

[14] W. Heitler, *The Quantum Theory of Radiation,* Dover, New York(1984).

[15] J.I. Pankove, *Optical Processes in Semiconductors,* Dover, New York(1971).

[16] K. Ploog and G.H. Doehler, "Compositional and doping superlattices in III-V semiconductors," Advances in Physics, vol. 32, pp. 285-359(1983).

[17] G.H. Doehler and P.P. Ruden, "Theory of absorption in doping superlattices," Physical Review B, vol. 30, pp. 5932-5944(1984).

[18] L. Esaki, L.L. Chang, and E.E. Mendez, "Polytype superlattices and multi-heterojunctions," Japanese Journal of Applied Physics, vol. 20, pp. L529-L532(1981).

[19] L.L. Chang, G.A. Sai-Halasz, L. Esaki, and R.L. Aggarwal, "Spatial separation of carriers in InAs-GaSb superlattices," Journal of Vacuum Science and Technology, vol. 19, pp. 589-591(1981).

[20] S.R. Forrest, "Optical detectors: Three contenders" Spectrum, vol. 23, pp. 76-84(May 1986).

[21] C.T. Elliott, "Infrared detectors," *Handbook on Semiconductors, vol. 4,* Ed. T.S. Moss, North Holland Publishing Company, Amsterdam, pp. 727-798(1981).

[22] D. Long, "Optical and infrared detectors," *Topics in Applied Physics, vol. 19,* Ed. R.J. Keyes, Springer Verlag, Berlin, pp. 101-147(1977).

[23] P.N.J. Dennis, *Photodetectors - An introduction to current technology,* Plenum, New York(1986).

[24] S.M. Sze, *Physics of Semiconductor Devices,* 2nd ed., Wiley Interscience, New York(1981).

[25] G.A. Walter and E.L. Dereniak, "Photodetectors for focal plane arrays. Part 1: Extrinsic silicon," Laser Focus/Electro-Optics, vol. 22, pp. 108-118(March 1986).

[26] G.A. Walter and E.L. Dereniak, "Photodetectors for focal plane arrays. Part 2: HgCdTe," Laser Focus/Electro-Optics, vol. 22, pp. 86-96(April 1986).

[27] G.E. Stillman, C.M. Wolfe, and J.O. Dimmock, "Far infrared photoconductivity in high purity GaAs," *Semiconductors and Semimetals, vol. 12,* Eds. R.K. Willardson and A.C. Beer, Academic Press, New York, pp. 169-290(1977).

[28] H.J.G. Meyer, "Infrared absorption by conduction electrons in germanium," Physical Review, vol. 112, pp. 298-308(1958).

[29] S.V. Kozyrev and A.Ya. Shik, "Capture of carriers by quantum wells in heterostructures," Soviet Physics-Semiconductors, vol. 19, pp. 1024-1025(1985).

[30] J.S. Smith, L.C. Chiu, S. Margalit, A. Yariv, and A.Y. Cho, "A new infrared detector using electron emission from multiple quantum wells," Journal of Vacuum Science and Technology, vol. B1, pp. 376-378(1983).

[31] A.Ya. Shik, "Intraband photoconductivity of quantum-well heterostructures," Soviet Physics-Semiconductors, vol. 20, pp. 1002-1006(1986).

[32] P.R. Bratt, "Impurity germanium and silicon infrared detectors," *Semiconductors and Semimetals, vol. 12,* Eds. R.K. Willardson and A.C. Beer,

Academic Press, New York, pp. 39-142(1977).

[33] B.F. Levine, K.K. Choi, C.G. Bethea, J. Walker, and R.J. Malik, "Quantum well avalanche multiplication initiated by 10 micron intersubband absorption and photoexcited tunneling," Applied Physics Letters, vol. 51, pp. 934-936(1987).

[34] F. Sibille, "Infrared detection and imaging," Reports on the Progress in Physics, vol. 49, pp. 119(1986).

[35] D.F. Barbe, "Imaging devices using the charge-coupled concept," Proceedings of the IEEE, vol. 63, pp. 38-67(1975).

[36] M.M. Blouke, C.B. Burgett, and R.L. Williams, "Sensitivity limits for extrinsic and intrinsic infrared detectors," Infrared Physics, vol. 13, pp. 61-71(1973).

[37] L.C. Chiu, J.S. Smith, S. Margalit, A. Yariv, and A.Y. Cho, "Application of internal photoemission from quantum-well and heterojunction superlattices to infrared photodetectors," Infrared Physics, vol. 23, pp. 93-97(1983).

[38] L.C. Chiu, J.S. Smith, S. Margalit, and A. Yariv, "Internal photoemission from quantum well heterojunction superlattices by phononless free-carrier absorption," Applied Physics Letters, vol. 43, pp. 331-332(1983).

[39] F. Capasso, J. Allam, A.Y. Cho, K. Mohammed, R.J. Malik, A.L. Hutchinson, and D. Sivco, "New avalanche multiplication phenomenon in quantum well superlattices: Evidence of impact ionization across the band-edge discontinuity," Applied Physics Letters, vol. 48, pp. 1294-1296(1986).

[40] N. Lifshitz, A. Jayaraman, R.A. Logan, and H.C. Card, "Pressure and compositional dependences of the Hall coefficient in Al[x]Ga[1-x]As and their significance," Physical Review B, vol. 21, pp. 670-678(1980).

[41] N.S. Rytova, "Resonance absorption of electromagnetic waves in a thin film," Soviet Physics Solid State, vol. 8, pp. 2136-2140(1967).

[42] A.Ya. Shik, "Anisotropy of the high frequency conductivity of size-quantized films," Soviet Physics JETP, vol. 29, pp. 931-933(1969).

[43] A.Ya. Shik, "Optical properties of semiconductor superlattices with complex band structures," Soviet Physics-Semiconductors, vol. 6, pp. 1110-1117(1973).

[44] A.Ya. Shik, "Superlattices - periodic semiconductor structures," Soviet Physics-Semiconductors, vol. 8, pp. 1195-1209(1975).

[45] S.Y. Yuen, "Fast relaxing absorptive nonlinear refraction in superlattices," Applied Physics Letters, vol. 43, pp. 813-815(1983).

[46] L. Esaki and R. Tsu, "Superlattice and negative differential conductivity in semiconductors," IBM Journal of Research and Development, vol. 14, pp. 61-65(1970).

[47] L.C. West and S.J. Eglash, "First observation of an extremely large-dipole infrared transition within the conduction band of a GaAs quantum well," Applied Physics Letters, vol. 46, pp. 1156-1158(1985).

[48] B.F. Levine, R.J. Malik, K.K. Choi, C.G. Bethea, D.A. Kleinman, and J.M. Vanderberg, "Strong 8.2 micron infrared intersubband absorption in doped GaAs/AlAs quantum well waveguides," Applied Physics Letters, vol. 50, pp. 273-275(1987).

[49] K.K. Choi, B.F. Levine, R.J. Malik, J. Walker, and C.G. Bethea, "Periodic negative conductance by sequential resonant tunneling through an expanding high-field superlattice domain," Physical Review B, vol. 35, pp. 4172-4175(1987).

[50] B.F. Levine, K.K. Choi, C.G. Bethea, J. Walker, and R.J. Malik, "New 10 micron infrared detector using intersubband absorption in resonant tunneling GaAsAs superlattices," Applied Physics Letters, vol. 50, pp. 1092-1094(1987).

[51] K.K. Choi, B.F. Levine, C.G. Bethea, J. Walker, and R.J. Malik, "Multiple quantum well 10 micron GaAs/$Al_xGa_{1-x}As$ infrared detector with improved responsivity," Applied Physics Letters, vol. 50, pp. 1814-1816(1987).

[52] F. Capasso, K. Mohammed, and A.Y. Cho, "Resonant tunneling through double barriers, perpendicular quantum transport phenomena in superlattices, and their device applications," IEEE Journal on Quantum Electronics, vol. QE-22, pp. 1853-1869(1986).

[53] F. Capasso, K. Mohammed, A.Y. Cho, R. Hull, and A.L. Hutchinson, "Effective mass filtering: giant quantum amplification of the photocurrent in a semiconductor superlattice," Applied Physics Letters, vol. 48, pp. 420-422(1985).

[54] F. Capasso, K. Mohammed, A.Y. Cho, and A.L. Hutchinson, "New quantum photoconductivity and large photocurrent gain by effective-mass filtering in a forward-biased superlattice p-n junction," Physical Review Letters, vol. 55, pp. 1152-1155(1985).

[55] F. Capasso, K. Mohammed, and A.Y. Cho, "Quantum photoconductive gain by effective mass filtering and negative conductance in superlattice pn junctions," Physica, vol. 134B, pp. 487-493(1985).

[56] D.D. Coon and R.P.G. Karunasiri, "New mode of IR detection using quantum wells," Applied Physics Letters, vol. 45, pp. 649-651(1984).

[57] D.D. Coon, R.P.G. Karunasiri, and L.Z. Liu, "Narrow band infrared detection in multiquantum well structures," Applied Physics Letters, vol. 47, pp. 289-291(1985).

[58] D.D. Coon, R.P.G. Karunasiri, and H.C. Liu, "Fast response quantum well photodetectors," Applied Physics Letters, vol. 60, pp. 2636-2638(1986).

[59] K.W. Goossen and S.A. Lyon, "Grating enhanced quantum well detector," Applied Physics Letters, vol. 47, pp. 1257-1259(1985).

[60] D.D. Coon and R.P.G. Karunasiri, "Effect of electric fields on long-wavelength response of infra-red detectors," Electronics Letters, vol. 19, pp. 284-287(1983).

[61] D.D. Coon, S.D. Gunapala, R.P.G. Karunasiri, and H.-M. Muehlhoff, "Photoionization of impurity atoms in semiconductors in the presence of an applied electric field," Electronics Letters, vol. 19, pp. 1070-1071(1983).

[62] D.D. Coon and R.P.G. Karunasiri, "Photoionization of impurity atoms in semiconductors in the presence of an applied electric field," Solid State Electronics, vol. 26, pp. 1151-1155(1983).

[63] D.D. Coon, S.D. Gunapala, R.P.G. Karunasiri, and H.-M. Muehlhoff, "IR detection by depletion of trapped charge in localized impurity of an extrinsic semiconductor," International Journal of Infrared and Millimeter Waves, vol. 5, pp. 197-205(1984).

[64] D.D. Coon, S.D. Gunapala, R.P.G. Karunasiri, and H.-M. Muehlhoff, "A high-sensitivity sampling IR detector," Infrared Physics, vol. 25, pp. 323-325(1985).

[65] D.D. Coon and A.G.U. Perera, "Spectral information coding by infrared photoreceptors," International Journal of Infrared and Millimeter Waves, vol. 7, pp. 1571-1583(1986).

[66] E.O. Kane, "Zener tunneling in semiconductors," Journal of Physical and Chemical Solids, vol. 12, pp. 181-188(1959).

[67] E.O. Kane, "Theory of tunneling," Journal of Applied Physics, vol. 32, pp. 83-91(1961).

[68] D.H. Seib and L.W. Aukerman, "Photodetectors for the .1 to 1. micrometer spectral region," *Advances in Electronics and Electron Physics, vol. 34,* Ed. L. Marton, Academic Press, New York, 95-221(1973).

[69] R.J. McIntyre, "Multiplication noise in uniform avalanche diodes," IEEE Transactions on Electron Devices, vol. ED-13, pp. 164-168(1966).

[70] R.J. McIntyre, "The distribution of gains in uniformly multiplying avalanche photodiodes: theory," IEEE Transactions on Electron Devices, vol. ED-19, pp. 703-713(1972).

[71] P.P. Webb, R.J. McIntyre, and J. Conradi, "Properties of avalanche photodiodes," IEEE Transactions on Electron Devices, vol. ED-19, pp. 234-278(1972).

[72] J. Conradi, "The distribution of gains in uniformly multiplying avalanche photodiodes: experimental," IEEE Transactions on Electron Devices, vol. ED-19,

pp. 713-718(1972).

[73] M.C. Teich, K. Matsuo, and B.E.A. Saleh, "Excess noise factors for conventional and superlattice avalanche photodiodes and photomultiplier tubes," IEEE Journal of Quantum Electronics, vol. QE-22, pp. 1184-1193(1986).

[74] F. Capasso, W.-T. Tsang, and G.F. Williams, "Staircase solid-state photomultipliers and avalanche photodiodes with enhanced ionization rates ratio," IEEE Transactions on Electron Devices, vol. ED-30, pp. 381-390(1983).

[75] K. Nishida, K. Taguchi, and Y. Matsumoto, "InGaAsP heterostructure avalanche photodiodes with high avalanche gain," Applied Physics Letters, vol. 35, pp. 251-253(1979).

[76] N. Susa, H. Nakagome, O. Mikami, H. Ando, and H. Kanbe, "New InGaAs/InP avalanche photodiode structure for the 1-1.6 micron wavelength region," IEEE Journal of Quantum Electronics, vol. QE-16, pp. 864-869(1980).

[77] O.K. Kim, S.R. Forrest, W.A. Bonner, and R.G. Smith, "A high gain $In_{.53}Ga_{.47}As$/InP avalanche photodiode with no tunneling leakage current," Applied Physics Letters, vol. 39, pp. 402-404(1981).

[78] S.R. Forrest, O.K. Kim, R.G. Smith, and G.F. Williams, "Excess-noise and receiver sensitivity measurements of $In_{53}Ga_{47}As$/InP avalanche photodiodes," Electronics Letters, vol. 17, pp. 917-919(1981).

[79] S.R. Forrest, O.K. Kim, and R.G. Smith, "Optical response time of $In_{53}Ga_{47}As$/InP avalanche photodiodes," Applied Physics Letters, vol. 41, pp. 95-99(1982).

[80] J.C. Campbell, A.G. Dentai, W.S. Holden, and B.L. Kasper, "High-performance avalanche photodiode with separate absorption 'grading' and multiplication regions," Electronics Letters, vol. 19, pp. 818-820(1983).

[81] F. Capasso, A.Y. Cho, and P.W. Foy, "Low-dark-current low-voltage 1.3-1.6 μm avalanche photodiode with high-low electric field profile and separate absorption and multiplication regions by molecular beam epitaxy," Electronics Letters, vol. 20, pp. 635-637(1984).

[82] G.E. Stillman, V.M. Robbins, and N. Tabatabaie, "III-V compound semiconductor devices: Optical detectors," IEEE Transactions on Electron Devices, vol. ED-31, pp. 1643-1655(1984).

[83] F. Capasso, H.M. Cox, A.L. Hutchinson, N.A. Olsson, and S.G. Hummel, "Pseudo-quaternary GaInAsP semiconductors: A new $Ga_{.47}In_{.53}As$/InP graded gap superlattice and its applications to avalanche photodiodes," Applied Physics Letters, vol. 45, pp. 1193-1195(1984).

[84] W.S. Holden, J.C. Campbell, and A.G. Dentai, "Gain uniformity of InP/InGaAsP/InGaAs avalanche photodiodes with separate absorption, grading, and multiplication regions," IEEE Journal of Quantum Electronics, vol. QE-21, pp. 1310-1313(1985).

[85] Y.K. Jhee, J.C. Campbell, W.S. Holden, A.G. Dentai, and J.K. Plourde, "The effect of nonuniform gain on the multiplication noise of InP/InGaAsP/InGaAs avalanche photodiodes," IEEE Journal of Quantum Electronics, vol. QE-21, pp. 1858-1861(1985).

[86] M.D. Petroff, M.G. Stapelbroek, and W.A. Kleinhans, "Detection of individual .4-28 micron wavelength photons via impurity-impact ionization in a solid state photomultiplier," Applied Physics Letters, vol. 51, pp. 406-408(1987).

[87] R. Chin, N. Holonyak, Jr., G.E. Stillman, J.Y. Tang, and K. Hess, "Impact ionisation in multilayered heterojunction structures," Electronics Letters, vol. 16, pp. 467-469(1980).

[88] F. Capasso, W.T. Tsang, A.L. Hutchinson, and G.F. Williams, "Enhancement of electron impact ionization in a superlattice: A new avalanche photodiode with a large ionization rate ratio," Applied Physics Letters, vol. 40, pp. 38-40(1982).

[89] F. Capasso, "New device applications of bandedge discontinuities in multilayer heterojunction structures," Surface Science, vol. 132, pp. 527-539(1983).

[90] K. Brennan, T. Wang, and K. Hess, "Theory of electron impact ionization including a potential step: application to GaAs-AlGaAs," IEEE Electron Device Letters, vol. EDL-6, pp. 199-201(1985).

[91] F.-Y. Juang, U. Das, Y. Nashimoto, and P.K. Bhattacharya, "Electron and hole impact ionization coefficients in GaAs–$Al_xGa_{1-x}As$ superlattices," Applied Physics Letters, vol. 47, pp. 972-974(1985).

[92] K. Brennan, "Theory of electron and hole impact ionization in quantum well and staircase superlattice avalanche photodiode structures," IEEE Transactions on Electron Devices, vol. ED-32, pp. 2197-2205(1985).

[93] P. Chakrabarti and B.B. Pal, "Optical characteristics of a superlattice avalanche photodiode," Solid State Electronics, vol. 30, pp. 675-679(1987).

[94] K. Brennan, "Comparison of multiquantum well, graded barrier, and doped quantum well GaInAs/AlInAs avalanche photodiodes: A theoretical approach," IEEE Journal on Quantum Electronics, vol. QE-23, pp. 1273-1282(1987).

[95] F. Capasso and W.T. Tsang, "Superlattice, graded band gap, channeling and staircase avalanche photodiodes towards a solid-state photomultiplier," IEDM Technical Digest, pp. 334-337(1982).

[96] G.F. Williams, F. Capasso, and W.T. Tsang, "The graded bandgap multilayer avalanche photodiode: A new low-noise detector," IEEE Electron Device Letters, vol. EDL-3, pp. 71-73(1982).

[97] H. Blauvelt, S. Margalit, and A. Yariv, "Single-carrier-type dominated impact ionisation in multilayer structures," Electronics Letters, vol. 18, pp. 375-376(1985).

[98] K. Brennan, "Theory of the doped quantum well superlattice APD: A new solid-state photomultiplier," IEEE Journal on Quantum Electronics, vol. QE-22, pp. 1999-2016(1987).

[99] K. Brennan, "Theory of the GaInAs/AlInAs-doped quantum well superlattice APD: A new low noise solid-state photodetector for lightwave communications systems," IEEE Transactions on Electron Devices, vol. ED-33, pp. 1683-1695(1985).

[100] K. Brennan, "The p-n quantum well APD: A new solid-state photodetector for lightwave communications systems and on-chip detector applications," IEEE Transactions on Electron Devices, vol. ED-34, pp. 782-792(1985).

[101] K. Brennan, "The p-n heterojunction quantum well APD: A new high-gain low-noise high-speed photodetector suitable for lightwave communications and digital applications," IEEE Transactions on Electron Devices, vol. ED-34, pp. 793-803(1985).

[102] F. Capasso, W.T. Tsang, A.L. Hutchinson, and P.W. Foy, "The graded bandgap avalanche photodiode: A new molecular beam epitaxial structure with a large ionization rates ratio," Institute of Physics Conference Series, No. 63, pp. 473-478(1982).

[103] C.J. Summers and K.F. Brennan, "New resonant tunneling superlattice avalanche photodiode device structure for long-wavelength infrared detection," Applied Physics Letters, vol. 51, pp. 276-278(1987).

[104] K.F. Brennan and C.J. Summers, "The variably spaced superlattice energy filter quantum well avalanche photodiode: A solid state photomultiplier," IEEE Journal on Quantum Electronics, vol. QE-23, pp. 320-327(1987).

[105] F. Capasso, "The channeling avalanche photodiode: A novel ultra-low-noise interdigitated p-n junction detector," IEEE Transactions on Electron Devices, vol. ED-29, pp. 1388-1395(1982).

[106] F. Capasso, "New ultra-low-noise avalanche photodiode with separated electron and hole avalanche regions," Electronic Letters, vol. 18, pp. 12-13(1982).

[107] K.F. Brennan, "Theory of the channeling avalanche photodiode," IEEE Transactions on Electron Devices, vol. ED-32, pp. 2467-2478(1985).

[108]H. Adamska and H.N. Spector, "Free carrier absorption in quantum well structures for polar optical phonon scattering," Journal of Applied Physics, vol. 56, pp. 1123-1127(1984).

[109]K. Ploog, A. Fischer, and H. Kunzel, "The use of Si and Be impurities for novel periodic doping structures in GaAs grown by molecular beam epitaxy," Journal of the Electrochemical Society, vol. 128, pp. 400-410(1981).

[110]P.A. Schumann, Jr., W.A. Keenan, A.H. Tong, H.H. Gegenwarth, and C.P. Schneider, "Silicon optical constants in the infrared," Journal of the Electrochemical Society, vol. 118, pp. 145-148(1971).

[111]E. Barta, "Optical constants of various heavily doped p- and n-type silicon crystals obtained by Kramers-Kronig analysis," Infrared Physics, vol. 17, pp. 319-329, (1977).

[112]S. Perkowitz and J. Breecher, "Characterization of GaAs by far infrared reflectivity," Infrared Physics, vol. 13, 321-326(1973).

[113]S. Perkowitz, "Far infrared free-carrier absorption in n-type gallium arsenide," Journal of Physical and Chemical Solids, vol. 32, 2267-2274(1971).

[114]G.D. Mahan, "Energy gap in Si and Ge: impurity dependence," Journal of Applied Physics, vol. 51, pp. 2634-2646(1980).

[115]J.R. Lowney and H.S. Bennett, "Effect of donors impurities on the conduction and valence bands of silicon," Journal of Applied Physics, vol. 53, pp. 433-438(1982).

[116]E.O. Kane, "Thomas-Fermi approach to impure semiconductor band structure," Physical Review, vol. 131, pp. 79-88(1963).

[117]T.N. Morgan, "Broadening of impurity bands in heavily doped semiconductors," Physical Review, vol. 139, pp. A343-A348(1965).

[118]K.P. Abdurakhmanov, Sh. Mirakhmedov, A. Teshabaev, and S.S. Khudaiberdiev, "Characteristics of the distribution of the density of states in heavily doped p-type GaAs," Soviet Physics-Semiconductors, vol. 10, pp. 393-397(1976).

[119]T.S. Moss, *Optical Properties of Semiconductors,* Academic Press, New York(1959).

[120]W.P. Dumke, "Quantum theory of free carrier absorption," Physical Review, vol. 124, pp. 1813-1817(1961).

[121]K. Seeger, *Semiconductor Physics,* Springer-Verlag, Berlin(1985).

[122]B. Jenson, "Quantum theory of free carrier absorption in polar semiconductors," Annals of Physics, vol. 80, pp. 284-360(1973).

[123]B.R. Nag, *Electron Transport in Compound Semiconductors,* Springer-Verlag, Berlin(1980).

[124]S. Ramo, J.R. Whinnery, and T. van Duzer, *Fields and Waves in Communications Electronics,* John Wiley and Sons, New York(1965).

[125]J.E. Bowers and C.A. Burrus, Jr., "Ultrawide-band long-wavelength p-i-n photodetectors," Journal of Lightwave Technology, vol. LT-5, pp. 1339-1350(1987).

[126]R.J. Seymour, E.S. Koteles, and G.I. Stegeman, "Far-infrared surface plasmon coupling with overcoated gratings," Applied Physics Letters, vol. 41, pp. 1013-1015(1982).

[127]A.K. Walton and S.F. Metcalfe, "Free-carrier absorption at low temperatures in uniaxially stressed n-type Ge, Si, and GaAs," Journal of Physics C, vol. 9, pp. 3605-3625(1976).

[128]H.N. Spector, "Free-carrier absorption in quasi-two-dimensional semiconducting structures," Physical Review B, vol. 28, pp. 971-976(1983).

[129]E.C. Jordan and K.G. Balmain, *Electromagnetic Waves and Radiating Systems,* 2nd ed., Prentice Hall(1968).

[130]H.L. Hackforth, *Infrared Radiation,* McGraw-Hill, New York(1960).

[131]L.L. Chang, "The conduction properties of Ge—$GaAs_{1-x}P_x$ n-n heterojunctions," Solid State Electronics, vol. 8, pp. 721-728(1965).

[132]L. Nordheim, "Zur Theorie der thermischen Emission und der Reflexion von Elektronen an Metallen," Zeitschrift fur Physik, vol. 46, pp. 833-855(1928).

[133]R.H. Fowler and L. Nordheim, "Electron emission in intense electric fields," Proceedings of the Royal Society, vol. A119, pp. 173-181(1928).

[134]K.H. Gundlach, "Zur Berechnung Des Tunnelstroms Durch eine Trapezformige Potentialstuff," Solid State Electronics, vol. 9, pp. 949-957(1966).

[135]C. Jacobini and L. Reggiani, "The Monte Carlo method for the solution of charge transport in semiconductors with applications to covalent materials," Reviews of Modern Physics, vol. 55, pp. 645-705(1983).

[136]C. Jacobini and L. Reggiani, "Bulk hot-electron properties of cubic semiconductors," Advances in Physics, vol. 28, pp. 493-553(1979).

[137]S. Adachi, "GaAs, AlAs and $Al_xGa_{1-x}As$: Material parameters for use in research and device applications," Journal of Applied Physics, vol. 58, pp. R1-R29(1985).

[138]W. Walukiewicz, L. Lagowski, L. Jastrzebski, M. Lichtensteiger, and H.C. Gatos, "Electron mobility and free carrier absorption in GaAs: Determination of the

compensation ratio," Journal of Applied Physics, vol. 50, pp. 899-908(1979).

[139]C.R. Crowell and S.M. Sze, *Physics of Thin Films, vol. 4,* pp. 325,328-9,367, Academic Press, New York and London, (1967).

[140]E.H. Putley, "Far infra-red photoconductivity," Physica Status Solidi, vol. 6, pp. 571-614, (1964).

[141]K.M. van Vliet, "Noise limitation in solid state photodetectors," Applied Optics, vol. 6, pp. 1145-1169(1967).

[142]P.W. Kruse, L.D. McGlauchlin, and R.B. McQuistan, *Elements of Infrared Technology: Generation, Transmission and Detection,* John Wiley, New York(1962).

[143]P.W. Kruse, "The photon detection process," *Topics in Applied Physics, vol. 19,* Ed. R.J. Keyes, Springer Verlag, Berlin, pp. 101-147(1977).

[144]J.S. Blakemore, "Semiconducting and other major properties of gallium arsenide," Journal of Applied Physics, vol. 53, pp. R123-R181(1982).

[145]J.P. Faurie, "Growth and properties of HgTe-CdTe and other Hg-based superlattices," IEEE Journal on Quantum Electronics, vol. QE-22, pp. 1656-1665(1986).

[146]Y.G. Chai, R. Chow, and C.E.C. Wood, "The effect of growth conditions on Si incorporation in molecular beam epitaxial GaAs," Applied Physics Letters, vol. 39, pp. 800-803(1981).

[147]J.R. Lowney and H.S. Bennett, "Effect of ionized donors on the electron and holes densities of states in silicon," Journal of Applied Physics, vol. 54, pp. 1369-1374(1983).

[148]P. Enquist, L.M. Lunardi, G.W. Wicks and L.F. Eastman, "Summary abstract: Effects of high levels of Be in GaAs by MBE," Journal of Vacuum Science and Technology, vol. B3, pp. 634-635(1985).

SUBJECT INDEX

absorption(See also losses)
- band to band 34,47-48,56,58-68
- due to tunneling 12,17,19-31
- free carrier 10,11,12-18,30,35,39-40,44-46,69-72,85,97-100,101-102,107,116-117
- from a dopant site 34,47-50
- intersubband 44,50-58,69
- phonon 45-46,97-98
- region 59-68
- spatially direct 19,20,26,30
- spatially indirect 19,20,26,30

absorption junction 1,11,19-31
array 34,44-46,53,116
band gap narrowing(degenerate doping) 71,105
barrier
- trapezoidal 35,82-85
- triangular 35,80-82,85

barrier height 39,44-46,50,53,73,78-79,87-95,101,104-105,107
collisions(See scattering)
cone of passage angle 90,95,105,106
coupling into structure
- photodetector 40-43,50,53,73-74
- solar cell 1,10-11,17,20,30,32

crosstalk(optical) 116
current
- background 75,77-78,96-98,102,109
- dark 50,75,96-97,102,105
- diffusion 58,68
- injection 5
- leakage 62
- optical 76,96
- signal 50,59,75-77,96-97
- thermionic emission 43,78-79,97,102-103,107-109
- tunnel(field emission) 22,35,58-59,79-85,96

D^* 45,75-76,96-100,102,109-112,113
deep dopant levels 50
density of states 39,43,44,52,69,71,89,93,105,116-117

dielectric constant
  metal 10,12,71
  oxide 12
  semiconductor 71,100
Drude theory 12,71-72
$E_{cb}-E_{cw}$ 44,80-85,89-94,101,107
$E_{cb}-E_F$ 39,40-44,50,53,78-79,88,93,95,101-103,105-106,107-108
E_F-E_{cw} 39,44,70-71,80,82,93,101,105,108
effective gap 19-31
efficiency
  photoconductor 39,43,47,50,53,56,58,69,75-77,87-95,97,98,101-106,107-112,116
  solar cell 4-10,20,32
escape(See well, escape)
fill factor 22
free carrier absorption(See absorption)
gain 39,44-45,50,53,56,64,76-80,96-97,107-112,116
heterojunction 19-20,26,62
impact ionization 39,44-45,53,58-68,85,88,107,116
impurity hopping 34,59
index of refraction(See dielectric constant)
intra-band absorption(See absorption, free carrier)
ionization ratio 58-59,62,64
losses
  propagation(Ohmic) 1,12-17,30,58
  structural 5-9,32
metal-insulator-metal diode 1,17,20
metal-insulator-semiconductor diode 1,11,17,20
mirror 5-10
Monte Carlo 89-95,109-112
multiplication region 59-68
narrow gap problems 34,47,58,116
noise
  avalanche 58-59
  amplifier 59,96
  background 45,58,75,96-98,102,109
  excess noise factor 58-68
  NEP 96
  RG 96,102-103
  shot 96

thermal 96
open well case 40-41,73-74,87-92,103-106,116-117
oxide-metal-oxide structure 12-17
partly closed well case 40-43,45,73,87-89,91-95,102-106,107-109,113,116-117
phonon
acoustic 87-88,101
elastic 88-89,101
general 35,87,117
inelastic 45,87-89,91,93-95,101,105,107
intervalley 40,43,87-88,102-104,105,107
negligible 88
nonnegligible 88
optical 40,43,87-88,102-104,105
photodetector
APD 34,47,58-59
channeling APD 68
effective mass filter IS-PC 47,56,68
extrinsic photoconductor 34-35,39,44,45,47-50,78,96,98,102,104,113,115,116
graded well SLIP 50
intrinsic photoconductor 34-35,45,47-50,56,98,102,104,113,115
IS-PC 53,68
one carrier detectors 34,47-50
photomultiplier 59
pin photodiode 34,47,102,113,115
quantum well IS-PC 56
resonant IS-PC 53-56
RTS-APD 68
SAM-APD 59-62
SLIP 2,34-46,47,50,53,69,75-77,80,85,87-89,96-100,101-106,107-114,116-117
staircase APD 64
superlattice APD 62
tunneling IS-PC 53,58,68,109
two carrier detectors 34-35,59
planar configuration 73
plasmons 1,10,12,17
pn junction 19,22-26
polarization of radiation 19-20,39-43,50-53,73-74,105
prism 10
propagation of radiation 10-11,19,22,35,39-43,50,53,69,73-74,76,85,103-104,106,107

recombination(collection) 25-26,39,85,109,116
reflection coefficient 5-9,73-74
scattering
  carrier-carrier 35,87-89
  general 40,43,72,73,91-95
  impurity 35,87-89,101,107
  phonon 35,50,87-89,93,101,107
semiconductor-insulator-semiconductor diode 1,19,20-22,30
solar cell
  MEG-SC 4,10-11,12-18
  multiple cell concepts 1,4-10,20,32
  spectrum splitting concept 4-10
  tandem cell concept 4-10,20
  weaknesses 4
superlattice
  conduction(or valence) band 34-46,50-58,85-86,107-112
  graded, type I 64
  nipi 20,26,30
  type I 20,26,56,62,68
  type II 20,26,30
temperature of operation 35,40,43,44,45,47,50,53,73,78-79,87,98,101-104,107,116
time
  escape 109-112
  lifetime 109-112,113,116
  RC 107,113
  relaxation 43,71,109,113
  response 45,50,58,59,62,68,113
transmission probability 80-85
tunnel(Esaki) diode 22-26,30
tunneling 1,10-11,12-18,19-22,35,50-58,68,75,79-85
2D effects 69,107
waveguide 1,10,12-18,19-20,30,40,74
well(quantum)
  doping of 35,88,104-105
  escape(excitation) 39-43,50,58,69,73-74,77,85,87-95,101,103,109,116
  fall into 39-43,45,50,85,89,91-95,109,116
  general 35,69,77,102,107
  levels 19,50-57